GERDA

## The GERmanium Detector Array for the search of neutrinoless $\beta\beta$ decays of ^{76}Ge at LNGS

Proposal to the LNGS P38/04

September 2004

Gerda

The GERmanium Detector Array for the search of neutrinoless $\beta\beta$ decays of ^{76}Ge at LNGS

I. Abt[j], M. Altmann[j], A.M. Bakalyarov[i], I. Barabanov[g], C. Bauer[c], M. Bauer[l],
E. Bellotti[f], S. Belogurov[g,h], S.T. Belyaev[i], A. Bettini[k], L. Bezrukov[g], V. Brudanin[b],
C. Büttner[j], V.P. Bolotsky[h], A. Caldwell[j], C. Cattadori[a,f], M.V. Chirchenko[i],
O. Chkvorets[c], H. Clement[l], E. Demidova[h], A. Di Vacri[a], J. Eberth[d], V. Egorov[b],
E. Farnea[k], A. Gangapshev[g], G.Y. Grigoriev[i], V. Gurentsov[g], K. Gusev[b],
W. Hampel[c], G. Heusser[c], W. Hofmann[c], L.V. Inzhechik[i], J. Jochum[l], M. Junker[a],
S. Katulina[b], J. Kiko[c], I.V. Kirpichnikov[h], A. Klimenko[b,g], K.T. Knöpfle[c],
O. Kochetov[b], V.N. Kornoukhov[g,h], R. Kotthaus[j], V. Kusminov[g], M. Laubenstein[a],
V.I. Lebedev[i], X. Liu[j], H.-G. Moser[j], I. Nemchenok[b], L. Pandola[a], P. Peiffer[c],
R.H. Richter[j], K. Rottler[l], C. Rossi Alvarez[k], V. Sandukovsky[b], S. Schönert[c],
S. Scholl[l], J. Schreiner[c], B. Schwingenheuer[c], H. Simgen[c], A. Smolnikov[b,g],
A.V. Tikhomirov[i], C. Tomei[a], C.A. Ur[k], A.A. Vasenko[h], S. Vasiliev[b,g], D. Weißhaar[d],
M. Wojcik[e], E. Yanovich[g], J. Yurkowski[b], S.V. Zhukov[i], G. Zuzel[c]

[a] INFN Laboratori Nazionali del Gran Sasso, Assergi, Italy
[b] Joint Institute for Nuclear Research, Dubna, Russia
[c] Max-Planck-Institut für Kernphysik, Heidelberg, Germany
[d] Institut für Kernphysik, Universität Köln, Germany
[e] Jagiellonian University, Krakow, Poland
[f] Università di Milano Bicocca e INFN Milano, Milano, Italy
[g] Institute for Nuclear Research of the Russian Academy of Sciences, Moscow, Russia
[h] Institute for Theoretical and Experimental Physics, Moscow, Russia
[i] Russian Research Center Kurchatov Institute, Moscow, Russia
[j] Max-Planck-Institut für Physik, München, Germany
[k] Dipartimento di Fisica dell'Università di Padova e INFN Padova, Padova, Italy
[l] Physikalisches Institut, Universität Tübingen, Germany

Contact Persons:

C. Cattadori
(Carla.Cattadori@lngs.infn.it)
S. Schönert,
(Stefan.Schoenert@mpi-hd.mpg.de)

Contents

1 Overview and executive summary

We propose the GERDA experiment, the **GER**manium **D**etector **A**rray for the search of neutrinoless double beta decay of ^{76}Ge. In the experiment germanium detectors made out of isotopically enriched material will be operated inside a cryogenic fluid shield. The facility would be located in Hall A of the Laboratori Nazionali del Gran Sasso (LNGS) and would serve a dual purpose:

- The experiment would probe the neutrinoless double beta decay of ^{76}Ge with a sensitivity of $T_{1/2} > 2 \cdot 10^{26}$ years at 90% confidence level (C.L.) corresponding to a range of the effective neutrino mass of <0.09 - 0.29 eV within ~ 3 years, thereby scrutinizing, with high statistical significance, the recent claim for evidence for neutrinoless double beta decay [Kla 04]. Existing enriched detectors from the previous Heidelberg-Moscow and IGEX experiments as well as a new set of detectors will be used.

- In addition the proposed experiment would be a pioneering low-level facility which would demonstrate the possibility of reducing backgrounds by 2-3 orders of magnitude below the current state-of-the-art; it would represent a major step on the way towards an ultimate ^{76}Ge double beta decay experiments aiming for a sensitivity in the 10 meV mass range.

The physics case. Since their discovery neutrinos have been an object of extensive experimental study and the knowledge about their properties has advanced our understanding of weak interactions significantly. Still unanswered, however, is the very fundamental question whether the neutrino is a Majorana particle like most extensions of the Standard Model assume. The study of double beta decay is the most sensitive approach to answer this question. If the decay occurs without the emission of neutrinos then their Majorana nature is proven. The potential of this method has increased considerably during the last years since a non-zero mass of the neutrinos has been established by the observation of neutrino flavor oscillation. In fact, the observation of neutrinoless double beta decay would not only establish the Majorana nature of the neutrino but also provide a measurement of its effective mass $m_{ee} = |\,|U_{e1}|^2 m_1 + |U_{e2}|^2 m_2 \exp{(i\alpha_2)} + |U_{e3}|^2 m_3 \exp{(i\alpha_3)}\,|$ where the U_{ei} are the mixing matrix elements between the flavor eigenstate e and the mass eigenstate i, m_i the mass eigenvalues, and $\alpha_{2,3}$ the CP violating phases due to the Majorana nature of the neutrino.

The experimental situation. Double beta decay experiments search for nuclear decays $(A, Z) \rightarrow (A, Z + 2) + 2e^- + 2\bar{\nu}_e$ where single beta decay is energetically forbidden. The neutrinoless reaction is only possible if neutrinos are Majorana particles. There is a long history of searches for neutrinoless double beta decay. The best lifetime limits come from the above mentioned experiments with the isotope ^{76}Ge, and it is $T_{1/2} > 1.9 \cdot 10^{25}$ years. Using calculations for nuclear matrix elements, lifetime limits can be used to constrain m_{ee}. Variations in the calculations introduce about a factor of three uncertainty in the mass limit. The current best limit is $m_{ee} < 0.33 - 1.3$ eV .

Recent evidence for neutrinoless double beta decay has been claimed by the group of Klapdor-Kleingrothaus [Kla 04], with a lifetime of about $1.2 \cdot 10^{25}$ years. Using more conservative errors for the matrix element calculations a mass range of $m_{ee} = 0.1 - 0.9$ eV is derived. The ongoing experiments CUORICINO and NEMO3 have in principal the sensitivity to confirm the neutrinoless double beta decay signal with ^{130}Te and ^{100}Mo. However, in case of a null result, they can not refute the claim because of the nuclear matrix element uncertainties involved. The KATRIN experiment would also see a signal for an effective electron neutrino masses above 0.2 eV.

Experimental considerations. The parameters determining the sensitivity of a neutrinoless double beta decay experiment are the mass of the relevant isotope, M, the running time, T, and the background index B (usually quoted in units of cts/(keV·kg·y)) in the relevant energy range. The kinetic energy spectrum of the outgoing electrons is measured, and the number of events in the window $Q \pm \delta_E$ is evaluated. In the case where no events are found, then the m_{ee} limit scales as $1/(M \cdot T)^{1/2}$. Once non-zero background is observed, then the m_{ee} limit varies as $a \cdot [(B \cdot \delta_E)/(M \cdot T)]^{1/4}$, with a being the fraction of enriched isotopes. A high sensitivity experiment will clearly need maximum detector mass as well as very small backgrounds.

We consider germanium as a good choice for such an experiment. The isotope ^{76}Ge has been successfully enriched at the level of 85 %. Germanium can be used both as source and detector, and excellent energy resolution is achieved. There is considerable experience with germanium, and many background sources have been identified. These can be classified as external and internal backgrounds. External backgrounds are those coming from the environment (natural radioactivity in the walls, air, etc.), from containment, support and shielding materials, and from detector surface contamination. Internal backgrounds arise from active radioisotopes within the detector itself (e.g., ^{60}Co) which are produced in cosmogenic reactions. The Heidelberg-Moscow collaboration has concluded that the dominant backgrounds are external. This background is at the level of $B \sim 0.1$ cts/(keV·kg·y), which should be reduced by more than two orders of magnitude to reach our objectives. We plan to achieve this background reduction by suspending bare germanium crystals in liquid nitrogen and applying various background reduction techniques. Liquid argon is considered as an alternative. Nitrogen can be highly purified such that it does not produce a significant source of background. On the other hand, the liquid nitrogen layer successfully suppresses radiation (primarily gammas) from the surroundings. The basic layout of our experiment follows ideas proposed several years ago [Heu 95] and is similar to the GENIUS [Kla 99] and GEM [Zde 01] proposals.

Proposed facility based on a cryogenic fluid shield. For cost and space reasons, we consider to use a combination of shields, rather than a single thick liquid nitrogen shield as in the original GENIUS proposal. The baseline option of the facility uses about 2 m of liquid nitrogen as a primary shield, contained in a vacuum-isolated copper cryostat, followed by about 3 m of highly purified water. This design is actually similar to the GEM proposal. The diameter of the cryostat is chosen such that the nitrogen shields the low residual activity of the cryostat walls. The outer water shield complements the shielding

against the rock and concrete. It also serves as a neutron shield and – encased in a diffuse reflecting foil and equipped with photomultipliers – as a veto against cosmic muons. While the response of potential suppliers is encouraging, the fabrication of a copper cryostat of the required dimensions by using only radiopure materials is non-trivial, and therefore a conventional vacuum-insulated steel cryostat is discussed as a backup option. To shield the activity of the steel, the inside of the tank would be lined with an additional (cold) lead or copper layer. Both options result in compact cryostats, important both for cost and safety aspects, since the volume of the cryogenic fluid is kept relatively small. A cleanroom and sophisticated lock and suspension systems on top of the cryostat allow to insert and remove detectors without introducing contamination into the vessel. Gas purification and handling systems make extensive use of the experience accumulated in BOREXINO.

Internal backgrounds must also be reduced to reach the desired sensitivity level. For germanium, these backgrounds are understood to come primarily from ^{68}Ge and ^{60}Co, and are the result of observing only a fraction of the energy carried by the decay products. It is critical to distinguish these types of energy deposits from those resulting from double beta decay. R&D is currently under way into producing segmented Germanium detectors which can resolve multi-site energy deposits. Another complementary approach is to discriminate multi-site deposits from the time structure of the signal. Both techniques will likely be necessary in order to reach the desired background levels. Furthermore, for the case of liquid argon as a cryogenic liquid shield, we study the possibility to suppress backgrounds by simultaneously measuring the scintillation of liquid argon. Signal recording and pulse shape analysis make use of recent developments where signals are sampled and digitized at high rate after minimal analog signal processing. In this way maximal information and flexibility is provided for a later digital post-processing.

Phases of the experiment.   The experiment will proceed in several phases. Phase I encompasses the installation of the cryostat and shields, the installation and operation of conventional Ge detectors to determine the background rejection and to screen materials and identify backgrounds by classifying their spectra, and the operation of almost 20 kg of existing enriched ^{76}Ge detectors, used in the past in the Heidelberg-Moscow and IGEX experiments. Within one year of measurement, the sensitivity of this setup should allow a statistically unambiguous statement concerning neutrinoless double beta decay with a lifetime around $1.2 \cdot 10^{25}$ y, as measured by [Kla 04].

Phase II: In parallel with the construction of the first phase of the experiment, techniques will be studied and implemented to provide improved enriched detectors to be used in a second phase. Enriched germanium will be produced in Russia. Detector geometry and segmentation will be optimized on the basis of detailed calculations of fields and pulse shapes, taking into account background simulations. Particular emphasis is devoted to minimize cosmogenic activation of detectors by reducing the exposure. Regardless of the outcome of the Phase I measurements, it is desirable to produce and operate a certain number of new detectors: In case of a positive result to provide a precise lifetime measurement, in case of a negative outcome to push the limits further and to demonstrate the background rejection. In particular in the second case, one would – funding permitting –

add enriched detectors up to the point where backgrounds start to show up.

At the end of Phase II with > 100 kg·years, the sensitivity will be $T_{1/2} > 2 \cdot 10^{26}$ years at 90% confidence level (C.L.) corresponding to a range of the effective neutrino mass of <0.09 - 0.29 eV.

Phase III: The ultimate experiment capable of reaching the 10 meV scale requires $\mathcal{O}(0.5 \text{ t})$ of enriched germanium and represents another huge step, which can only be afforded in the context of a world-wide collaboration. Options for detector shielding and detector arrangements will have to be re-evaluated on the basis of results achieved by the proposed experiment and by studies following other approaches, such as the copper shield foreseen in the Majorana proposal [Maj 03]. It is likely that by that time the proposed facility will have reached its limits - in fiducial size, in background shielding, or in both – and will need to be upgraded or replaced by an improved facility. On the scale of the cost of 1 t of enriched germanium, costs for such a new facility are modest. At the current time, it is, however, clearly premature to speculate about the kind of modifications needed, or the space required by and the potential location of such a future experiment.

It is also undisputed that such an ultimate ^{76}Ge experiment would be carried out in the framework of a world-wide collaboration, merging the different current efforts. Close contacts with the Majorana collaboration have already been established with the goal to provide a large degree of transparency between the collaborations and to coordinate the R&D work, and to work ultimately towards a merger of the collaborations.

Time scale, cost, and requests to LNGS. We estimate that the cryostat and auxiliary system could be set up on a time scale of less than 2 years. We will make use of the available know-how concerning gas purification in BOREXINO, and ideally also of the BOREXINO water purification system. After installation of the ^{76}Ge detectors a measurement time of at least three years is required. The cost of the cryostat, the auxiliary systems and the modification of the existing detectors is estimated to be 3.9 M€.

Phase II – the production of new enriched detectors – will start concurrently with Phase I. About two years will be required until the first detectors are available. The cost of Phase II depends on the amount of additional detectors, and on the production mode. Detector costs are roughly 100 €/g, including the raw material, the enrichment and the crystal growing, plus a certain offset since the crystal growing requires a certain amount of additional material (which can be recovered for a second lot of detectors). Currently requested funding for Phase II will allow to procure about 20 kg of new detectors.

The facility for Phase I and II could be located in the free space in Hall A of LNGS. Electronics, experiment control and gas control could be housed partly on top of the cryostat, partly in (stacked) containers. Additional space is required for liquid gas tanks. Safety issues regarding the cryogenic fluid system and gas handling will be addressed in close collaboration with LNGS safety officers.

2 Introduction and experimental overview

2.1 Introduction

Double beta decays are transitions between nuclei of the same atomic mass number (A) that change the nuclear charge (Z) by two units under emission of light particles. Double beta decay is only observable in absence of the concurring process, the cascading decay via two single beta decays. This condition is only satisfied, if the mass of the intermediate nucleus is larger than that of the initial one, or if the single beta transition to the intermediate nucleus is highly hindered. Double beta transitions for both signs of nuclear charge change are possible: two neutrons transform into two protons, or vice versa, two protons into two neutrons. For simplicity, we consider here only the first.

The transformation can occur under emission of two neutrinos ($\beta\beta(2\nu)$),

$$(A, Z) \rightarrow (A, Z + 2) + e_1^- + e_2^- + \bar{\nu}_{e1} + \bar{\nu}_{e2}, \tag{1}$$

conserving lepton number. In contrast, the neutrinoless decay ($\beta\beta(0\nu)$)

$$(A, Z) \rightarrow (A, Z + 2) + e_1^- + e_2^- \tag{2}$$

violates lepton number by two units and is forbidden in the standard electroweak theory. Another decay mode involves the emission of a light neutral boson ($\beta\beta(0\nu, \chi)$), a majoron, as postulated in some extensions of the standard electroweak theory:

$$(A, Z) \rightarrow (A, Z + 2) + e_1^- + e_2^- + \chi \tag{3}$$

The different decay modes are distinguishable by the shape of the spectrum of the electron sum energy. For the $\beta\beta(2\nu)$ mode, the summed kinetic energy of the two electrons displays a continuous spectrum with a broad maximum below half the endpoint energy. In contrast, the $\beta\beta(0\nu)$ mode exhibits a mono-energetic line at the endpoint ($Q_{\beta\beta}$), as the electrons carry the full available energy. For a light majoron, the spectrum is also continuous with a broad peak located above half the endpoint energy.

Neutrinoless double beta decay can be mediated by various mechanism. Here we consider only the simplest case of the left-handed $V - A$ weak currents and the exchange of a light massive Majorana neutrino. The half life is then (e.g. [Ell 02])

$$[T_{1/2}^{0\nu}(0^+ \rightarrow 0^+)]^{-1} = G^{0\nu}(E_0, Z)|M_{GT}^{0\nu} - g_V^2/g_A^2 M_F^{0\nu}|^2 m_{ee}^2 \,, \tag{4}$$

where $G^{0\nu}$ is the phase-space integral, $M_{GT}^{0\nu}, M_F^{0\nu}$ are the nuclear matrix elements, and m_{ee} the effective electron neutrino mass. Under the assumption of three light massive Majorana neutrinos ν_i ($i = 1, 2, 3$), the weak eigenstate neutrinos ν_e, ν_μ and ν_τ can be written as a superposition of the mass eigenstates ν_i with the mixing matrix U_{li}. The electron neutrino ν_e is then given as $\nu_e = \sum_i^3 U_{ei}\nu_i$ and the effective neutrino mass is defined as

$$m_{ee}^2 = \left| \sum_i^3 U_{ei}^2 m_i \right|^2 = \left| \sum_i^3 |U_{ei}|^2 e^{\alpha_i} m_i \right|^2 . \tag{5}$$

Here, $\alpha_1 = 0$ by convention and $\alpha_{2,3}$ are CP violating Majorana phases which can cause cancellations in the sum.

From the measurements of the mass differences $\Delta m_{ij}^2 = |m_i^2 - m_j^2|$ and the mixing angles in neutrino oscillation experiments, the range for m_{ee} is substantially constrained. Figure 1 displays the range of m_{ee} as a function of the lightest neutrino mass m_1. One distinguishes
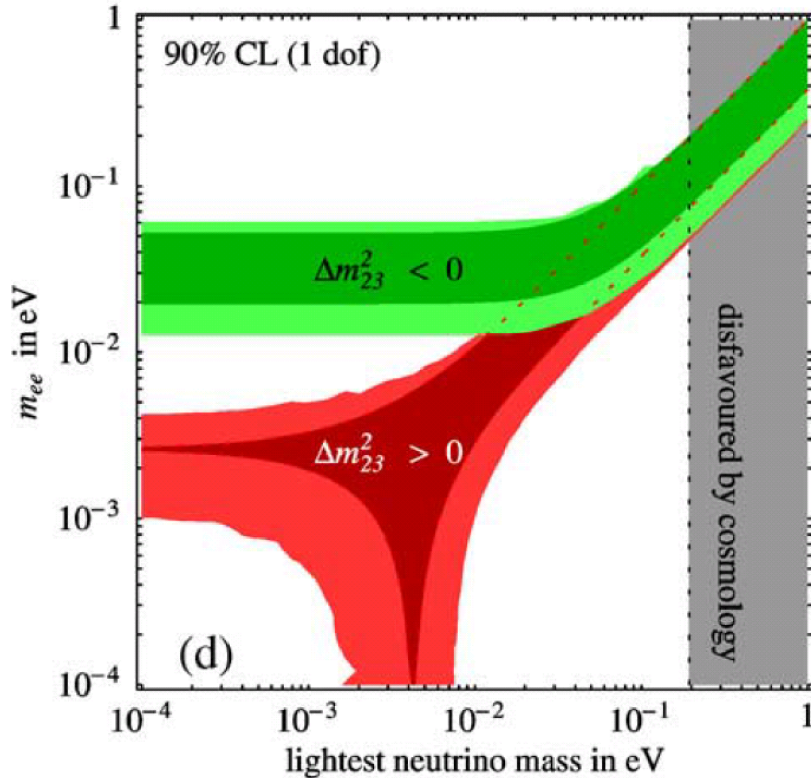
Figure 1: Predictions for the effective neutrino mass m_{ee} as a function of the lightest neutrino mass m_1 derived from oscillation experiments [Fer 03]. The different bands in parameter space correspond to the normal mass hierarchy ($\Delta m_{23} > 0$), to the inverted mass hierarchy ($\Delta m_{23} < 0$) and to the degenerate mass scheme (lightest mass $\gg \Delta m_{23}$). The dark colors use the measured oscillation data without errors to emphasize the contribution of the Majorana CP phases. The lighter colors include the current experimental errors of the mixing parameters.

the parameter range corresponding to normal, inverted and degenerated mass schemes. In the normal hierarchy, the mass splitting driving solar neutrino oscillations occurs between the lightest neutrinos with masses m_1 and m_2, and that driving atmospheric oscillations between m_2 and m_3. In the inverted hierarchy the splitting is arranged in the reverse order. If the values of Δm_{ij}^2 are small compared to the actual values of m_i, the mass spectrum is called degenerate. Large parts of the parameter space for m_{ee}^2 predicted by

neutrino oscillation experiments will be experimentally accessible with the next generation of experiments.

2.2   Past and present experiments

Major experimental progress has been achieved during the last ten years. For a comprehensive review the reader is referred to [Ell 02]. Direct measurements of double beta decay accompanied by the emission of two neutrinos ($\beta\beta(2\nu)$) have been carried out for more than ten nuclei. Recent results for $\beta\beta(2\nu)$ include ^{76}Ge, ^{100}Mo, ^{150}Nd, ^{116}Cd and ^{96}Zr. The measured half-lives are in the range of $10^{19} - 10^{21}$ years.

Today the central focus in double beta decay research is the neutrinoless mode ($\beta\beta(0\nu)$). Most stringent limits have been derived from experiments using enriched ^{76}Ge detectors. The leading two experiments - IGEX and Heidelberg-Moscow (HdM) - have been running for several years with a background around $Q_{\beta\beta}$ close to 0.2 cts/(keV·kg·y) before pulse shape discrimination and about 0.06 cts/(keV·kg·y) after. Limits for the life time close to $2 \cdot 10^{25}$ y have been derived corresponding to a limit for an effective neutrino mass m_{ee} of 0.3 - 1.0 eV [Aal 99, Kla 01]. Both experiments have stopped data taking recently.

In 2001, the group of Klapdor-Kleingrothaus claimed evidence for neutrinoless double beta decay at a 2 σ confidence level [Kla 01] based on 52 (kg·y) of data from the HdM experiment. Based on a data set of 72 (kg·y) the claim has been strengthened recently [Kla 04]. The derived access counts are 28.8 ± 6.9 events above a background of approximately 60 events.

Operational experiments are currently NEMO3 and CUORICINO. The NEMO experiment is carried out at the Modane Underground Laboratory, France. During five years of R&D phase using the NEMO2 detector, the collaboration has performed measurements of the $\beta\beta(2\nu)$ decay of ^{100}Mo, ^{82}Se, ^{116}Cd and ^{96}Zr. The final detector, NEMO3 [Arno04], consists of a large tracking calorimeter surrounding 10 kg of thin source foils of different enriched materials, mainly 7 kg of ^{100}Mo. The aim is to reach after five years of data taking a limit for the half-life of $5 \cdot 10^{24}$ years, corresponding to an effective mass of 0.2-0.3 eV. NEMO3 started data taking in 2003.

The CUORICINO experiment at LNGS searches for neutrinoless double beta decay with TeO$_2$ bolometers [Arn 03]. The setup consists of an array of 62 crystals with a total mass of about 40 kg. The counting rate in the region of neutrinoless double beta decay is ~0.2 cts/(keV·kg·y). No evidence for neutrinoless double beta decay is found with the present exposure of about three months during 2003. The corresponding limit for the lifetime is $5.5 \cdot 10^{23}$ y (90% C.L.) and for the effective neutrino mass between 0.37 and 1.9 eV [Arn 04]. The expected sensitivity after three years of data taking will be $4 \cdot 10^{24}$ y or 0.2-0.5 eV [Giu 03].

2.3   Proposed and suggested future experiments

The next generation of double beta decay experiments aims for probing Majorana masses down to 0.1 eV and below. Many different isotopes and detector concepts have been

suggested. Recent reviews of the field can be found in [Ell 02, Giu 03]. Here, we briefly discuss the more advanced projects as listed in Tab. 1 including this proposed new ^{76}Ge experiment at Lngs.

Table 1: Characteristics of operating and proposed future $\beta\beta(0\nu)$ experiments. The corresponding references are: Nemo3 [Aug 03], Cuoricino [Giu 03], Nemo-Next [Aug 03], Cuore [Arn 03], Majorana [Maj 03], Exo [Dan 00]. The three phases of our proposed ^{76}Ge experiment are discussed in the following sections.

Experiment	Source	Description	FWHM at $Q_{\beta\beta}$ (keV)	Sensitivity $T^{0\nu}_{1/2}$ (y)	m_{ee} (eV)	Year
Nemo3	^{100}Mo	7 kg ^{enr}Mo tracking	90	$5 \cdot 10^{24}$	0.2-0.3	2008
Cuoricino	^{130}Te	40 kg TeO$_2$ bolom.	7	$4 \cdot 10^{24}$	0.2-0.5	2007
Nemo-Next	^{100}Mo	0.1 t ^{enr}Mo track.	50	$1 \cdot 10^{26}$	0.04-0.07	
Cuore	^{130}Te	0.76 t TeO$_2$ bolom.	5	$3 \cdot 10^{26}$	0.03-0.05	
Majorana	^{76}Ge	0.5 t ^{enr}Ge diodes	4	$4 \cdot 10^{27}$	0.02-0.07	
Exo	^{136}Xe	1 t ^{enr}Xe	120	$8 \cdot 10^{26}$	0.05-0.14	
Gerda	^{76}Ge	^{enr}Ge in LN/LAr	4			
Phase I		15 kg (15 kg y)		$3 \cdot 10^{25}$	0.3-0.9	2007
Phase II		35 kg (100 kg y)		$2 \cdot 10^{26}$	0.09-0.29	2010
Phase III		$\mathcal{O}(500$ kg$)$ - world-wide collaboration				

Nemo-Next would be based on the Nemo3 tracking concept, however with an increased mass of approximately 100 kg of foils enriched in ^{100}Mo or ^{82}Se and improved energy resolution. A sensitivity of $> 10^{26}$ y or of $0.04 - 0.07$ eV for m_{ee} is projected.

The Cryogenic Underground Observatory for Rare Events (Cuore) has been proposed to be operated at the Gran Sasso laboratory. It is planned to use 1000 crystals of TeO$_2$ with a total mass of 760 kg as cryogenic bolometers [Arn 03]. The detector is arranged into 25 separate towers of 40 crystals. A prototype tower is operated in Cuoricino. Assuming an energy resolution of 5 keV and a background of 0.01(0.001) cts/(keV·kg·y), the expected sensitivity of Cuore is $0.9(3.0) \cdot 10^{26}\sqrt{t}$ years. One year of measurements would provide bounds for m_{ee} in the $0.04 - 0.15$ eV range [Arn 03].

The Majorana experiment plans to employ 500 kg of Ge, isotopically enriched to 86% in ^{76}Ge, in the form of about 200 detectors in a densely packed array. Each crystal will be segmented, and the signals from each segment will be subjected to pulse shape analysis. A half-life sensitivity is predicted of $4 \cdot 10^{27}$ y or 0.02 - 0.07 eV for m_{ee} after approximately ten years of operation.

The Enriched Xenon Observatory (Exo) proposes to use 1-10 tons of xenon enriched to 60-80 % in ^{136}Xe. In contrast to other proposals, it is planned to discriminate backgrounds by identification of the daughter isotope ^{136}Ba with laser spectroscopic methods. If realized successfully, all backgrounds but the $\beta\beta(2\nu)$ mode could be suppressed. Two different

detector concepts are under study: high-pressure gas TPC or liquid xenon scintillator. Sensitivities of $8 \cdot 10^{26}$ y, or $0.05 - 0.14$ eV for m_{ee}, are projected.

Other interesting projects have been proposed including MOON [Eji 00] (34 t of natural molybdenum in a sandwich Mo/scintillator configuration), CAMEO [Bel 01] (1 t of scintillating ^{116}CdWO$_4$ crystals situated within the BOREXINO detector), and COBRA [Zub 01] (CdTe of CdZnTe semiconductors).

In the GERDA project for LNGS, presented in this Proposal, we intend to operate bare germanium diodes enriched to 86% in ^{76}Ge in a high-purity cryogenic medium for shielding against external radiation. The concept, detailed in the following sections, is based on the observation that the background signals are largely dominated by external radiation. By removing most of the cladding and contact materials, and immersing the crystals in an ultra-pure environment, one can operate the diodes largely free of background. Provided that the background can be reduced to 10^{-3} cts/(keV·kg·y), it will be possible to operate crystals free of backgrounds up to exposures of 100 (kg·y). The experimental strategy is based on three phases, in each incrementing the target mass. In Phase I it is planned to operate the existing enriched germanium detectors which have been used in the IGEX and Heidelberg-Moscow experiment. Conservatively, it is assumed that 15 out of almost 20 kg will be operational. About 20 kg of additional ^{76}Ge crystals are conceived for Phase II. The third phase has to be defined during Phase II and depends on the physics result and the experimental performance. Already after completion of Phase I, it will be possible to test the recent claim of evidence for neutrinoless double beta decay.

2.4   Dark Matter experiments

As an experiment searching for very rare events a detector set up to search for neutrinoless double beta decay could as well be used for the direct search for dark matter particles.

There is strong observational evidence that most of the mass density in the universe consists of dark non-baryonic matter. Unobserved weakly interacting massive particles (WIMPs) could be an explanation. Supersymmetric extensions of the standard model predict such particles. LEP II measurements contain their masses to be larger than ≈ 40 GeV. In this context WIMPs are well motivated candidates as a solution of the dark matter problem. The direct detection of such particles could be possible by elastic scattering on nuclei. The expected count rates are extremely low. The presently best limits correspond to a few events per kg of target mass per keV of recoil energy and per year (cts/(keV·kg·y)). As for the search for double beta decay, a sensitive dark matter search requires high purity detectors with minimized radioactive contaminations and a highly efficient shielding against radiation from the surrounding.

Presently the best results for direct dark matter searches come from cryogenic detectors. By the simultaneous measurement of a calorimetric signal together with a signal from ionization or scintillation, these detectors are capable to distinguish nuclear recoils from electron recoils. For nuclear recoils the ionization or light yield is smaller than the observed calorimetric energy. Since most of the background is due to γ's or β decays, the sensitivity to low count rates of recoil signals can be increased by orders of magnitude [Ake 04, Ben 02,

Ang 04]. With GERDA electron and nuclear recoils cannot be discriminated. Consequently the sensitivity to dark matter entirely depends on the efficiency of the shielding and on an extreme reduction of impurities.

Section 3.7 discusses the current experimental limits and possible contributions of our experiment to the WIMP search. Due to limited man power little emphasis has been given by our collaboration to this topic until now.

3 Performance

The performance of GERDA depends on the background level and the sensitive mass of the germanium detectors. The improvements of this proposal relative to past experiments are the superior shielding against external radiations, the reduction of impure materials close to the germanium detectors, and the lower intrinsic contamination and segmentation of newly produced diodes. The level achievable and the resulting sensitivity will be discussed in this section.

First, general design considerations and the understanding of the background contributions of the Heidelberg-Moscow experiment are discussed. Afterwards different sources of backgrounds and discrimination techniques are analyzed. In the following section, the physics sensitivity for $T_{1/2}$ of the neutrinoless double beta decay for the two phases of the experiment are calculated.

3.1 General design considerations

A reduction of the background by two to three orders of magnitude relative to existing experiments to a level of 10^{-3} cts/(keV·kg·y) is the goal of this proposal.

While such a tremendous background reduction is difficult to predict reliably, the contributions of many well identified background sources can be extrapolated with Monte Carlo techniques. For the suppression of external radiation, shielding of the germanium diodes with ultra-pure materials, such as liquid nitrogen (LN) or liquid argon (LAr), is one of the key prerequisites [Heu 95]. Following this idea the GENIUS [Kla 99] and GEM [Zde 01] experiments were proposed. A more conventional approach with shielding by copper and lead is pursued by the MAJORANA collaboration [Maj 03].

An artist's view of our baseline solution of the experimental design is shown in Fig. 2 and is discussed in section 6. Similar to the GEM design the diodes are operated in liquid nitrogen or argon. The superinsulated copper cryostat is contained within a water vessel.

Water can be purified to a level comparable to liquid nitrogen and is therefore a cheap replacement of the cryogenic liquid. In addition, it serves as neutron moderator and Cherenkov medium for a muon veto system.

While this design reduces background from external sources to the required level, contaminations intrinsic to the germanium detectors remain. The latter can only be reduced in an optimized production procedure or its influence can be minimized with vetoing techniques which are described below.

3.2 Background sources of the Heidelberg-Moscow experiment

A good understanding of the available data is useful to estimate the background level of GERDA, especially since the existing enriched germanium diodes are used in the first phase. Most important are contaminations in the diodes themselves like ^{60}Co or ^{68}Ge.

For the energy range of 2000 to 2100 keV the primordial decay chains of U and Th external to the diodes are identified as the main contamination sources, with 38% and
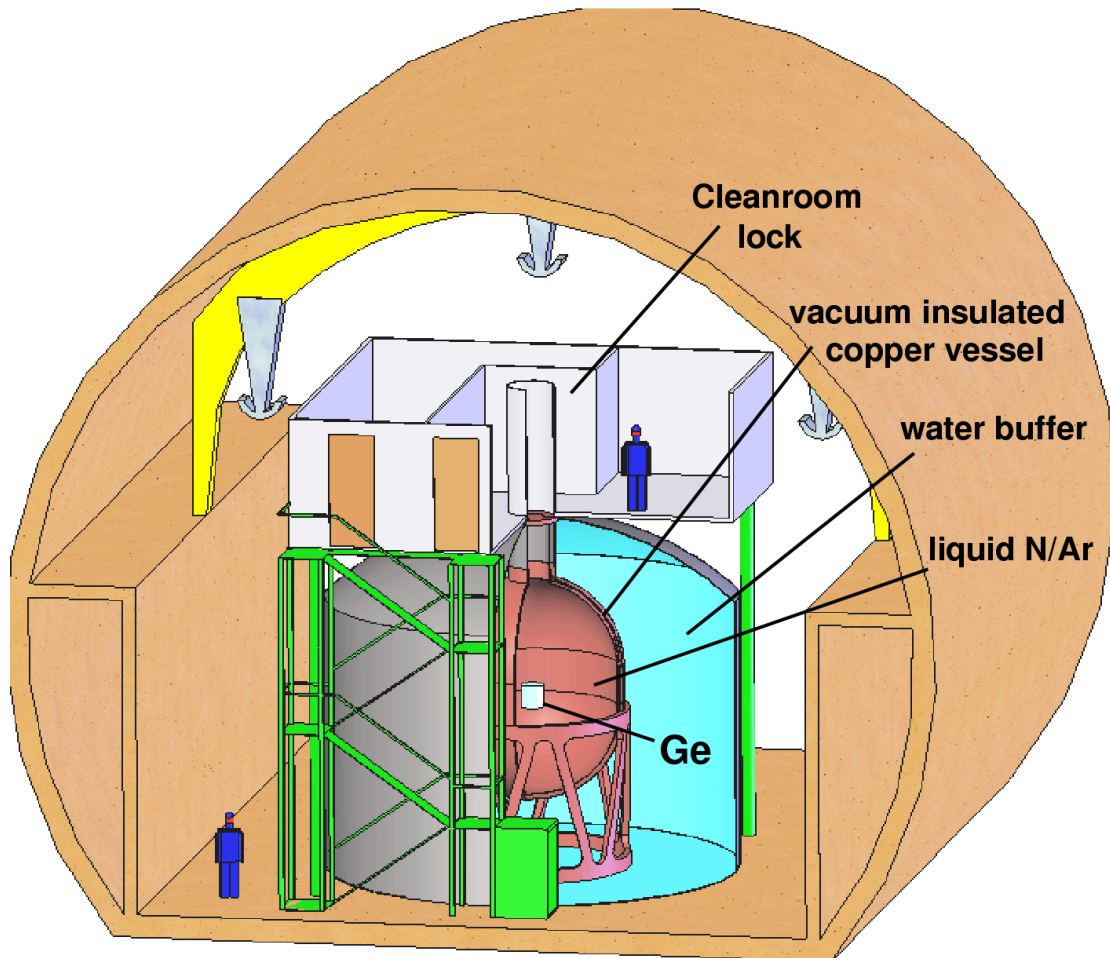
Figure 2: An artist's view of the baseline design of GERDA placed in LNGS Hall A. In reality the detector will be placed asymmetrically to allow access to the LVD experiment.

41%, respectively [Kla 03, Dör 03]. Smaller background contributions originate from the cosmogenic radio-nuclide ^{60}Co in the copper holder (16%), anthropogenic contaminations and neutron/muon induced events (5%). Reference [Dör 03] finds no indication for intrinsic contaminations of the diodes. The sum of the simulated backgrounds is 660 ± 93 events while the data has 803 entries. It is worth mentioning that the simulation has large uncertainties and does not explain the data entirely.

The intrinsic diode background may be estimated in a different way. A detailed history of the detector storage locations and times is available and has been used to calculated the activation of the germanium detectors during the diode production process [Mai 96]. According to these calculations a total activity of about 36 μBq of ^{60}Co can be estimated at the beginning of the main measurement period of the Heidelberg-Moscow experiment in November 1995. Using an uptime of the experiment of about 80% and a Monte Carlo estimate for the fraction of decays depositing an energy close to the Q value of the double beta decay $Q_{\beta\beta}$, one finds a background contribution of ^{60}Co of about 9% at $Q_{\beta\beta}$.

This number is in contradiction to the result of [Dör 03], but is supported by an ongoing independent analysis of the Moscow group of the Heidelberg-Moscow collaboration.

By the beginning of 2006, the above mentioned total ^{60}Co activity will decay to about 10 μBq. This corresponds to a background index of $5 \cdot 10^{-3}$ cts/(keV·kg·y). Other contaminations like ^{68}Ge have a much shorter lifetime and will not contribute. For the sensitivity estimate of phase I of our proposal, we assume a factor of two uncertainty for the ^{60}Co contamination and hence a background index of 10^{-2} cts/(keV·kg·y).

3.3   Background simulations

The sources of background can be classified by the location of the radioactive isotope: within the germanium diode, on the surface of the detector, or external in the material for the diode contacts, the shielding, and in the concrete/rock of the laboratory.

This section focuses on the simulation of the backgrounds considered to be most serious. The discussion of the internal background applies to newly built detectors (Phase II of the GERDA) while the external backgrounds affect the design of the vessel.

For most simulations GEANT4 (version 5.2) [GEA 03] was used. Only a simplified setup consisting of a vessel filled with liquid nitrogen or argon and an ensemble of 27 germanium detectors was simulated, see Fig. 3. Each detector has a height of 78 mm and a diameter of 78 mm which corresponds to a weight of 2 kg. The detectors will be "p-type" and hence a dead layer of 0.7 mm at the outside was included in the simulation. In the middle, a cylindrical hole of 10 mm diameter and a length of 58 mm is included for the p contact. The crystals are arranged in a $3 \times 3 \times 3$ array with a spacing of 12 mm.
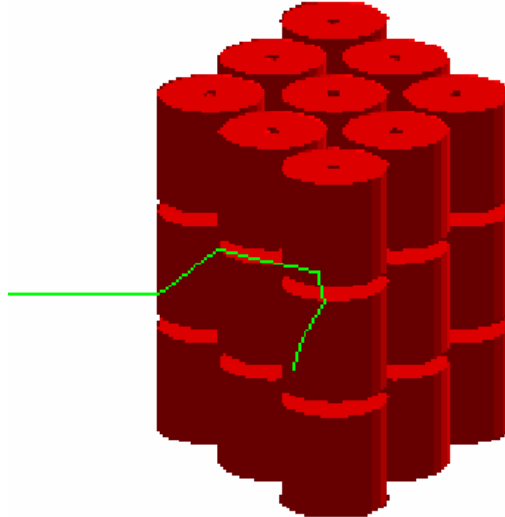

Figure 3: Drawing of the setup of 27 germanium diodes used in the GEANT4 simulation. This display shows the interaction of a 2.6 MeV photon in the array.

In addition, a CPU time optimized Monte Carlo for extensive simulations of gamma

interactions is used. This program simulates Compton scattering, pair production and photo electric effect and performs about a factor of 30 faster than GEANT4. However, only geometries with a single diode have been implemented. Simulations were carried out for internal as well as for external background.

3.3.1 The internal background from cosmogenic isotopes

During storage above ground the germanium is exposed to hadronic radiation, especially neutrons. These cause spallation in the germanium and hence a variety of radioactive isotopes are produced. These processes can be simulated and past experience shows that the results of simulations agree with measurements within a factor of two [Avi 92, Mai 96].

Most important for the neutrinoless double beta decay are the decays of ^{68}Ge and ^{60}Co since Q values above $Q_{\beta\beta} = 2039$ MeV occur in the decay chain, and the lifetimes are in the range of years. Relevant for ^{60}Co spallation production is the time between the zone refinement and the storage underground. For one detector a production time of less than 10 days was achieved (see section 7.4). Here, we assume an average time of 30 days.

Relevant for ^{68}Ge spallation production is the time between the isotope separation and the storage underground. Here we will assume 180 days. It seems feasible to store the enriched material between processing steps underground and this option will be pursued in contacts with the enrichment company ECP. A substantial reduction of the activation time is therefore expected. To compensate uncertainties in the spallation cross sections we take the above mentioned conservative activation times in our background estimates. The time between the storage underground and the start of the measurement is taken as an additional 180 days.

Cosmogenic ^{60}Co background in the germanium diode

The cosmogenic production of ^{60}Co in a germanium detector is about 4 atoms/(kg d) above ground [Avi 92]. Therefore an exposure of one day corresponds to an activity of $4\ln(2)/T_{1/2} = 0.017\,\mu$Bq/kg. This number agrees within a factor of 1.6 with the value of reference [Bau 99a].[1]

A 30 day exposure time results in an activity of $0.5\,\mu$Bq/kg which corresponds to 15 decays/(kg y). Fig. 4 shows the simulated energy deposited inside the diode. In one out of 6000 decays the deposited energy is at $Q_{\beta\beta}$ within a 1 keV window. The resulting background index is therefore $2.5 \cdot 10^{-3}$ cts/(keV·kg·y).

Cosmogenic ^{68}Ge background in the germanium diode

According to calculations in reference [Avi 92], the production rate of ^{68}Ge in ^{76}Ge is about 1 atom/(kg d). Within an exposure time of 180 days and $T_{1/2} \simeq 270$ days about 40% of the saturation activity is reached.

The saturation activity is 1 decay/(kg d) at the time the detector is brought underground which corresponds to 400 ^{68}Ge atoms/kg. After 180 days of storage and for 40%

---

[1]The value given in reference [Bau 99a] of 0.18 μBq/kg after a 10 day exposure and 3 years of storage underground corresponds to 0.027 μBq/kg for a one day exposure without underground decay time.
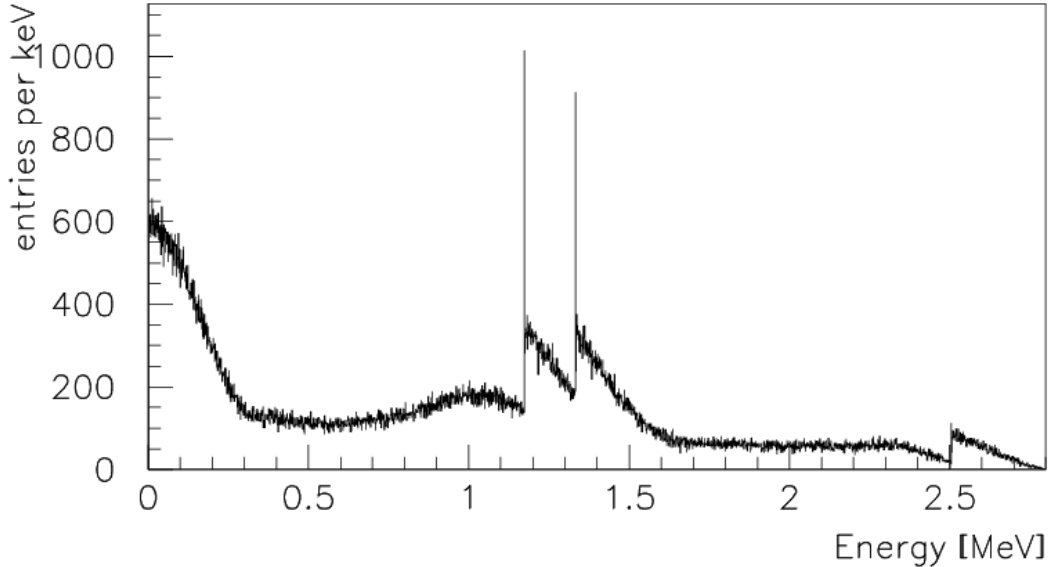
Figure 4: Energy deposition in a germanium detector from ^{60}Co decays located inside the crystal. The decay chain starts with a β^- emission of an endpoint energy of 300 keV followed by two prompt γ quanta of 1.173 and 1.332 MeV.

saturation activity 96 ^{68}Ge atoms/kg remain. 60% of these will decay in the first year. Fig. 5 shows the spectrum of deposited energy. In about one out of 5000 decays the energy is within 1 keV of $Q_{\beta\beta}$. This yields a background of $12 \cdot 10^{-3}$ cts/(keV·kg·y)

3.3.2 External backgrounds

The external background consists of photons from primordial decay chains, neutrons and muon induced background. So far, most of our emphasis is focused on the suppression of the 2.615 MeV photons from ^{208}Tl decays. This background influences the design of the vessel considerably.

^{208}Tl background

The activity in the concrete and the rock in LNGS Hall A from ^{208}Tl results in a flux of $(0.031 \pm 0.09)\, \gamma/(\text{sec·cm}^2)$. This flux has recently been determined by our collaboration [Chk 04]. Fig. 6 shows the directional distribution of the flux in hall A. Within a factor of 2-3 it is isotropic. The integral flux is a factor of two larger than previous published numbers for hall C [Arp 92]. To be conservative we dimension the shielding for a flux of 0.0625 $\gamma/(\text{sec·cm}^2)$. The GEANT4 simulation of such a flux for the complete vessel is too CPU intensive. There are three alternatives to estimate the background. With GEANT4 one can simulate smaller vessels of different size and then extrapolate to the background
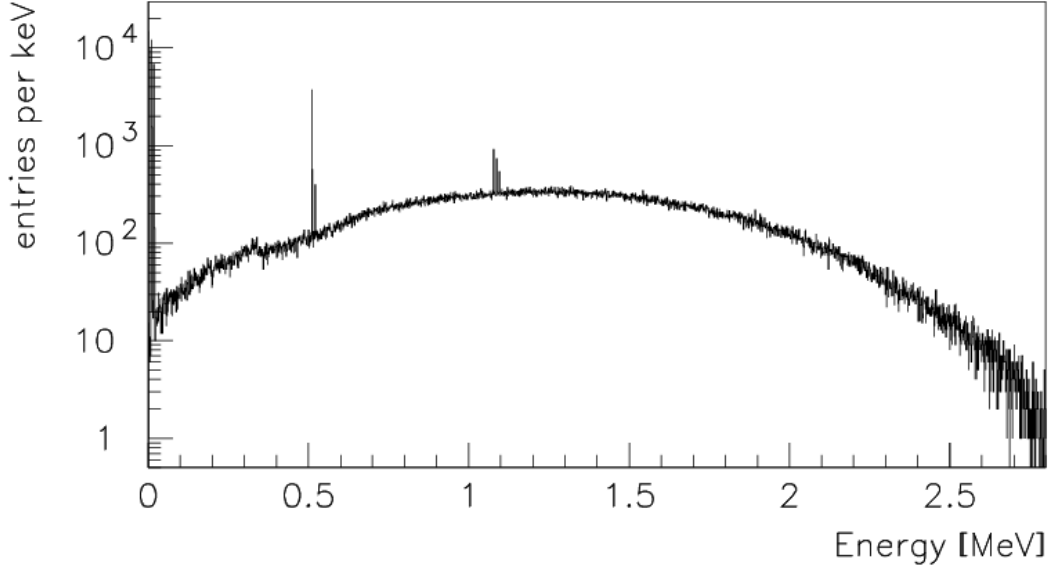
Figure 5: Energy deposition in a germanium detector from ^{68}Ga decays inside the crystal.

for the full size. Alternatively, the fast simulation program mentioned above was used.

The third method is based on an approximate calculation. Inputs are the peak to Compton ratio C and the detection efficiency ϵ of a ^{208}Tl source. The peak to Compton ratio C is defined as the number of events in the 2.615 MeV peak to the number of events in the energy interval of 2.00 - 2.08 MeV. Here the detection efficiency ϵ is defined as the fraction of ^{208}Tl photons that deposit the entire energy in the detector. Then, the absorption coefficient μ of the ^{208}Tl photon is used to analytically calculate the background index B for a given shielding thickness d and flux of photons (surface activity) A.

If ϵ is measured or calculated for a detector of mass m using a source at a distance r then B is given by

$$B = \frac{\epsilon}{C} \frac{\pi r^2}{m \; 80 \, keV} A \cdot e^{-t \cdot \mu} \tag{6}$$

with $80 \, keV$ being the width of the "Compton" interval.

With a GEANT simulation one finds for $r = 1 \, m$ and $m = 2 \, kg$ for the efficiency $\epsilon = 5.8 \cdot 10^{-5}$. C depends on the shielding. For no shielding the simulation gives $C \sim 6$ while for thicknesses $t \cdot \mu > 5$ one finds

$$C \simeq \frac{10}{t \cdot \mu} \tag{7}$$

For a photon flux of 0.0625 $\gamma/(\text{sec·cm}^2)$ the background index B can therefore be approximated by

$$B = 2250 \cdot t \cdot \mu \cdot e^{-t \cdot \mu} \frac{cts}{keV \; kg \; y} \tag{8}$$
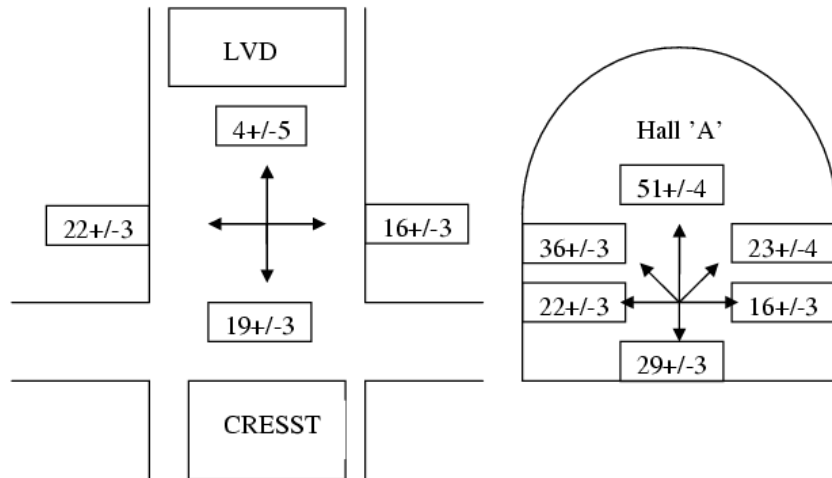
Figure 6: Flux of ^{208}Tl decay photons in LNGS hall A in units of $1/(\text{sec} \cdot \text{m}^2 \cdot \text{steradian})$.

All methods predict within a factor of two the same background suppression.

Different design options for GERDA are discussed in section 6. The resulting background indices are calculated with above formula.

Neutron induced background

The main sources of neutrons in the LNGS are from spontaneous fission (dominated by the ^{238}U isotope) and from (α,n) reactions in the concrete and the rock. The maximum neutron energy from these processes is about 9 MeV. Neutrons above this energy originate from muon interactions which have a much smaller flux. No detailed measurements of the neutron energy spectrum exist. Instead the spectral shape is taken from a simulation of the above processes [Wul 03]. The predicted integral flux of $4 \cdot 10^{-6}$ neutrons/(cm$^2 \cdot$sec) is in agreement with measurements.[2] The energy spectrum is shown in Fig. 7. The peak in the spectrum at 6.75 MeV is due to (α,n) reactions on magnesium and carbon. Neutrons above 7 MeV are from fission.

A spherical vessel of 7 m diameter plus a variable thickness of polyethylene as a moderator is simulated. The results shown here will not depend on the exact shape of the vessel. Hermetic moderator shielding is assumed in the simulation.

The simulation in GEANT4 is based on cross section tables for all the relevant isotopes. Tables are available for elastic scattering, capture (n,γ) and inelastic reactions like (n,nγ), (n,p), (n,pγ) etc. In Table 2 the neutron flux and the mean neutron energy after the polyethylene moderator is given. With increasing thickness more and more slow neutrons are captured, and consequently the spectrum becomes harder. Since nitrogen acts as an additional moderator, neutrons are a more critical background for the argon filling, and we primarily address this case. In liquid argon neutrons loose only a few percent of their energy per elastic scattering and the mean free path is 15-20 cm above a kinetic energy

---

[2]For a more detailed discussion see [Wul 03] and references therein.
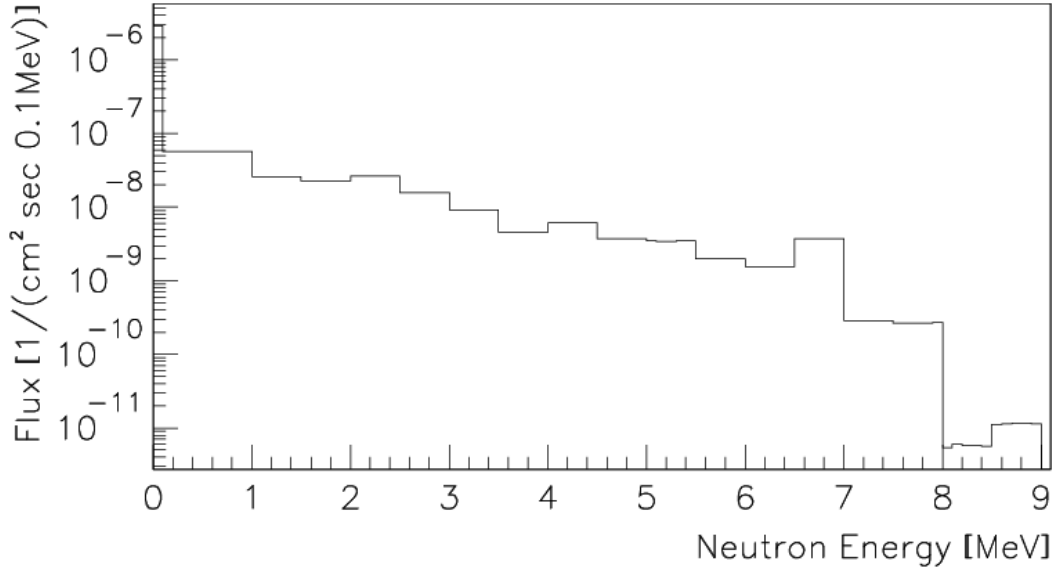
Figure 7: Prediction of the energy spectrum of neutrons in Lngs Hall A from fission and
(α,n) reactions [Wul 03].

of 0.5 MeV. Consequently, the total path length of neutrons is many meters and they are typically stopped in the moderator.

Table 2: Relative neutron flux Φ and average neutron energy E after a polyethylene moderator for different moderator thicknesses.

thickness	0 cm	10 cm	20 cm	30 cm	40 cm	50 cm
Φ	1	0.22	0.031	$6 \cdot 10^{-3}$	$1.3 \cdot 10^{-3}$	$3.8 \cdot 10^{-4}$
E [MeV]	0.52	0.61	0.81	0.97	1.09	1.16

A moderator thickness of 40 cm was simulated in detail. In Fig. 8 a) the neutron energy spectrum is shown for those neutrons that pass the moderator and 3 m of liquid argon. Part b) shows the initial energy of the same neutrons. All slower neutrons are captured and only the neutrons with large initial energy reach the germanium diodes. Here elastic scattering dominates again and almost no neutron is captured in the germanium. The Monte Carlo sample size corresponds to twice the integrated flux for one year. No event was observed in the energy region of $Q_{\beta\beta}$.

For nitrogen the neutron background is even less of a problem, since the energy loss

22
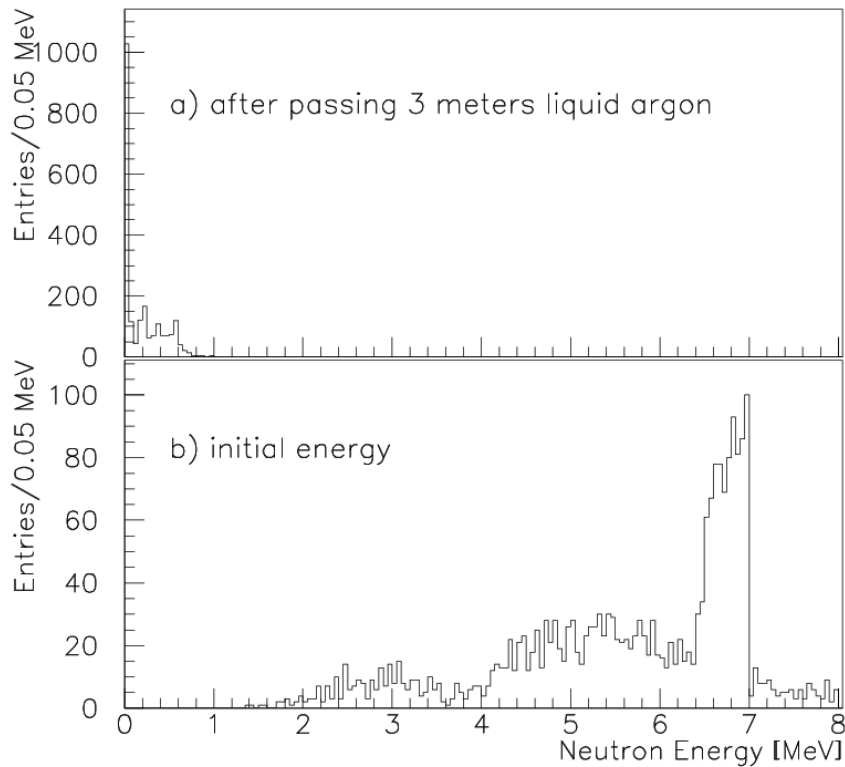
Figure 8: a) Neutron energy after 40 cm of polyethylene moderator and 3 m of liquid argon. b) Initial energy of these neutrons.

per scattering is almost a factor of 3 larger and the cross sections are typically a factor of 10 larger. Water will provide a similar shielding as polyethylene.

Presently all options include a thick layer of water (>100 cm) as shield. This will ensure a negligible neutron background.

Muon induced backgrounds

The Gran Sasso overburden of 3500 m.w.e. suppresses the cosmic muon flux to $1.1/(\text{h·m}^2)$ and shifts the mean energy to 320 GeV. Muons penetrating our detector will loose energy not only by electromagnetic interactions (ionization, bremsstrahlung and pair production) but also in inelastic reactions with nuclei. In the latter processes radioactive isotopes and high energy neutrons may be produced. The neutrons will cause inelastic interactions themselves and produce more isotopes and neutrons.

It is foreseen to instrument the water buffer with photo multipliers for the detection of Cherenkov light which is produced when muons pass through the detector. In addition scintillators will be installed on top of the experiment for hermetic coverage (see section 6.5). These signals in coincidence with an energy deposition in the germanium can be used as a veto. To estimate the background from muons a 90% detection efficiency for the veto is

23
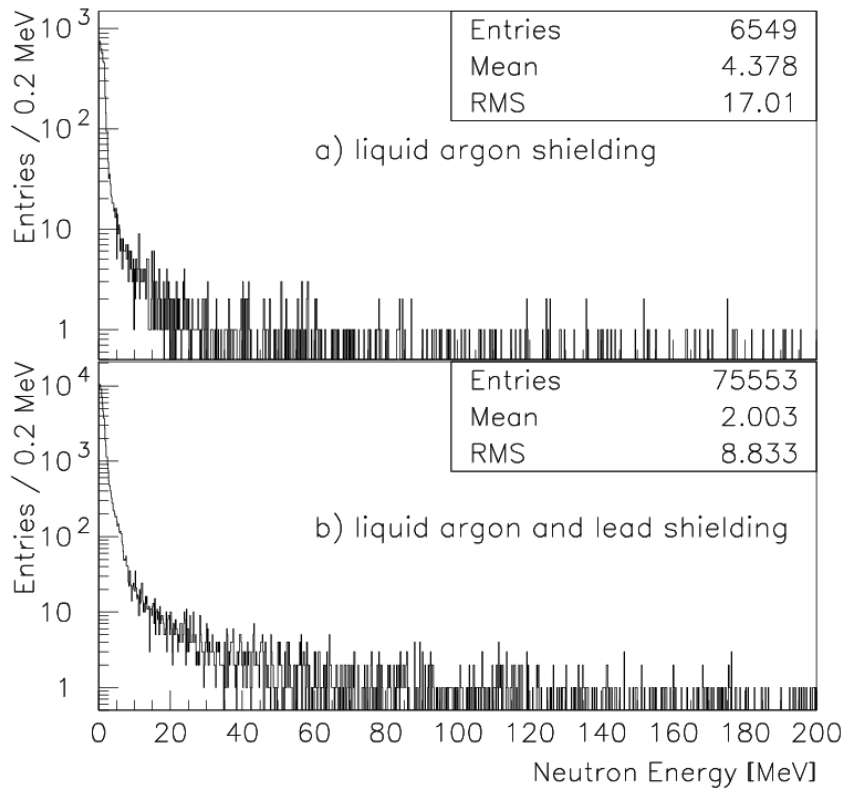
Figure 9: Neutron spectrum due to interactions of 270 GeV muons in the germanium and liquid argon (part a). Part b) contains the spectrum for the case of an additional layer of lead at the outside. The statistics corresponds to a flux of 3 months. "Mean" is the average neutron energy and "RMS" is the root-mean-square of the distribution.

assumed at this point. Delayed energy deposition from the decay of radioactive isotopes can not be identified this way. Therefore the level of isotope production has to be studied.

In a first step muon interactions have been simulated with GEANT4 (version 6.2) using a simplified geometry: a spherical vessel of 4 m diameter with an optional layer of 20 cm of lead on the outside and a large amount of germanium at the center. So far the muon energy was fixed at 270 GeV.[3] The "quark-gluon-string-plasma" (QGSP) physics list was used which includes inelastic muon and neutron interactions. Hence the production of radioactive isotopes was enabled. Simulations were performed for argon and nitrogen fillings, with and without the lead layer.

Fig. 9 shows the neutron spectrum generated in inelastic interactions for liquid argon filling. In the upper plot no lead was included. If the lead is included (lower plot) the

---

[3]At the energy of 270 GeV the neutron production rates agree with the simulation result for the full spectrum for the FLUKA package[Wul 03].

total number of neutrons produced increases by more than a factor of 10. About $260 \cdot 10^{-5}$ n/(g/cm^2) are generated per muon at this energy. This agrees within a factor of two with results from a FLUKA simulation [Wul 03] for the number of neutrons N_n

$$N_n = 2.06 \cdot 10^{-5} \, A \, \big[\frac{cm^2}{g} \big] \quad \text{per muon} \tag{9}$$

Here A is the atomic mass of the nucleus. The energy deposition in a muon event is
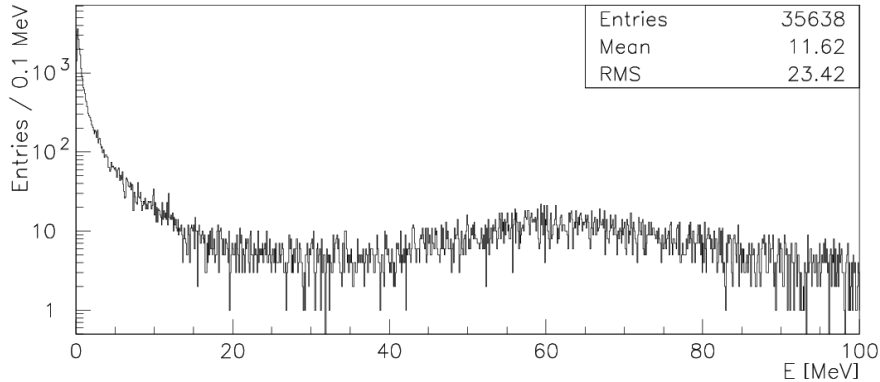
Figure 10: Energy deposition in a 2 kg detector in muon background events.

typically large. Fig. 10 shows the distribution of the deposited energy in 2 kg detector. The resulting background index is $\sim$ 0.01 cts/(keV·kg·y). For a muon veto with 90% efficiency this number reduces to 0.001 cts/(keV·kg·y). According to the simulation of a large array of dioded more than 90% of the events have an energy deposition in a second crystal resulting in a background index of $1 \cdot 10^{-4}$ cts/(keV·kg·y). All four cases yield very similar results indicating that the electromagnetic energy losses are similar for all cases.

For the radioactive isotope production this is not true since the number of produced neutrons is much larger if the lead is included. The total number of atoms produced inside the germanium and with a Q value of the decay above $Q_{\beta\beta}$ is about 0.5 atoms/(kg·y) for the argon filling with lead shielding. For the nitrogen case with lead it is reduced by 50% and for the shielding without lead it is reduced by 70%. In the latter case the isotope production is dominated by photonuclear reactions.

The production of 0.5 atoms/(kg·y) is much smaller than the decay rate from ^{60}Co of 15/(kg·y) or from ^{68}Ge of 60/(kg·y). A simulation of the decays for the relevant isotopes yields a background index of about 10^{-4} cts/(keV·kg·y) which can be reduced by vetoing techniques described below.

The muon and neutron flux will also generate radioactive isotopes in liquid argon and, at a much reduced level, in liquid nitrogen. A simulation of these decays yields a negligible contribution to the background.

Muons passing through the rock will also produce high energy neutrons. Their flux for energies above 14.5 MeV is 175/(y·m^2) [Dem 97] which is about half of the corresponding flux produced by muon interactions in the lead and argon. Since the original muon is

not passing through our detector, the neutron interactions can not be vetoed. These events have not been simulated so far. Due to the reduced flux and the thick water buffer surrounding the cryostat we do not expect a large contribution to the background from this source.

The simulation performed so far contained many simplifications concerning the geometry and the muon energy spectrum. More realistic versions are in progress. Also a cross check of the isotope production rates is needed.

Background from contaminations of the liquid nitrogen / argon

^{222}Rn and impurities of ^{232}Th and ^{238}U in the cryogenic liquid are possible sources of background for the double beta decay signal.

The BOREXINO collaboration has measured upper limits for the contamination of their liquid scintillator of less than $3.5 \cdot 10^{-16}$ g/g for ^{238}U and less than $4.4 \cdot 10^{-16}$ g/g for ^{232}Th [Ali 98]. Similar limits are expected for LN/LAr since they are also produced by fractional distillation. These limits correspond to 32 ^{238}U decays and 11 ^{232}Th decays per m^3 and year for liquid nitrogen. Backgrounds at $Q_{\beta\beta}$ from these activities are negligible.

Due to heat losses some of the liquid will evaporate and will be lost. An upper limit of 200 μBq/m^3 for the ^{222}Rn contamination is assumed for the liquid supply [MPI 03]. This corresponds to 95 atoms/m^3. For a boil off of 1% per day and a volume of 60 m^3 about 200 m^3 of liquid has to be supplied per year. Thus 19000 decays, about 320 decays/m^3, have to be taken into account. Alternatively, if the contamination does not decay with $T_{1/2} = 3.8$ d but stays constant (due to permanent emanation), 6300 decays/m^3 have to be taken into account per year. A simulation shows that even this very conservative assumption leads to an upper limit of $0.1 \cdot 10^{-3}$ cts/(keV·kg·y) for the background index.

If the choice of the liquid is argon, then additional background from ^{42}Ar decays have to be taken into account. The upper limit of the activity from ^{42}Ar is 40 μBq/kg [Ash 03]. A simulation shows that this results in a background of $< 10^{-4}$ cts/(keV·kg·y). Beta decays of ^{39}Ar have a Q value of 0.6 MeV and do not contribute to the background for neutrinoless double beta decay.

Background from the detector surface and the holder material

The experience of many low background experiments shows that surface contaminations are often larger than bulk activities.

For the detectors of the Heidelberg-Moscow experiment there is clear evidence for surface contamination for two of the five detectors [Die 99, Bak 03]. The level is of the order of 45 decays of ^{210}Pb per year and detector. For the ^{232}Th decay chain the intensity is approximately a factor of 4 smaller and consequently one would expect about 4 ^{208}Tl decays on the detector surface per year. According to simulation, 2.5% of these decays deposit energy in the 2.0 to 2.08 MeV range. The resulting background index is $0.6 \cdot 10^{-3}$ cts/(keV·kg·y). This can be reduced substantially by anti-coincidence methods described below. For the other detectors the contamination by ^{210}Pb is about a factor of 10 smaller or not seen at all. This example shows that surface contaminations can be limited to an

acceptable level.

Alternatively, an upper limit for surface contaminations can be defined. For p-type detectors the inner well is most critical. A background index of 10^{-3} cts/(keV·kg·y) corresponds to a surface activity of ^{208}Tl of 0.01 μBq/cm^2 in the well. Using the below described anti-coincidence method this limit may be relaxed to 0.25 μBq/cm^2. The background contribution from ^{214}Bi decays is about a factor of 10 smaller for the same activities.

For contaminations in the holder material of the diodes the fraction of decays depositing energy in the interval 2.0 to 2.08 MeV is similar to the case of surface contaminations. The behavior concerning additional background rejection methods is also similar. Therefore for 10 gram holder weights per diode and a background index of 10^{-3} cts/(keV·kg·y), the contamination of the material should be below 20 μBq/kg of ^{208}Tl ($1.5 \cdot 10^{-11}$ g/g of ^{232}Th).[4] If the anti-coincidence methods are applied this number can be larger by up to a factor of 25. For the acryl material used by SNO, a contamination level of 10^{-12} g/g for ^{232}Th was found, resulting in a background index of $\leq 10^{-4}$ cts/(keV·kg·y).

3.4 Background reduction techniques

Several methods exist to reduce backgrounds:

- Anti-coincidence between different detectors in the setup: This method relies on the fact that the total Q value of background decays is larger than $Q_{\beta\beta}$. Consequently, a part of the energy is deposited elsewhere and may be detected. The rejection depends on the location of the detector within the setup. For the suppression factor a corner location was used which gives the smallest rejection power.

- Segmentation of readout electrodes: For signal events the energy deposition is very localized (single site events) whereas Compton scattered photons deposit their energy often at several positions within the diode (multiple site events). Also, for the cases where the background is due to the summation of two photons or an electron and a photon the energy deposition is typically not localized. In the simulation a four-fold segmentation of the n-contact along the axis of the coaxial detector is studied. This applies only for new detectors for phase II.

- Pulse shape analysis (PSA): Again, the non-localized energy deposition for background events is explored. Due to the non-uniform (radial) electric field in the diode there is a correlation between the charge sensitive preamplifier output and the location of the energy deposition. A superposition of energy deposits from background events can in principle be disentangled using this information. No detailed simulation of the pulse shape has been performed so far. Beside the methods used in previous Ge experiments or proposed for the MAJORANA experiment [Maj 03, Kla 04], there is also the possibility to extend the method used by the GNO experiment for the discrimination of multiple site events in proportional counters [Pan 04]. A conservative estimate is that 1/3 of the background events are rejected.

---

[4]The background from ^{214}Bi decays is about a factor of 10 smaller for the same contamination level.

- Waiting: For many cosmogenic backgrounds the decay time is short enough such that waiting for the decay of the isotope is an option. For ^{68}Ge about 60% of the atoms decay in one year.

- Coincidences in the decay chain: The electron capture of ^{68}Ge from the K shell results in a $\sim$10 keV energy deposition when the empty K shell location is filled. The β^+ decay of ^{68}Ga follows with a half lifetime of $T_{1/2} = 68$ min. The time correlation of the two decays is therefore a powerful rejection tool. About 86% of the ^{68}Ge decays occur via electron capture from the K shell. If the trigger threshold is low enough a large fraction of the ^{68}Ge decays can be vetoed.

- Scintillation light detection: Liquid argon is pursued as one option for the cryogenic fluid. In this case an energy deposition in argon by a background process may be detected by the observation of scintillation light. This solution is very attractive and will be discussed in section 3.6. Since this is not our baseline design at the moment no background rejection factor is assumed for our sensitivity estimate.

Table 3 lists for the most relevant background sources the remaining fraction of events after a rejection method has been applied. For the combination of the anti-coincidence of diodes and segments within a diode the fractions should be multiplied. Since the segmentation discriminates against multi site events at different axial positions and the pulse shape analysis discriminates against events with different radial energy depositions we assume that the discrimination factors are also multiplicative for the PSA. The cumulative rejection power of the combined methods is rather large, however, not all methods may be applicable in the different phases of the experiment.

Table 3: Fraction of background events remaining after the individual rejection methods. The labels "^{60}Co" and "^{68}Ge" stand for intrinsic background decays of these isotopes. The label "^{208}Tl" stands for 2.615 MeV gammas from the concrete and "holder material" for ^{208}Tl decays originating very close to the diode. "combined" corresponds to the multiplication of all individual rejection factors.

method	^{60}Co	^{68}Ge	^{208}Tl	holder material
diode anti-coin.	0.51	0.72	0.66	0.15
segm. anti-coin.	0.19	0.25	0.55	0.25
pulse shape	0.66	0.66	0.66	0.66
waiting 1 y	0.87	0.39	-	-
decay chain coin.	–	0.2	-	-
combined	0.06	0.01	0.24	0.02

3.5   Background summary

Phase I: The external background will be reduced to a level of 10^{-3} cts/(keV·kg·y). As discussed in sec. 3.2 we are confident that the background of the existing diodes can be reduced by at least a factor of 20 once the diodes with contacts of reduced mass are immersed in LN/LAr. This includes also possible intrinsic contaminations from ^{60}Co. The total background index is then 10^{-2} cts/(keV·kg·y).

Table 4: Summary for the background index B for Phase II of GERDA (for the assumptions see text). The external γ background is for shielding with LN. For the column "after bkg. rej." the background rejection due to the anti-coincidence of detectors, pulse shape analysis and decay chain coincidence is assumed. The column "after add. det. segm." lists the background index if the detector segmentation cut is applied in addition. The suppression factors are taken from table 3.

source	B $\frac{10^{-3}\text{cts}}{\text{keV·kg·y}}$	B after bkg. rej. $\frac{10^{-3}\text{cts}}{\text{keV·kg·y}}$	B after add. det. segm. $\frac{10^{-3}\text{cts}}{\text{keV·kg·y}}$
ext. γ from ^{208}Tl, ^{228}U	1	0.4	0.2
ext. neutrons	≤ 0.05	≤ 0.03	≤ 0.02
ext. muons	≤ 0.1	≤ 0.05	≤ 0.03
internal ^{68}Ge	12	1.1	0.3
internal ^{60}Co	2.5	0.8	0.2
^{222}Rn in LN/LAr	0.2	≤ 0.1	≤ 0.1
^{208}Tl, ^{228}U in holder mat.	≤ 1	≤ 0.1	≤ 0.1
surface contamination	≤ 0.6	≤ 0.1	≤ 0.1

Phase II: A summary of the estimated background contributions is given in Table 4. For the estimate of the internal background, the above mentioned rather pessimistic assumptions for the fabrication times are made (sec. 3.3.1).

The column "after bkg. rej." lists the background index after the background rejection due to the anti-coincidence of the detectors in the setup, the pulse shape analysis, and the decay chain coincidence (relevant for ^{68}Ge). These methods do not require any new experimental techniques like segmentation and are also applicable to the existing detectors. However a trigger threshold below 10 keV and a close packing of many detectors is needed. The resulting total background index is dominated by the intrinsic sources in this scenario and a factor of 2-3 larger than the design goal.[5] To ensure a background index less than 10^{-3} cts/(keV·kg·y) segmentation of one detector contact is needed.

---

[5]For the existing detectors only the ^{60}Co background at a level of 10^{-2} cts/(keV·kg·y) contributes. With the anti-coincidence of diodes and the pulse shape analysis this can be reduced to $3 \cdot 10^{-3}$ cts/(keV·kg·y), somewhat larger than 10^{-3} cts/(keV·kg·y).

3.6 Performance with instrumented shield for LAr

The design of our proposal consists of germanium diodes immersed in liquid nitrogen or argon. The liquid serves as a high purity *passive* shield against radiation. Ionizing radiation that creates background signals in the diodes with energies close to $Q_{\beta\beta}$ typically has energies greater than the one deposited in the germanium crystals. Part of this energy is dissipated in the shielding liquid and is 'invisible'. An option under study is to instrument the shielding medium and to measure the energy deposition which can be used as an anti-coincidence signal. Liquid nitrogen provides only weak signals from scintillation and Cherenkov light emission. The scintillation properties of liquid argon are well established, see [Kub 79, Dok 90, Hit 83, Cen 99]: about 40,000 photons are emitted per MeV of deposited energy. This is approximately four times the number observed in organic liquid scintillators. Photons are emitted in the de-excitation of the Ar_2^* excimer with a wavelength of 128 nm. Decays from singlet and triplet excited states give rise to a fast 6 ns and a slow 1.6 μsec component with an intensity ratio of 0.3 for excitation with electrons, and of 1.3 for alpha particles [Kub 79].

In order to use the scintillation light in anti-coincidence with the germanium diodes, one has to detect the 128 nm scintillation photons with high efficiency. The use of wavelength shifting materials to move the photon wavelength into the region of maximal sensitivity of Bi-alkali photomultipliers is under investigation. Technical details of this developments are summarized in section 6.8.1. A Monte-Carlo simulation of a 2 kg diode immersed in liquid argon demonstrates the potential power of the method. We assume that a threshold of 100 keV can be achieved for the detection of scintillation light.

Figure 11 displays the results of simulations of ^{42}K decays, the progeny of ^{42}Ar ($Q_\beta = 0.6$ MeV, $t_{1/2} = 33$ y), homogeneously distributed in the liquid argon. ^{42}K has a maximum electron energy of 3.5 MeV and a weak γ line at 2.424 MeV and thus is a possible background for double beta decay. A ratio of ^{42}Ar/^{nat}Ar of $3 \cdot 10^{-21}$ has been assumed [Bar 02] for the simulation. A background suppression of more than a factor of 100 is achieved in the $Q_{\beta\beta}$ region.

Figure 12 shows a simulation of cosmogenic ^{60}Co decays which are placed homogeneously inside a germanium crystal. An activity of 0.18 μBq/kg is assumed. Again, one gains two orders of magnitude in background suppression.
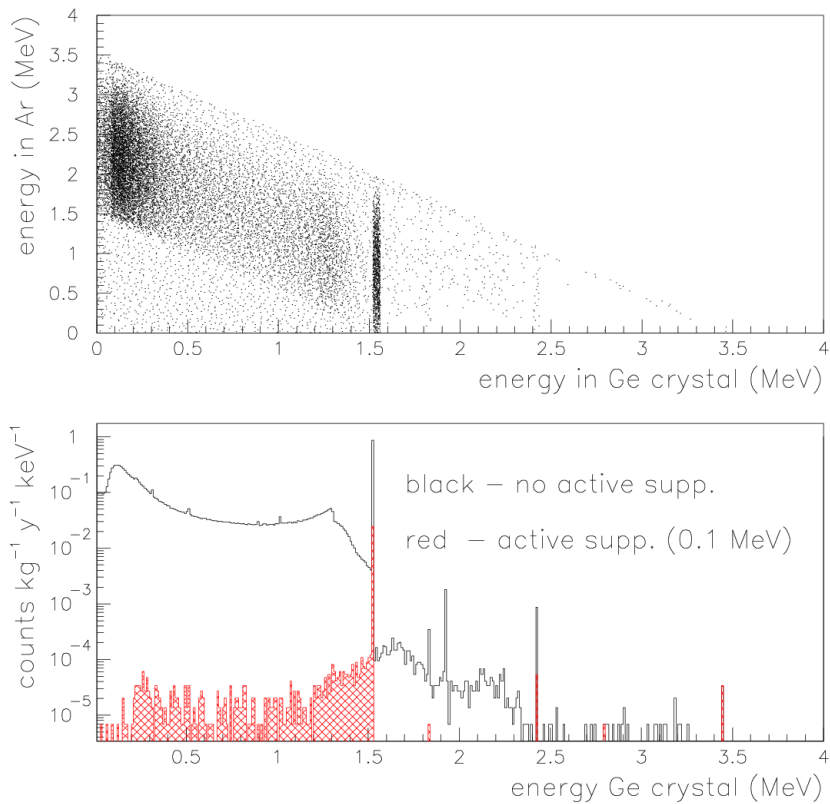
Figure 11: Suppression of external ^{42}K (^{42}Ar progeny): Scatter plot of the energies deposited in the liquid argon and the Ge diode (top), and the energy spectrum seen by the germanium crystal with and without anti-coincidence assuming a threshold of 100 keV (bottom).
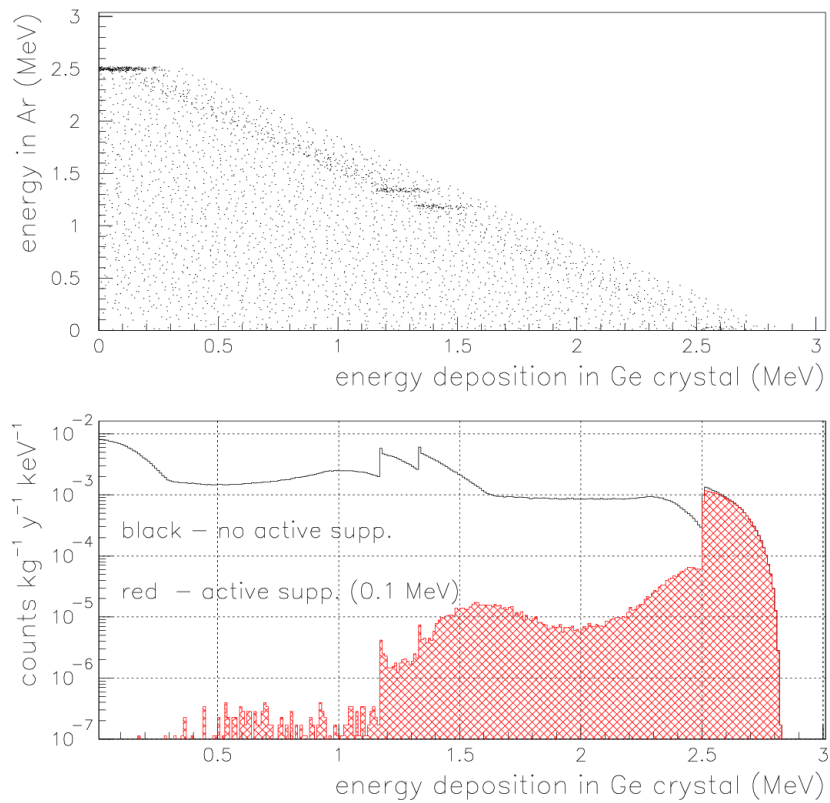
Figure 12: Suppression of internal ^{60}Co activity: Scatter plot of the energies deposited in the liquid argon and the Ge diode (top), and the energy spectrum seen by the germanium crystal with and without anti-coincidence assuming a threshold of 100 keV (bottom).

3.7 Performance for dark matter search

The CDMS experiment has currently the most sensitive limit [Ake 04] on WIMP searches with an exposure time of 30 kg·days. This experiment is about a factor of 20 more sensitive than Heidelberg-Moscow [Bau 99b] and about a factor of 10 more sensitive than IGEX [Ira 02]. The latter experiments are limited by background. The CDMS limit will improve linearly with time and mass until the first background events will be observed. Even in case they do not reach their goal of a 10-20 times better limit, it can be expected that the current CDMS limit will improve considerably. Similar limits are expected from EDELWEISS and CRESST in the future. Here the CDMS limit is taken as a guideline for a first estimate of our competitiveness concerning dark matter.

We can reach a similar sensitivity as the current CDMS limit for a background index of ≤ 1 cts/(keV$_{rec}$·kg·y) for energies ≥ 30 keV$_{rec}$. Here the subscript "rec" refers to nuclear recoil energy. The measured ionization energy is smaller by the quenching factor of ~ 3 and is referred to by the subscript "ee". This background index is a factor of 20 lower than the one of Heidelberg-Moscow. To compete with the future CDMS results the reduction factor should be 400.

So far we have performed only a small number of simulations to estimate our low energy background. This will be discussed in the following section. Here we assume that the dark matter measurement is done with natural germanium detectors of our setup. Hence the sensitivity will not be restricted by background from $2\nu\beta\beta$ decays of ^{76}Ge. For the limits we assume all detected events to be signal events, i.e. no background subtraction is foreseen.

3.7.1 Backgrounds

External background

The sensitivity to dark matter of the Heidelberg-Moscow experiment was limited by external radiation and surface contaminations. For GERDA the background at $Q_{\beta\beta}$ from external sources and surface contaminations will be reduced by a factor of 200. Taking additional background suppression methods into account a factor of 400 is expected. From past experience we expect a similar suppression at low energies. So far no simulations have been performed to quantify this statement, and a prediction of the limitation due to external backgrounds or surface contaminations is difficult at the moment.

We assume in the following a background index of 0.05 cts/(keV$_{rec}$·kg·y) for the contributions from external backgrounds.

Cosmogenic background

Due to quenching the energy region where most WIMP signals could be expected with GERDA is concentrated to a few keV above the threshold, which we assume to be just above the X-ray line from ^{68}Ge decays. The analysis threshold is then 11 keV$_{ee}$, i.e. 30 keV$_{rec}$ recoil energy. In principle the trigger threshold and hence the analysis threshold can be lower. Whether the background below 10 keV$_{ee}$ permits a more competitive analysis
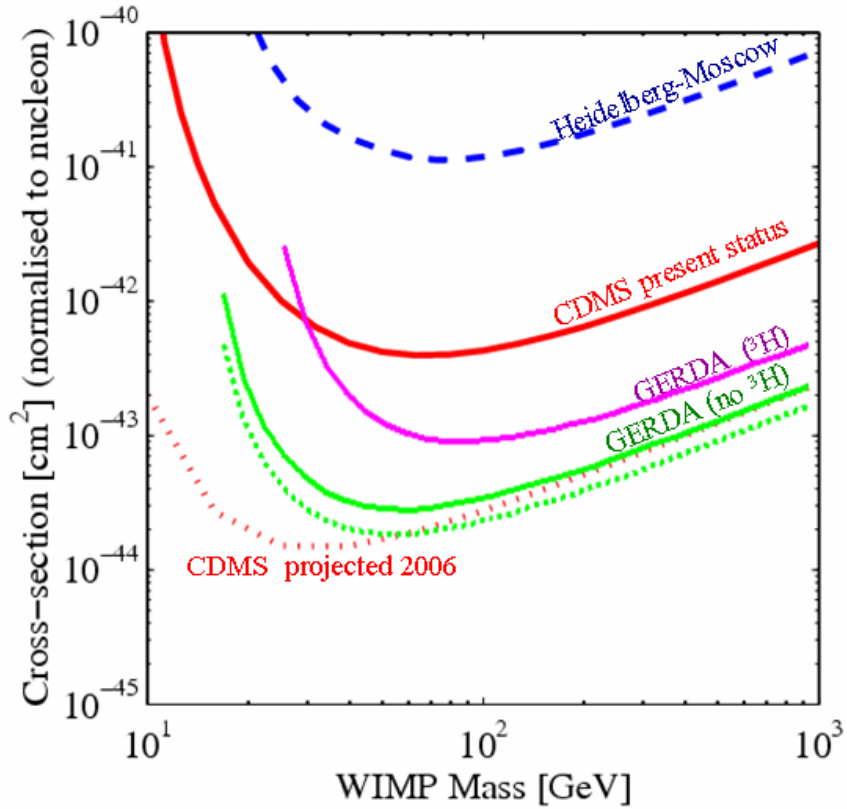
Figure 13: Comparison of the present and projected limits from CDMS with the sensitivity of GERDA for a background of 0.05 cts/(keV$_{rec}$·kg·y). The lower lines for GERDA labelled "(no ^{3}H)" are assuming that there is no relevant ^{3}H contamination and thus a threshold of 30 keV$_{rec}$. The full line can be reached with an exposure of 100 kg·y, and the dotted line shows the background limitation (infinite statistics). The line labeled "(^{3}H)" shows the case for 100 kg·y and a threshold of 57 keV$_{rec}$. Also shown is the limit from Heidelberg-Moscow.

remains to be seen.

The contaminations, which we considered so far are ^{60}Co, ^{68}Ge and ^{3}H in the detectors and ^{42}Ar and ^{39}Ar for liquid argon. The levels of expected internal background are compiled in table 5. The background from ^{68}Ge, and ^{60}Co can be estimated from the Monte Carlo simulations discussed in section 3.3.1.

The background from tritium can be estimated from a conservative limit on the production rate of tritium above ground of 140/(kg·d) [Avi 92]. We assume 30 days of exposure. About 1/5 of all ^{3}H decays have an energy above the detection threshold. Comparing the numbers from table 5 with the level of 0.05 cts/(keV$_{rec}$·kg·y) assumed for the external background one can see, that ^{68}Ge and ^{60}Co will not limit our sensitivity.

Tritium is the source with the highest background, which would limit the sensitivity to the present level of CDMS. However, one can do a dark matter analysis above the ^{3}H endpoint, which is more competitive given the high background rate expected at lower en-

Table 5: Background between 30 keV$_{rec}$ and 40 keV$_{rec}$ for some intrinsic contaminations.

	cts/(keV$_{rec}$·kg·y)
^{68}Ge	$0.3 \cdot 10^{-3}$
^{60}Co	$3 \cdot 10^{-3}$
^{3}H	2

ergies. The largest effect of a higher threshold is a shift of the lower limit of the sensitivity to higher masses. This is shown in Fig. 13 for a background index of 0.05 cts/(keV$_{rec}$·kg·y) above the analysis threshold. Since we do not know the concentration of ^{3}H in the detector crystals, two cases are considered: For the case of a large ^{3}H background with a threshold of 19 keV$_{ee}$ (labeled "GERDA (^{3}H)") and for the extreme optimistic case without any ^{3}H background and a lower threshold (labelled "GERDA (no ^{3}H)"). Even with an increased threshold our sensitivity after several years of data taking is within a factor of three comparable with the anticipated future CDMS limits, also shown in Fig. 13.

Shielding with liquid argon

Cosmogenic production of ^{42}Ar and ^{39}Ar in argon lead to decay rates of $\leq 40\,\mu$Bq/kg and 1 Bq/kg, respectively.

The results from the Monte Carlos for the expected count rate at low energies in the germanium detectors from ^{42}Ar and ^{39}Ar decays in the LAr shield are summarized in table 6. The expected spectrum caused by ^{39}Ar decays is shown in figure 14.

Table 6: Background indices at 30 keV$_{rec}$ as expected from Monte Carlos due to cosmogenic produced Ar in the LAr shield. Numbers with and without a veto using the readout of the argon scintillation signal are given.

	no veto cts/(keV$_{rec}$·kg·y)	with veto (threshold 100 keV) cts/(keV$_{rec}$·kg·y)
^{39}Ar	$10 - 13$	$1 - 2$
^{42}Ar	$3 \cdot 10^{-3}$	negligible

^{42}Ar will not be a limiting factor with or without the veto based on the scintillation in LAr – but ^{39}Ar is! Even using scintillation the background from ^{39}Ar will limit the sensitivity to the present level achieved by CDMS. In principle one could reduce this background, if the threshold of the scintillation veto were lower than 100 keV. But since most of the relevant decays are from the close vicinity of the detector surfaces, and from the inner contacts of the diode, it will be very difficult, if not impossible, to veto these
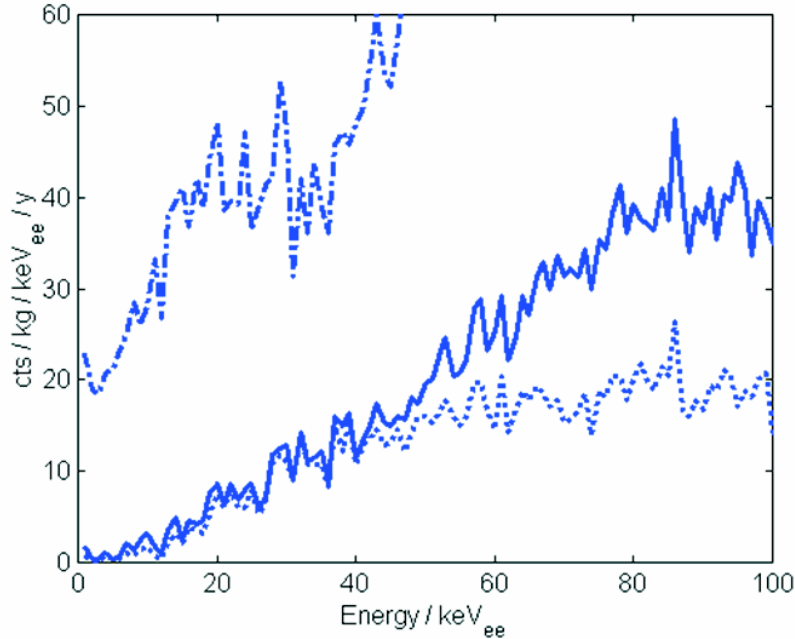
Figure 14: Background spectrum in the germanium detectors expected from ^{39}Ar decays in the LAr shield. The dash-dotted line shows the result without the LAr scintillation veto. The full (dotted) line assumes a veto with a threshold of 100 keV (50 keV). The background in keV$_{rec}$ is reduced relative to this figure by the quenching factor of $\sim$3.

events. This means, GERDA with a LAr shield will not be competitive in dark matter search unless it becomes possible to subtract the ^{39}Ar background.

For liquid nitrogen the argon concentration is very low and the ^{39}Ar contamination is therefore negligible.

3.7.2   Summary

If the evidence from the DAMA experiment were true [Ber 03], GERDA should see about 5-10 cts/(kg·y), i.e. a few hundred counts per year - enough to look for a few percent annual modulation.

For the limit calculations all observed events are treated as signal events, i.e. no background subtraction is performed. In principle an analysis looking for annual modulation can reach a higher sensitivity since the background which is constant in time can be subtracted. However, the signal of the modulation is only about 3% of the WIMP recoil signal, and an analysis based on annual modulation only helps after a large statistics is accumulated. For the assumed background index of 0.05 cts/(keV$_{rec}$·kg·y) the modulation analysis yields a better limit for a data sample larger than about 2000 kg·y.

To carry out a competitive dark matter search, the background has to be reduced by at least a factor of 400 compared to the present level achieved in the Heidelberg-Moscow experiment. At the moment it is uncertain whether this is realistic.

Due to the high background introduced by cosmogenic ^{39}Ar, the sensitivity to dark matter will be very limited, if liquid argon is used for shielding. At the moment only the liquid nitrogen option is considered competitive.

Of the considered contributions the tritium background will dominate and limit the sensitivity to the current CDMS result. An analysis threshold above the end point of ^{3}H avoids this problem. Especially for WIMP masses below 50 GeV the sensitivity is then strongly compromised. However, in the context of supersymmetric models these masses are almost excluded by LEP II measurements. For higher masses a sensitivity is reachable which is somewhat worse than the CDMS projected sensitivity for the next few years. It should be stressed again that these results are only based on a limited number of simulations. The numbers given can only serve as a rough estimate of the potential of the experiment. In the long run, better sensitivities will probably be reached by discriminating detectors, such as cryogenic calorimeters.

Even then, it is likely that in future dark matter experiment, germanium plays a role (CDMS, EDELWEISS, etc.). Also there, the electromagnetic background before discrimination needs to be reduced as much as possible. In this respect, double beta decay experiments are more advanced today than CDMS and EDELWEISS for example. The latter have presently a count rate of about 1000 cts/(keV$_{rec}$·kg·y). How far the limits of α-, β-, and γ-background can be pushed, is best tested with GERDA. It will thus provide important information for the future of dark matter searches and contribute in any case.

4 Physics reach

As discussed before GERDA will have several phases. In the first phase the existing enriched germanium detectors will be used while new segmented diodes need to be fabricated for the second phase. The sensitivities are discussed in the following.

4.1 Phase I

For the case that no background events are observed, the 90% confidence limit (C.L.) on the half lifetime for the neutrinoless double beta decay of ^{76}Ge is given by

$$T_{1/2} > 2.4 \cdot 10^{24} \cdot \epsilon \cdot a \cdot M \cdot t \quad [y] \tag{10}$$

with ϵ being the detection efficiency, a being the enrichment fraction of the ^{76}Ge isotope, M being the total active mass of the diodes in kilograms and t being the measurement time in years.

If the number of background events is large and Gaussian errors can be assumed, the same confidence level limit is given by

$$T_{1/2} > 4.3 \cdot 10^{24} \cdot \epsilon \cdot a \sqrt{\frac{M \cdot t}{B \cdot \Delta E}} \quad [y] \tag{11}$$

with B being the background index in cts/(keV·kg·y) and ΔE being the energy resolution (FWHM) at $Q_{\beta\beta}$ in keV.

For the first phase of the experiment only existing enriched detectors will be used. In total, the active mass of the existing enriched detector is almost 20 kg. Here we will only assume an active mass of 15 kg, since some of the detectors might not work reliably.

The reduction of the external backgrounds to a level of less than 10^{-3} cts/(keV·kg·y) is ensured by the design of the vessel and the reduction and selection of the detector mounting material. For the intrinsic background we assume a level of 10^{-2} cts/(keV·kg·y) as discussed in section 3.2.

Assuming one year of data taking and an energy resolution of 3.6 keV, the expected number of background events is 0.5 counts. If no event is observed (60% chance), a 90% C.L. of $T_{1/2} > 3.0 \cdot 10^{25}$ y can be established for a detection efficiency of $\sim 95\%$ and an enrichment fraction of 86%. This results in an upper limit on the effective neutrino mass of $m_{ee} < 0.24 - 0.77$ eV. The mass range is determined by the matrix elements quoted in [Ell 02]. If the possibility of a non-zero event count is taken into account (with weights determined by a Poisson distribution of mean 0.5 events) then the upper limit becomes $T_{1/2} > 2.2 \cdot 10^{25}$ y or, translated into an effective neutrino mass, $m_{ee} < 0.28 - 0.9$ eV.

The current claim of a signal for neutrinoless double beta decay [Kla 04] is based on an excess of 28.8 ± 6.9 events for a total statistics of 71.7 kg·y. With a statistics of one year data taking of 15 kg·y and a similar detection efficiency we would observe 6.0 ± 1.4 events above a background of 0.5 counts. If no event is observed, the claim would be ruled out with 99.6% confidence level. If one event would be observed, it would be a 97.8%

confidence level. However, if six or more events would be observed, this would correspond to a 5 sigma confirmation.

While we are confident that the current coarse simulations are reliable enough to dimension the shields and to estimate the background rejection, more detailed simulations will be needed to study the shielding in regions such as the neck of the cryogenic vessel, to determine the exact shape and thickness of additional lead shield underneath and on top of the vessel, and to optimize the arrangement and segmentation of the diodes. Detailed simulations will also be required to compared measured and expected background characteristics and to trace potential sources of excess background.

If some of the detectors exhibit a larger background index the same sensitivity can be reached with a subset and a correspondingly larger running time.

4.2   Phase II

In the second phase of the experiment new segmented germanium detectors will be added to the setup. A background index of 10^{-3} cts/(keV·kg·y) is achievable, if the detector exposure can be kept to the limits discussed in section 3.3.1.

It is foreseen to accumulate statistics of about 100 kg·y within ≈3 years. With an energy resolution of 3.6 keV, 0.36 background counts are expected. Consequently there is a large chance that no event is observed. The limit on $T_{1/2}$ would improve by a factor of six to $2 \cdot 10^{26}$ y. This translates to an upper limit of the effective neutrino mass of 0.09 - 0.29 eV, depending on the nuclear matrix element used.

If the background index for the existing diodes does not reach the goal of 10^{-3} cts/(keV·kg·y) a longer running time may be necessary.

5 Simulation studies and plans

Simulations will take the geometry of the detectors, support materials, readout materials, and all shielding materials into account. All relevant physics processes will need to be simulated in detail to produce a reliable background spectrum. There should be enough information stored in the event records so that one can make similar cuts as on data. I.e., all information stored for data should also be stored for Monte Carlo (detector identification, ADC count time spectrum, possible environmental variables if relevant in the simulation), in addition to truth information (source, location, type of initiating energy deposit).

Most existing simulations have been performed with GEANT4 [GEA 03]. This program is used in many particle physics experiments, there is worldwide support for it, and all relevant physics processes are implemented. Therefore, we anticipate that GEANT4 will be the main simulation program of the experiment.

The following subtasks are anticipated:

- A precise and complete description of the geometry of the detectors and supports. This will need close coordination with the engineers who are designing the detector supports, calibration devices (since these will require other material), etc. The relative location of detectors will need to be measured and introduced into the simulation. As an example Fig. 15 shows how the rejection factor due to the anti-coincidence of diodes changes as a function of the detector spacing. This example is for the particular case of background from intrinsic ^{68}Ge.

- The design of the plastic scintillator and the water Cherenkov detector for the muon veto. A good starting point is the BOREXINO layout but the correct position of the PMTs in the water and the size of the area covered with plastic scintillators has to be studied.

- A precise and complete description of materials, including information of radioactive impurity concentrations. This will be needed for the detectors, supports, nitrogen, tank, water shield, other materials, etc. A database will be set up where individual items are listed. This database will be linked to the simulation program and kept updated.

- Verification of the simulation for low energy processes as well as neutron production by high energy muons. A series of tests will be specified to qualify the simulation and to check that all relevant physics processes are correctly simulated. One example of a check of intrinsic radioactive impurities is the study of relative rates of escape lines. Many such tests will need to be devised to guarantee that the simulation is accurate.

  The implementation of many hadronic processes such as isotope production in muon interactions or neutron interactions have to be carefully checked. For example, the number of neutrons produced in muon interactions are by a factor of two larger in
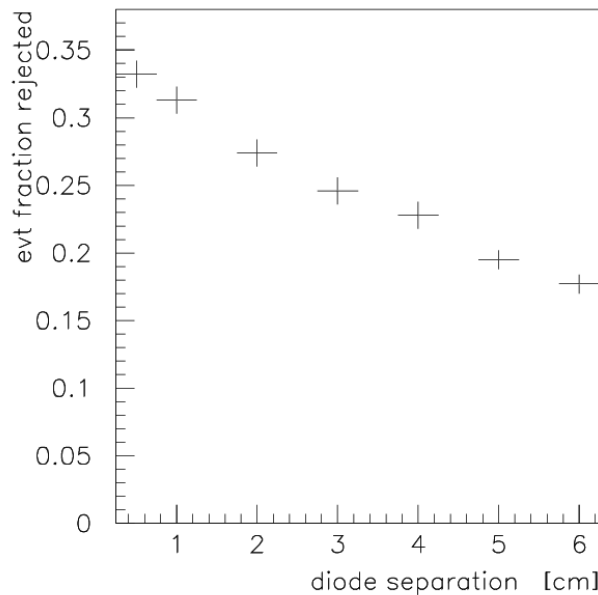
Figure 15: Fraction of events that can be rejected by the anti-coincidence of detectors for ^{68}Ge decays as a function of the separation between the diodes. The analysis is performed for a detector at a corner location of the setup shown in Fig.~reffig:simusetup.

FLUKA than in GEANT4. Also, some simulations are only correct on average due to simplified reaction models.[6]

- A code management system will be needed to keep track of different versions of the simulation. The number of detectors and configurations will change during the life of the experiment, and different running periods will have different simulation setups.

- Simulation programs will be needed to develop optimized geometries and segmentation for the new detectors of phase II. The new detector designs need to be tested with the full simulation to understand the gain we are expecting from segmentation.

- The simulation requires an implementation of the time development of the pulse, and possible detector differences from different geometries, segmentation, E-field configurations, electronic readout, etc. This could initially be developed in standalone code, but should eventually be migrated to the full simulation so that we can generate events with all effects included.

  The calculation of the pulse shape is an important aspect of the simulations. This requires a calculation of the electric field and the charge collection inside the diode.

---

[6]For example, the Q value for neutron capture on ^{14}N is 10.8 MeV and this energy is released in a cascade of photons. GEANT4 is simulating this cascade only on average correctly, i.e. only the average of the released energies is equal to the Q value.

Expertise for such simulations exists in our collaboration. For the AGATA experiment, these simulations have been performed for n-type detectors [Krö 01, Med 04]. The HLL (semi-conductor laboratory) of the Max-Planck-Institute regularly performs simulations for silicon strip detectors [Ric 96] and simulations in 3-D have begun for Germanium detectors. Both codes or updated versions are able to perform simulations for p-type germanium detectors. The simulation of the preamplifier might be included in a later step. The calculations may also be used for an optimization of the detector geometry and segmentation.

There are clearly many important aspects to the simulation. We anticipate forming a task group which will undertake the job of fulfilling the requirements listed above in a coordinated way.

For many items discussed here there is an overlap with the MAJORANA efforts. To profit from mutual experience and knowledge a close contact between the collaborations has been established.

6 Technical aspects of the experiment

6.1 Overview

Figure 16 shows a schematic of the experimental setup. The Ge diodes are brought via the cleanroom to the lock through which they are installed in the cryogenic vessel filled with either liquid nitrogen (LN) or liquid argon (LAr). The cryofluid serves both as cooling and shielding medium for the diodes. The detector suspension and contacts are made out of a minimum of carefully screened materials of ultra-high radiopurity. The cryostat is enclosed by a water shield which serves as neutron absorber and medium for the detection of muons by Cherenkov radiation. Scintillators on top of the vessel increase the power for muon rejection. The signals of the Ge diodes are led via feed-throughs into the electronic cabin
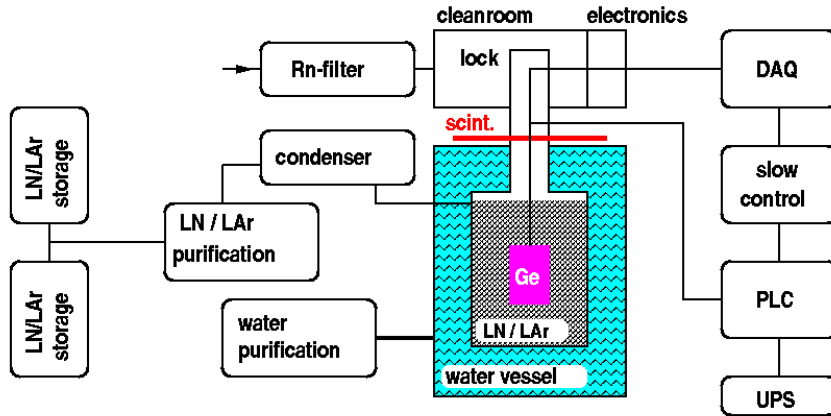
Figure 16: Schematic of the experimental setup.

on top of the vessel where their pulse shapes are digitized in flash ADCs. The PC based data acquisition system allows the processing, visualization, quality control, and storage of the incoming data. The slow control supervises all auxiliary systems including the low and high voltage power supplies and the monitoring of the parameters characterizing the status of the experiment like temperature, pressure, detector currents, etc. The programmable logic controller (PLC) is an autonomous system of high reliability for the monitoring of safety relevant parameters like vessel pressure, oxygen concentration, and temperature. An uninterruptible power supply (UPS) allows the system to continue data taking or to reach a safe state in case of an electrical power outage.

The cryogenic and water vessel system will be isolated against vibrations from the floor. The cryogenic vessel is sealed with metal gaskets and operated at 0.2 bar overpressure to prevent contamination of the cryofluid by radon from the environment. Moreover, the cleanroom will be operated with Rn-reduced air. Activated carbon adsorber columns will be used to supply fresh Rn free cryofluid as substitution for evaporated LN/LAr. In case of LAr it might be, however, more economic to re-condense the LAr vapor with a cryogenerator. Purification of the shielding water is needed to establish sufficient transparency for

the detection of Cherenkov light.

In the following section we will discuss some of the components in more detail and outline planned R&D activities.

6.2 Cryogenic and water vessel system

The basis for the following discussion are measurements of the ^{208}Tl 2.615 MeV gamma activity in Hall A of the LNGS from which we adopt the value of 0.0625 cts/cm^2. We assume that the background index at Q$_{\beta\beta}$=2.039 MeV is dominated by the Compton tail of this ^{208}Tl gamma line. From measurements and Monte Carlo studies, it has been concluded (see section 3.3.2) that for above surface activity the background index B in a shielded Ge diode can be approximated by B=2250$\cdot X \cdot \exp{(-X)}$ cts/(keV·kg·y) for $X > 5$ where $X = t \cdot \mu$ is the product of the thickness t of the shielding material and its absorption coefficient μ. The condition $B = 10^{-3}$ cts/(keV·kg·y) yields $X = 17.5$, and hence $t = 563$ cm for LN. In order to fit the shield within Hall A, a graded shield has to be considered in which part of the LN is substituted by materials of larger absorption coefficients and appropriate radiopurity (see Table 7). Due to its high radiopurity, water represents an ideal substitute for LN

Table 7: Linear absorption coefficients μ for 2.615 MeV γ rays in various materials and the material's intrinsic ^{228}Th 'mass' activities A_M assumed in the present discussion. The 'surface' activity $A_S(^{208}$Tl$)$ is calculated according to $A_S = 0.356 \cdot (A_M(^{228}Th) \cdot \rho \cdot \mu^{-1}) \cdot (1 - \exp{(-\mu \cdot \text{t})}$ where ρ, μ and t are the material's density, absorption coefficient and thickness, respectively. The factor of 0.356 is due to the 35.6% branch from ^{228}Th to ^{208}Tl.

material	μ [cm^{-1}]	ρ [g / cm^3]	$A_M(^{228}$Th$)$ [μBq/kg]	$A_S(^{208}$Tl$)$ [μBq/cm^2]
LN	0.0311	0.81	*	*
Water	0.0427	1.0	1	t>1 m: 0.01
LAr	0.050	1.39	*	*
Steel	0.299	7.87	2·10^4	t=2 cm: 84.5
Cu	0.338	8.96	25	t=3 cm: 0.15
Pb	0.484	11.35	30	t>10 cm: 0.25

* negligible

and the discussion below will outline several options for a shielding system consisting of a cryostat for LN and LAr immersed into a water vessel.

6.2.1 General considerations

The design of the cryogenic and water vessel system has to fulfill the following requirements:

1. The ^{208}Tl 2.615 MeV gamma activity of the surrounding concrete has to be suppressed by the factor of $\exp{(-17.5)} = 2.5 \cdot 10^{-8}$ in order to obtain the background index of

44

10^{-3} cts/(keV·kg·y) in case that the cryogenic vessel is filled with LN. Replacing the LN by LAr should yield a background index of 10^{-4} cts/(keV·kg·y), or better.

2. The thickness of the water layer should be at least 1.50 m in order to serve not only as neutron moderator but also as Cherenkov medium for the detection of muons.

3. The dimensions of the vessel arrangement are constraint by the available space in Hall A of LNGS to a diameter of 12 m and a height of 9 m. This leaves a height of about 3 m on top of the vessel system that is needed for the lock and cleanroom through which the Ge detectors can be installed in the vessel.

4. For safety reasons the liquid gas volume has to be kept as small as possible.

5. Both construction and operating costs should be reasonably low.

Table 7 list absorption coefficients and activities of various materials which are considered to be used for the shielding system. The quoted activities have been measured for materials used in the BOREXINO and LENS projects or for the present study. For a mix of materials the background index B is estimated

$$B = 2250 \cdot X \cdot \exp\left(-X\right) \text{ cts/(keV} \cdot \text{kg} \cdot \text{y)} \quad \text{with} \quad X = \Sigma_i \left(\mu_i t_i\right) > 5$$

where μ_i and t_i are the absorption coefficient and thickness of the various materials i. For pure LN, water, and Pb the thicknesses ($X = 17.5$) are 562 cm, 410 cm, and 36.2 cm, respectively. Thus, by a suitable mix of these materials, the vessel assembly can be made to fit into the available space. It is also easily verified that a LAr fill will yield a background index that is lower by at least a factor of 10 if the liquid gas thickness is larger than about 125 cm.

Another factor influencing the overall size of the setup is the choice of thermal insulation for the cryogenic vessel. Most efficient will be the use of superinsulation which at thermal losses of about 2 mW/m^{2}K needs marginal space, typically less than 25 cm. Its implementation requires a special double-walled container that is able to maintain a vacuum of better than 10^{-3} Pa between both shells. The alternative, a standard powder (perlite) insulation as used in flat bottom vessels, needs to be much thicker, typically 1 m, due to its much higher thermal conductivity ($\approx$40 mW/m·K).

We will discuss below two designs of superinsulated cryogenic vessels that have a diameter of about 4 m, a size that allows them to be carried by road/water/air from the factory to the LNGS. A powder/foam insulated cryogenic vessel is discussed as a third option; its diameter of about 6.5 m would require it to be built in the LNGS Hall A. The Ge diode array is assumed to be of cylindrical shape with 50 cm height and 50 cm diameter.

6.2.2 Baseline design

The baseline design considers the cryogenic vessel to be fabricated from copper with an ^{228}Th activity of at most 25 μBq/kg. For NOSV copper an upper limit of 23 μBq(^{228}Th)/kg has been recently measured. A double-walled vessel with a total wall thickness of 3 cm would then exhibit a ^{208}Tl surface activity of 0.15 μBq/cm^2 which could be shielded to

the desired level of 1.6 nBq/cm^2 by a 147 cm thick layer of LN. On the other hand, a 303 cm thick water layer will reduce the ^{208}Tl surface activity in Hall A just to the same 0.15 μBq/cm^2. Neglecting the attenuation in the copper walls, the sum of the ^{208}Tl activities at the inner vessel wall is 0.3 μBq/cm^2 so that the thickness of the LN has to be increased by additional 22 cm to 169 cm. Taking the extension of the Ge array into account, the inner diameter of the inner vessel has to be 388 cm in order to achieve the desired background index of 10^{-3} cts/(keV·kg·y).

Fig. 17 shows the cross section of a superinsulated cryogenic vessel designed according to the German codes for cryogenic and pressure vessels using copper of the DIN type DHP R240. A summary of its characteristics is given in Table 8. The inner vessel is fabricated from two hemispheres of 380 cm diameter which are connected by a cylinder of 94 cm height. With less than 10 cm allocated for the space housing the superinsulation, the outer vessel diameter is 402 cm. The connection between both vessels is made at the end of a 150 cm long superinsulated neck. A major part of it is fabricated from stainless steel for obtaining a high thermal impedance. Thus the inner vessel is suspended via the neck in the outer vessel without any further thermal contact.

Two about 2 m long pipes serve to maintain the insulation vacuum of less than 10^{-2} Pa. Four further nipples will be used to connect safety and pressure relieve valves as well as a manometer. Not yet shown is a further connecting pipe which will be needed for filling (emptying) the vessel and for the connection to a refrigerator.

The pressure vessel code limits the thickness of the DHP R240 copper plates to 15 mm. This constraint implies that the earthquake tolerance of 0.6 g can be fulfilled for horizontal accelerations only; in vertical direction 0.5 g can be tolerated. If this would be not acceptable, the present rather elegant and efficient support of the inner vessel which minimizes the use of 'dirty material' will be modified e.g. by using plastic pads for the support of the inner vessel. Fig. 18 shows the copper cryostat immersed in a water container of 10 m diameter and 9 m height in a slightly asymmetric position in Hall A. Laterally, the space of 2 m is available which is required for the exchange of LVD modules. On top, 3 m of height are available for cleanroom and lock. The lack of 1 m water shield in vertical direction will be compensated by lead (t = 8.8 cm) or copper (t = 12.6 cm) plates; the precise location and respective thicknesses need still to be optimized.

The overall setup, a superinsulated copper cryostat within a water buffer of several meters of thickness resembles very much to that proposed and discussed in the GEM proposal [Zde 01]. In our LoI [LoI 04] we still considered a copper cryostat to be too expensive and technically difficult to be realized. With the advent of a commercial electron beam welding facility with a vacuum chamber of $7 \times 6 \times 14$ m^3 [pro 04] the situation has changed, however, and a feasibility study for the optimum fabrication of this copper vessel using electron beam welding is in progress. At affordable costs, this procedure would not only warrant highest quality of weld seams but also the much desired extreme cleanliness during fabrication.
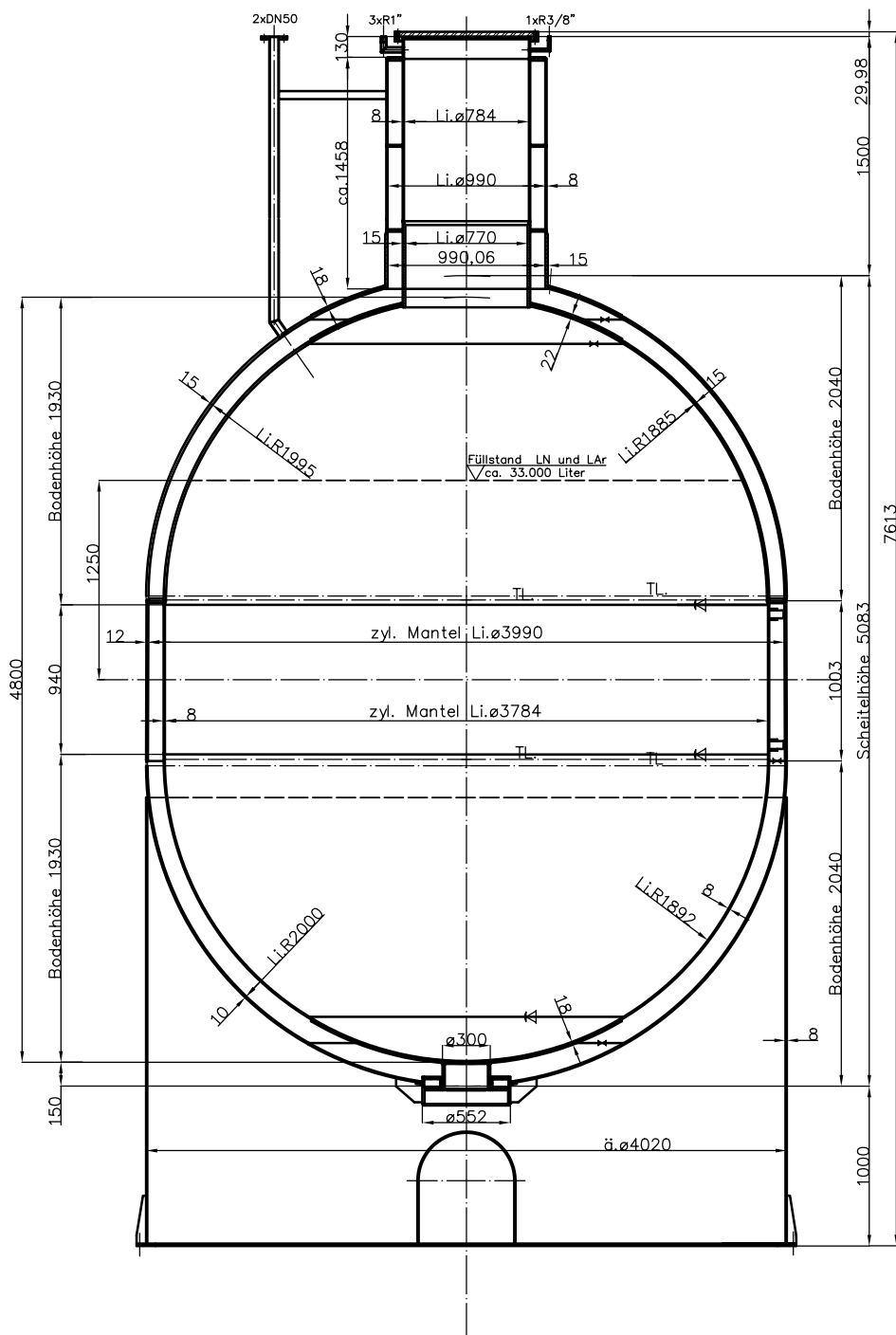
Figure 17: Cross section of a superinsulated vessel for LN or LAr fabricated from copper except a part of the neck which is made out of stainless steel.
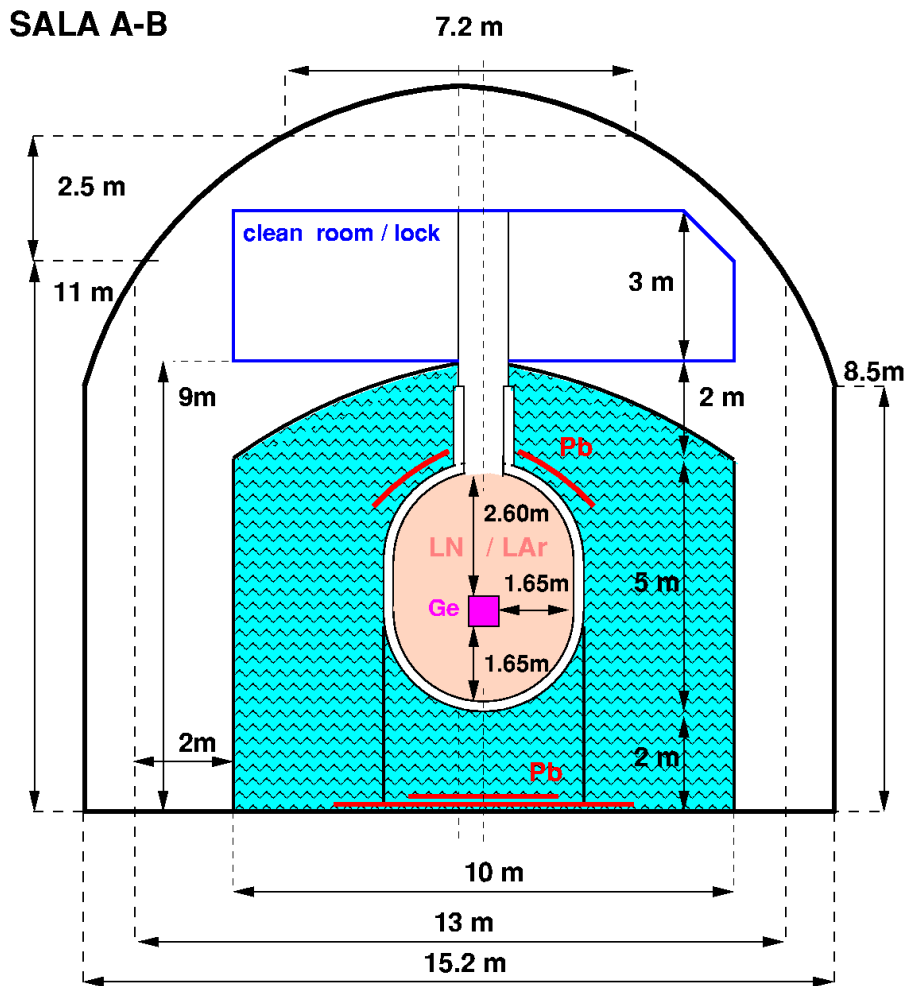
Figure 18: Cross section of the baseline cryogenic and water vessel system with clean room and lock on top. The outer contour line shows the cross section of Hall A.

Table 8: Characteristics of two superinsulated cryogenic vessels: a custom baseline design and an alternative designed by Cryogenmash [CRM 04].

| Design	baseline	alternative	
Material			
	Cu-DHP R240	X10CrNiTi18_9	
radiopurity ^{232}Th	<30 μBq/kg*	20 mBq / kg	
radiopurity ^{238}U		61 mBq / kg	
Geometry			
overall dimensions $\varnothing_o \times$h	4034×7613	4052×8750	[mm^2]
outer vessel $\varnothing_o \times$h	4020×5083	4032×6900	[mm^2]
inner vessel $\varnothing_i \times$h	3784×4600	3500×6500	[mm^2]
neck height	1500	1395	[mm]
neck inner diameter	800	1150	[mm]
inner vessel volume	41	58	[m^3]
volume for liquid gas	33	55	[m^3]
Masses			
empty vessel	17,700	20,700	[kg]
inner vessel		7,700	[kg]
max. load inner vessel		200,000	[kg]
LN fill	26,600	45,000	[kg]
LAr fill	46,000	77,000	[kg]
Pb shield	none	<50,000	[kg]
total max. mass	63,700	147,000	[kg]
Pressures			
inner vessel operating pressure	0.1	0.5	[10^5 Pa]
inner vessel maximum pressure	1.5/-1	3.0	[10^5 Pa]
pressure for LN emptying		0.8	[10^5 Pa]
pressure for LAr emptying		1.2	[10^5 Pa]
outer vessel overpressure	-2	-3	[10^5 Pa]
Superinsulation			
number of superlayers	tbd	45	
nominal insulation vacuum	tbd	10^{-2}	[Pa]
leakage rate	tbd	10^{-5}	[m^{3}Pa/s]
thermal loss (calc./upper limit)	tbd	150 / 300	[W]
corresponding daily loss of LN	tbd	0.15 /0.30 %	
		83 / 165	[ℓ]
Safety			
construction code	AD 2000 HP	PB 03-576-03	
	DGRL 97/23 EG		
earth quake tolerance	h/v : 0.6/0.5 g	0.6 g	

* established for NOSV copper
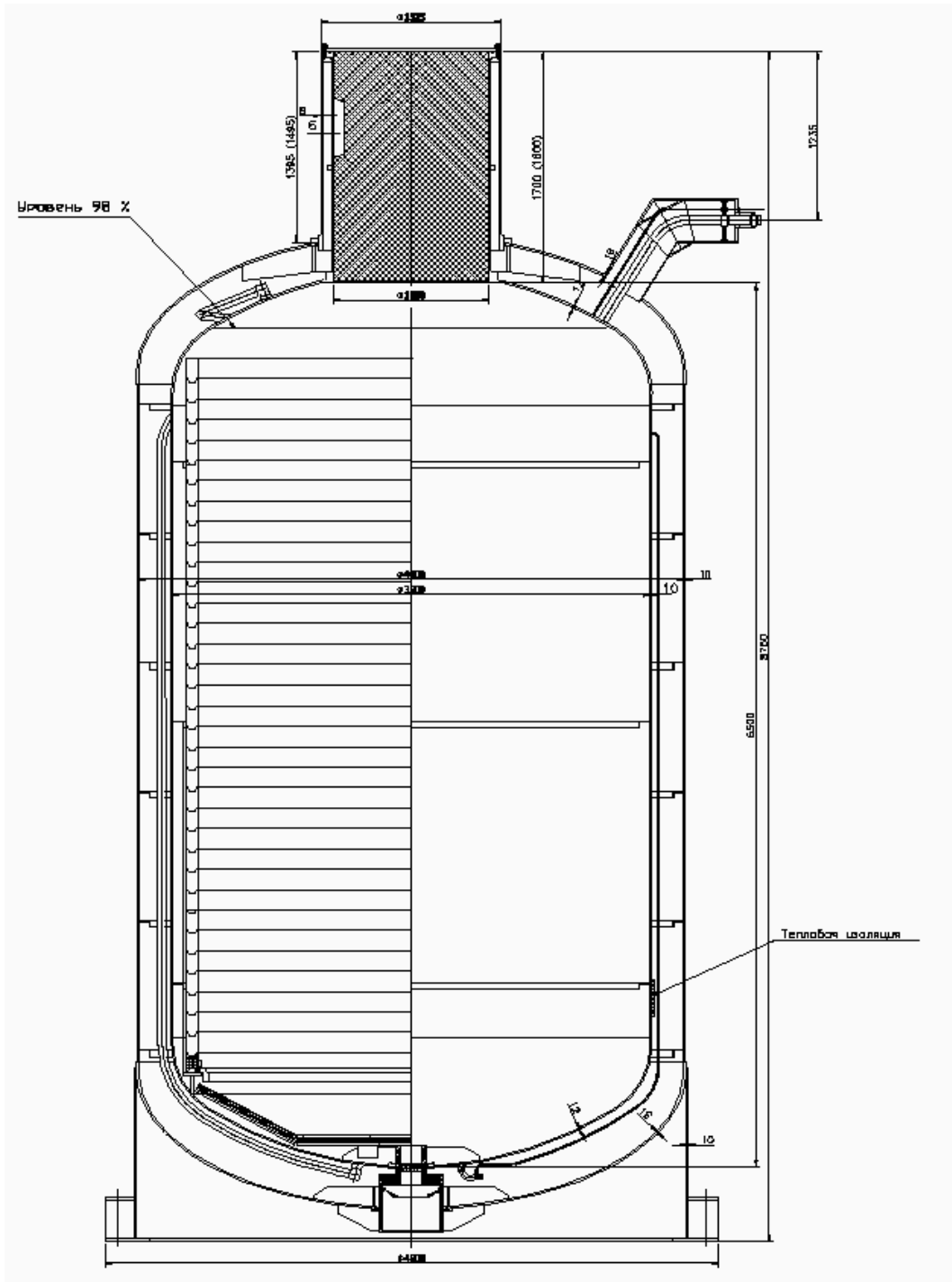
Figure 19: Cross section of a modified commercial cryogenic vessel with superinsulation which is able to carry an internal load − liquid gas and Cu/Pb shield − of 200 tons (design by CRYOGENMASH [CRM 04]).

6.2.3   Alternative design

Our alternative vessel layout is derived from a mature commercial design for superinsulated liquid gas containers engineered by the Russian leader of cryogenic machinery CRYOGENMASH [CRM 04]. The modifications on the conventional cylindrical cryostat include the addition of a 140 cm long neck, an increase of the outer vessel diameter to 400 cm, and reinforcements to carry the additional Pb shield within the inner vessel, see Fig. 19 and Table 8 for a detailed list of specifications. The use of ribs to reinforce the cylindrical vessel walls allows a virtually unlimited height of the vessel. Similar as in case of the copper cryostat, the inner vessel is suspended within the outer vessel by a joint on top of the neck. At bottom the inner vessel is kept centered by a plug entering a socket which warrants the earthquake tolerance of 0.6 g. All necessary pipes are collected at a single superinsulated socket. The superinsulation consists of 45 layers of double-sided aluminized Mylar of 18 g/m^2 and a spacer of 11 g/m^2. Despite of the large inner neck diameter (Ø= 1.15 m) the maximum thermal loss is expected to be less than 0.3% of the liquid gas volume of 55 m^3.

The double-walled vessel is made out of 1 cm thick stainless steel plates with a ^{228}Th activity of 20 mBq/kg. To suppress the corresponding ^{208}Tl surface activity of 85 μBq/cm^2 to the desired level of 1.6 nBq/cm^2, a LN layer of 351 cm thickness would be required which is much larger than the cryostat's inner radius of 175 cm. In fact 163 cm of LN are just enough to reach the desired level if selected Pb of 30 μBq(^{228}Th)/kg (250 nBq(^{208}Tl)/cm^2) is used as graded shield within the cryogenic liquid. The thickness of Pb has to be chosen such that the surface activity of the steel is reduced to a fraction of that of the lead; for a 10% fraction (25 nBq/cm^2 ^{208}Tl), the Pb thickness has to amount to 16.8 cm. Similarly, the thickness of the water shield has to be chosen such that it suppresses the external ^{228}Th activity to a fraction of the steel surface activity; for a 10% fraction the required water thickness is 209 cm.

The effective vertical LN level is about 6 m; by placing the Ge detector array (Ø 50× 50 cm^2) at a distance of 190 cm from the bottom, the LN thickness above the array amounts to 360 cm so that no Pb shield against the steel is needed on top. Moreover, the thickness of lead in front of the cylindrical wall can be reduced taking into account that photons hitting the Ge array see otherwise at non-perpendicular incidence relative to the cylinder wall a larger effective Pb thickness than needed.

Fig. 20 shows a diagram of the infrastructure for the cryostat. A pumping system is foreseen to keep the insulation vacuum below 10^{-2} Pa. The differential manometer is used to determine the liquid gas level. A refrigerator of typically 4 kW power is used to re-condense evaporated liquid. At a maximum thermal loss of 300 W, about 165 ℓ of LN (0.3%) would else be evaporated per day. The pressure specification of the inner vessel allows to empty the vessel by applying the suitable overpressure for LN resp. LAr (see Table 8).
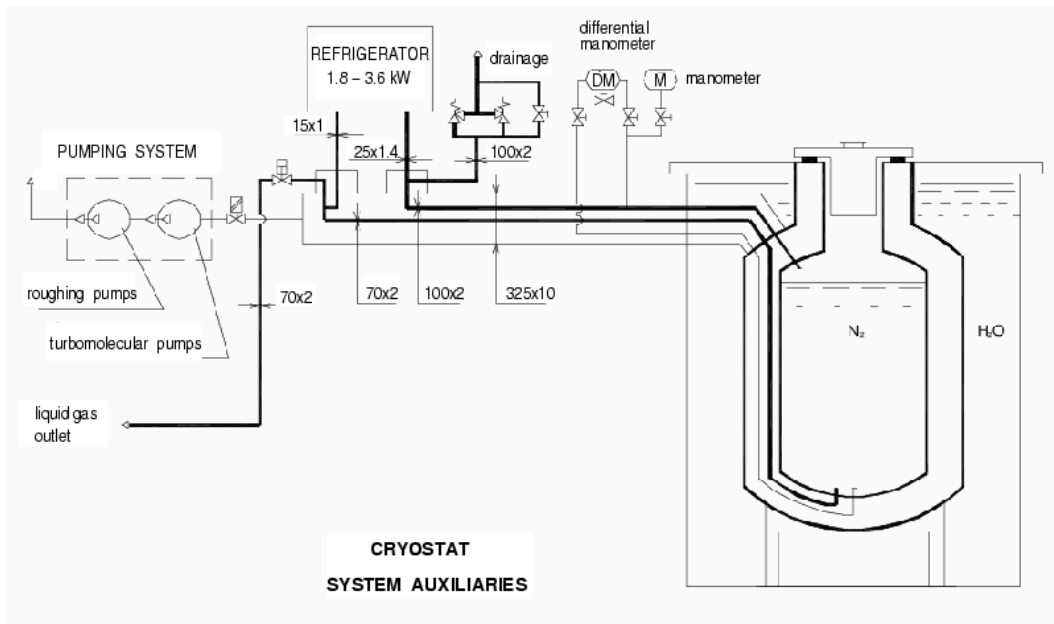
Figure 20: Infrastructure for the CRYOGENMASH cryostat (design by CRYOGENMASH [CRM 04]).

6.2.4   Backup design

A solution similar to option B of our LoI is shown in Fig. 21 which has been developed in collaboration with CMP [Cmp 04], a producer of cryogenic flat bottom vessels. Starting point was a commercial flat bottom vessel with standard perlite/foam insulation of about 1 m thickness. As above, a Pb shield (30 μBq/kg ^{228}Th) inside the cryofluid immediately in front of the inner wall is needed as shield against the activity of the stainless steel (7 mBq/kg ^{228}Th) and the insulation materials which must not exceed the steel's activity. The lead wall can be stacked such that it is self-supporting and exhibits the required stability against earthquakes [JLG 04]. The total load by the Pb shield (170 tons) is, however, too large to be accommodated by a standard flat bottom vessel, and thus both the bottom and ceiling of the vessel need to be modified including a reinforcement by ribs. Compared to the superinsulated stainless steel vessel discussed above, its larger effective internal diameter of 398 cm is of advantage; however, the height of the complete vessel setup of more than 11 m is rather large and cannot be economically reduced. We estimate the cost of this set up to be significantly higher than that of the baseline or alternative designs discussed above, and consider it thus only as a backup solution.

52
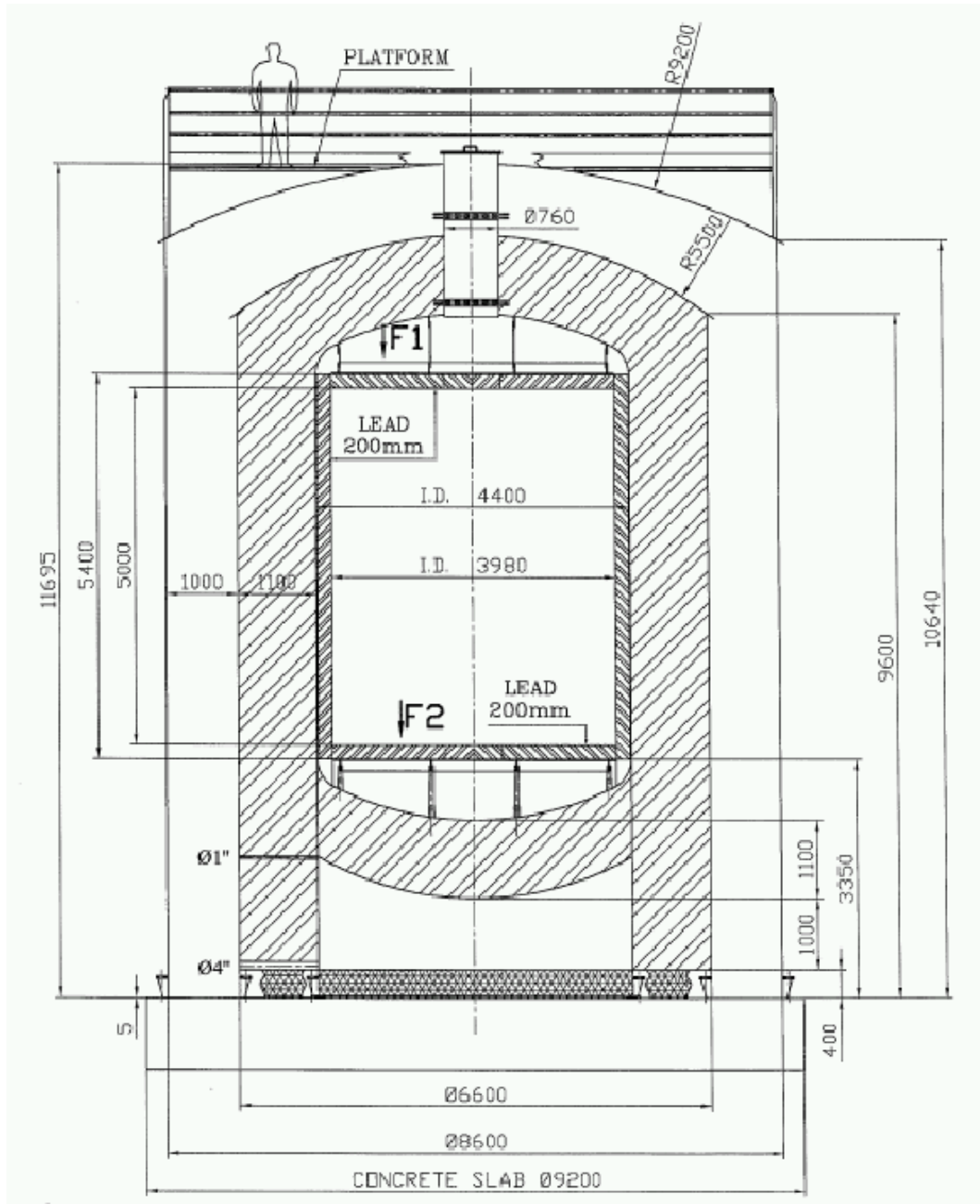
Figure 21: Cross section of a cryogenic vessel with perlite insulation and support structures for the internal Pb shield (design by CMP Arles [Cmp 04]).

6.2.5 Conclusions

Since the LoI, further contacts with manufacturers of cryogenic equipment and an engineering study have established the feasibility to build a superinsulated cryostat from copper or stainless steel that would fulfill the requirements for the proposed experiment. Other than envisaged in the LoI, the solution based on a standard commercial flat bottom vessel turned out to be problematic requiring major redesign in order to accommodate the additional load by the internal Pb shield. Due to high cost and an unfavorable height we consider this design to be a backup solution only.

While the stainless steel cryostat takes advantage of the proven design for commercial high volume production, the custom engineered copper cryostat will still need further optimization of the neck region in order to minimize thermal losses. If the earth quake tolerance of 0.5 g in vertical direction achieved so far is not acceptable also a re-design of the inner vessel support will be needed. Further work is in progress in order to establish that copper with the structural specifications of DHP R240 can be produced with the same radiopurity as NOSV copper ($<23\ \mu$Bq/kg).

Table 9 shows a comparison between the baseline and alternative design as well as with the corresponding specifications for GENIUS and GEM. Obviously, both chosen op-

Table 9: Characteristics of the two design options for the cryogenic and water vessel system. For comparison the corresponding information is listed also for GENIUS and GEM.

Item		baseline	alternative	GENIUS/GEM
Cryostat material		copper	stainl. steel	stainl. steel / copper
Ø×H, overall	[m^2]	10×9	8×10.3	14×19 / 11×11
Ø×H, cryostat	[m^2]	4×7.6	4×8.8	14×19 / Ø 5
Liquid gas volume	[m^3]	33	55	1250 / 50
Water volume	[m^3]	<660	<420	0 / 1000
Mass of Lead	[ton]	≈ 6	<50	0 / 0

tions are more compact than the GENIUS and GEM designs, a consequence of the use of Pb as shielding material and of LAr in order to reach the ultimate background index of 10^{-4} cts/(keV·kg·y). Both cryostats exhibit a diameter of 4 m which allows them to be fabricated in an industrial plant and to be transported to the LNGS. The major difference of baseline and alternative design is that in the latter case a significant amount of lead has to be installed in the liquid gas volume in order to reduce the surface activity of the stainless steel walls to a level that can be sufficiently shielded by LN. This feature might increase total cost, will increase the effective surface of the inner vessel and hence the probability of surface contaminations, and it is also not optimal with respect to the adopted shielding philosophy which aims at keeping large amounts of high Z material as far away from the Ge diodes as possible. Concerning the overall dimensions, the alternative option is more compact in lateral direction; the reduction of its quoted height of 10.3 m to the

desired 9 m would be straightforward by covering part of the bottom of the water vessel with a 10 cm thick Pb shield.

A final decision between both options will be made as soon as the design of the copper cryostat is finalized and a complete cost analysis is available.

6.3   Platform, cleanroom and lock

A platform on top of the vessel supports a penthouse which will feature a local control room, an electronics room, and a cleanroom (class 10,000 or better, with radon reduced air) with the lock into the interior of the vessel. Fig. 22 depicts a possible floor plan of the penthouse as well as some infrastructural details of the cleanroom. The penthouse covers 10 m × 10 m. In addition there is an outdoor area for access. The air supply infrastructure for radon reduction is not yet integrated. The cleanroom with its integrated lock system will allow the insertion and withdrawal of detectors in a modular way. It will take two or three people to assemble detector packages or lower them into the vessel. The complete penthouse together with the water vessel will form a Faraday cage.

The main components of the cleanroom infrastructure can be located through their numbers in Fig. 22. Personnel enter the cleanroom through a classical personnel lock and an airshower. In the lock private storage space will be available. All materials, especially detectors, enter the cleanroom through a material lock suitable for containers up to l=60 cm×d=50 cm×h=40 cm. The lock can be evacuated, heated and flushed with nitrogen. The stations 4-7 will be laminar flowboxes. When not in use they are closed and flushed with nitrogen. As a result, detectors which are under preparation do not have to be transferred if unpredicted breaks are necessary. All station specific tools are kept in holders within the station.

The material lock opens towards the container loading station (4). A passive roller system is foreseen. Storage space for 4 containers will be provided under the workbench. Station 5 will be used to prepare detectors and cables. All work that can be done before the integration of a detector into a package, see sect. 6.4, will be done here. There will be a microscope and probably a small wire bonder. Suction systems will allow mechanical and gluing work.

Stations 6-8 are connected via a rail system below the ceiling. Detector packages are hung on movable hooks. Packages can be rotated. The windows between the stations are opened to allow the transfer from one station to the next. The maximal package height is 150 cm. Lowered tables with integrated suction systems allow easy access to the hanging packages. Packages can be temporarily stored in the area close to the outer wall. During the final assembly the detectors are integrated into the relevant packages, see sect 6.4, and all cables are combined into easily pluggable units. While open the laminar flow consists of synthetic, radon reduced air. During transfer to the outer lock both stations are filled with nitrogen.

The outer lock always contains an ultrapure nitrogen atmosphere. While closed off against the inner lock and the final assembly station it can be evacuated, heated [50 °C] and flushed. After the last cleaning cycle the outer lock will be flooded with nitrogen (or
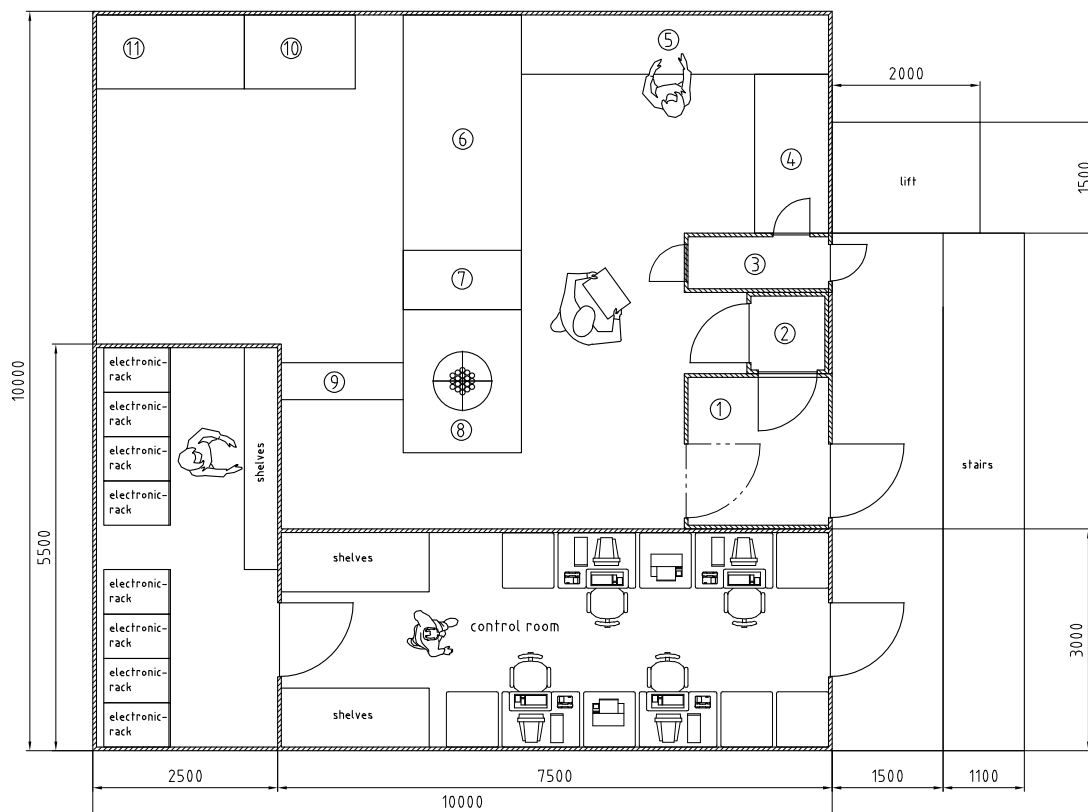
Figure 22: Floor plan of the penthouse on top of the vessel. Some components in the cleanroom are marked with numbers denoting 1: personnel lock, 2: airshower, 3: material lock, 4: container loading station, 5: detector preparation tables, 6: final assembly station, 7: outer lock, 8: inner lock, 9: cable bridge, 10: detector storage unit, and 11: tool-cabinet.

argon) from the boil-off of the vessel and the connection to the inner lock will be opened. A mechanical arm grabs the cables hanging inside the inner lock. After they are pulled into the outer lock they are connected with the help of a glove box integrated in the outer lock. The glove box is shuttered off during non operation and constantly flushed. After the cables are connected the package is transferred into the inner lock.

During normal running the boil-off from the vessel goes through the inner lock. A part of it goes through a valve into the outer lock. The inner lock has the same pressure as the vessel, 1.2 bar. The outer lock has a pressure which is intermediate between the inner lock and the cleanroom. During transfers from the outer to the inner lock both volumes are kept under 1.2 bar. The neck of the vessel opens into the inner lock. It is basically a part of the volume of the vessel. Boil-off from the cryostat has to be brought up to the inner lock through the complete neck insulation system. The central part of the neck insulation

system is a movable plug that is part of the shielding during operation and is pulled up into the lock during loading. Detector packages are hooked to the bottom of the plug. The plug has recesses built into the outer edge to provide space for the cables which go outside. It also contains valves for a controlled gas flow into the inner lock. The holding structure of the plug allows a lead lid to be closed at the floor level while the plug is positioned inside the neck. The lock contains the end part of all mechanical devices needed to attach packages and lower the plug. Steering and control happens from the outside. Cables enter through a panel from the cable bridge (9). They are fixed to holders inside the lock. The inner lock has a webcam for constant surveillance.

The detector storage unit allows the storage for detectors and other materials under radon-free nitrogen atmosphere. The tool cabinet holds all non station specific tools, especially the ones needed for mechanical operations steered from the outside of the lock. This cabinet has normal cleanroom atmosphere.

Cleanroom control and safety. All workstations and the cleanroom itself will have particle counters. In addition the oxygen content and humidity will be controlled.

6.4   Detector suspension

The detectors will be arranged horizontally in layers and vertically in strings. The maximum foreseen load of 5 layers with 19 detectors in each layer is schematically depicted in Fig. 23. The typical distance between detectors is 1 cm. With approximately 2 kg per detector the full load would be ≈ 200 kg.

The suspension system groups the detectors vertically into strings. Such strings can be composed of as little as one or two detectors. Strings on the outside of the package can be moved separately. The seven inner strings are combined into a so called inner tier. Fig. 24 shows the inner tier for 5 layers (left) and an outer string (right).

The detectors in a single string are only held by loops around the detectors. The details will have to be worked out after the final detector specifications are available. In Fig. 24 the detectors in the inner tier are standing on plates. This design as it is would introduce too much material. However, we foresee the necessity for some spacers and holders, even if we adopt a similar design as for the single strings. Detailed MC simulation is under way to optimize the detector arrangement for optimum background suppression by anti-coincidences as well as the placement of irreducible material.

The cabling within each package will be provided by Kapton cables. These have been tested to keep their properties in liquid nitrogen, even after moderate mechanical stress such as multiple rolling cycles. The details of the cabling still have to be worked out and the cables are not shown in Fig. 24. The radiopurity measurement of Kapton cables is pending.

The positioning of the vertical cables holding all packages is guaranteed through copper rings at least 50 cm above the highest detector. Everything below and including the ring is preassembled before the package is transferred into the inner lock as described in sect. 6.3.

At a very early stage of the experiment it is also possible that the inner tier will be broken up into individual strings to test various approaches to reduce material and
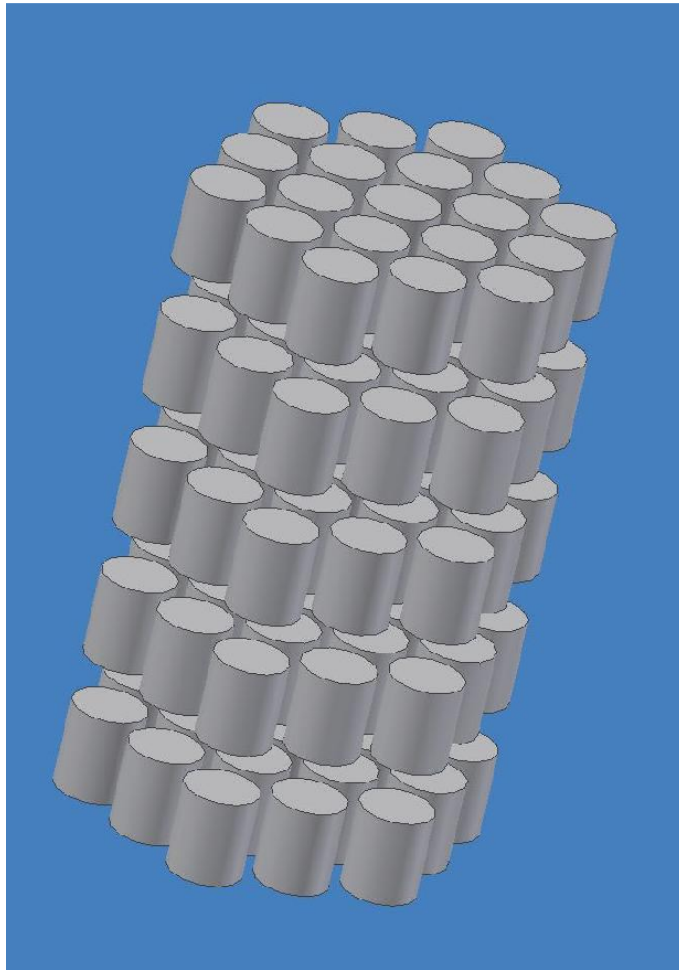
Figure 23: Arrangement of the maximal foreseen load of 95 detectors.

improve its radiopurity. Figure 25 shows one possibility based on high performance fibers and spacers made of polyamide-imides (e.g. TORLON or VESPEL). Here 4 detectors from the Heidelberg–Moscow experiment are combined to form a compact string.

The fiber is tied such that the force is carried up to the top where the spring together with gravity compresses the four crystals into a stable unit. The length of the fiber is only four times the diagonal crystal height and one times the diameter (below each spacer). This results in a total mass of about 0.6 g including the knots (bowline hitch). This mounting should give enough load to the crystals against their spacers so that the incorporated contact points reach the required electrical conductivity.

Detector contacts.   The example shown in Fig. 25 depicts the case of the Heidelberg–Moscow (HDM) crystals (original size). In this case the signal contact has to be pressed against the core bottom. The contact stem can be either made from the same thermoplastic as the spacers with a thin wire running over the tip and fixed onto the two broadenings (to
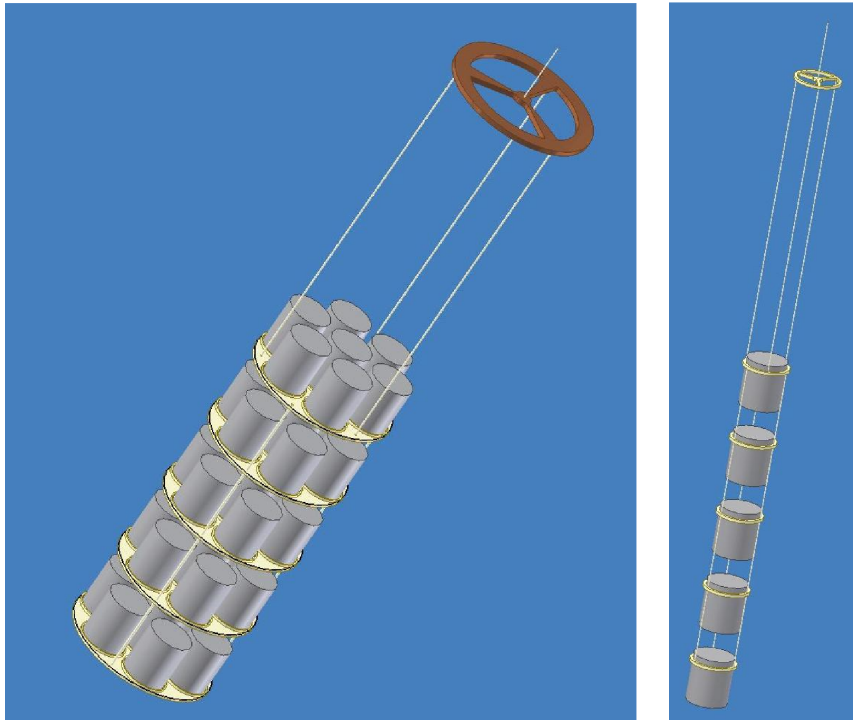
Figure 24: Inner tier[left] and a single outer string[right]. Cabling is not shown.

guide the stem within the core) or of electro-formed copper. A spring coil below the stem maintains the pressure under variable temperature conditions. In the GENIUS TF a similar solution is applied. As to the inner contact of the IGEX type diodes (and presumably of the new enriched diodes), a steel spring wire of 0.5 mm diameter could be applied, or alternatively a Chinese hat, again made of electro-formed copper. The spring wire solution would allow to save material in the core but also at the spacer (no spring and a much thinner connecting bar).

The HV contact is in both cases (HDM and IGEX) a thin copper braid wire which opens up behind the feed through point like a flower, so that a rather flat structure is facing the beveled rim of the crystal. A thin gold foil could be added between the braid and the diode to improve the contact quality. For the IGEX type diodes this fixture has to be placed at the very rim before the flat bottom area starts. The earlier discussed solution with a spring wire tightly – by use of a tiny spanner nut – laid around the outer surface of the Ge cylinder is a backup possibility for both mountings. Tests with natural isotopic diodes of the same type are foreseen.

Radiopurity. High performance fibers have been intensively studied in BOREXINO and KAMLAND. The general outcome was that they are subject to potassium contamination, mostly originating from coatings. This is also the case for the so far investigated DYNEEMA qualities, our favored fiber in view of temperature compatibility. The measurements yielded
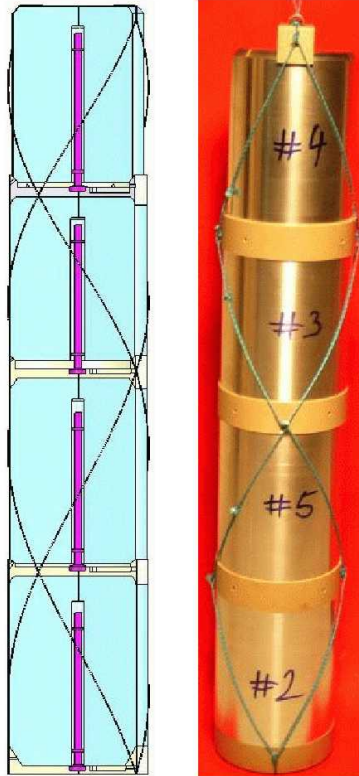
Figure 25: String out of four diodes of the HDM type. The numbered Al mockups represent the actual size of the respective detectors.

^{40}K concentrations between 0.3 and 1 Bq ^{40}K/kg. A very rough scaling from the potassium contamination in the cladding material of the HDM detectors (average about 700 μBq ^{40}K/kg) by the same reduction factor as envisioned for the background index at 2 MeV 10^{-3} cts/(keV·kg·y), shows that the K contamination needs to be reduced by about three orders of magnitude. For ^{226}Ra and ^{228}Th the situation is less dramatic. A highly sensitive measurement with GEMPI below the present upper limits in the 50 mBq/kg range for both sub-chains is underway. Detailed Monte Carlo calculations for the rope (about 0.6 g around each crystal) and also for the other materials are required to overcome the present uncertainty in the allowed impurity. We continue the search for fibers of higher radio-purity. For example, TENSYLON, an ultra high molecular weight polyethylene, of which the holding ropes of the BOREXINO inner vessel are made has about 20 times less potassium [Arp 02]. A rope made of TENSYLON needs to be slightly thicker for the same strength but has a slightly lower creep than DYNEEMA. Creep plays an important role in long term considerations of the suspension at least at the room temperature section of the ropes. The low temperature behavior of TENSYLON has still to be tested. We also investigate the possibility to wash off the potassium containing compound of DYNEEMA as advised by the producer.

The radio-purity situation in case of the thermoplastic spacers is more relaxed, at least no indications for K, Ra and Th impurities above a few 10 mBq/kg have been detected by us for VESPEL. TORLON, which is somewhat better suited for liquid nitrogen temperature will be analyzed next for its radio purity. However, the mass of each spacer is between 20 to 30 g, i.e. about two orders of magnitude more mass compared to the fiber is seen by the middle detectors.

The springs will be made from brass. For this material we are more confident to find clean charges. Some material selected for the HDM and GEMPI detectors is left and will be remeasured at higher sensitivity. The top spring to tighten the fiber on each string can be shielded by e.g. Ge-metal against the diode if required. The 0.5 g steel spring wire was tested at some ten mBq/kg level (upper limits) at Heidelberg.

6.5 The muon veto system

In section 3.3.2 the muon induced background is discussed. A first version of the simulation results in an unacceptable large index of 0.01 cts/(keV·kg·y), if no discrimination of these events is foreseen. To reduce this background, we plan to instrument the water buffer as a Cherenkov detector. Moreover, plastic scintillator panels on top of the detector will tag muons which enter the cryostat through the neck without intersecting the water buffer. In case that LAr is used as cryogenic shield, its scintillation light can be used as an additional muon veto signal.

6.5.1 Plastic scintillator muon detectors

The region above and around the cryostat's neck will be covered with plastic scintillators since here the efficiency of the water Cherenkov detector is zero or poor. The precise geometrical coverage of the system has still to be determined by Monte Carlo simulations; a first estimate yields an area of about 4×4 m^2.

The scintillator modules will be fabricated along the design developed for the new central and forward muon counters for CDF II [Art 04]. The typically 0.5 m wide and 2 m long modules (Fig. 26) are made from a high quality polystyrene-based scintillator material (UPS 923A) of 4 to 5 cm thickness for excellent photon/muon separation. A novel light collection technique uses wavelength shifting (WLS) fibers (Kuraray Y-11(250)M) to extract the scintillation light from the longer side of the module reducing so the path length of the light in the bulk material and in consequence deteriorating transmission effects present in conventional designs. A further equalization of light collection efficiency is obtained by a suitable arrangement of light absorbing black strips on the module's surface. The use of the fiber bundle eliminates the need of lucite light guides and features in particular a rather small cross section that allows to use PMTs of small diameter. We envisage to use the Hamamatsu H6780 model which includes high voltage divider and integrated high voltage power supply or the H5784 model with an extra integrated amplifier. The total number of modules and PMT channels will be about 25 including spares.
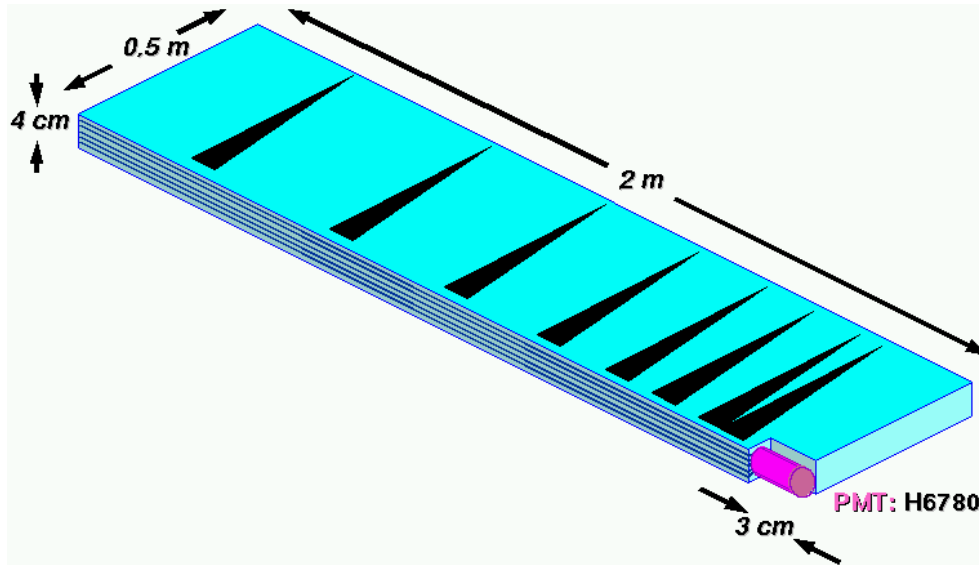
Figure 26: Scintillator module using a WLS fiber light guide for readout as well as a set of black strips for equalizing light collection.

6.5.2 Water Cherenkov muon detector

The concept and design of the water Cherenkov detector follows earlier work for the BOREXINO Outer Detector, one part of the muon identification system [Obe 98]. The results of the MC simulations can be adapted for our design provided that the thickness of the water buffer, the PMT area density and the type of reflectors are similar. The minimal thickness of the water buffer in BOREXINO is 2.15 m compared to 2 to 3 m in this experiment. However, the distance between the bottom of the cryogenic vessel and the floor may be as low as 1 m and thus will require a higher PMT area density. An optimized distribution of PMTs on the bottom side of the outer vessel will be worked out once the design of the cryostat and support structure is frozen.

The number of PMTs will also depend upon the medium that will be used to reflect the Cherenkov light from the vessel walls. In case of BOREXINO the well proven Tyvek plastic foil has been used for this purpose. Recent work with wavelength shifting mirror foils indicates that an alternative design with improved performance and reduced costs might be feasible. The decision which design to implemented will be taken after completion of a comparative design study.

The region between the water vessel (generic dimensions: diameter and height approx. 10 m, volume 785 m^3, surface 471 m^2) and the cryogenic vessel (diameter 4 m, height 6 m, volume 75 m^3, surface 100 m^2) is filled with about 700 m^3 of ultra-clean water. In the baseline design the outer wall of the cryogenic vessel and the inner surface of the water vessel are covered with 0.2 mm thick Tyvek plastic sheets. Tyvek is a white polyolefin plastic with a diffuse reflectivity of over 90% for visible light. Its spectral reflectivity has been

measured and is displayed in Figure 27 (left) together with the PMT quantum efficiency and the primary photon spectrum. Cherenkov photons can impinge either directly on the
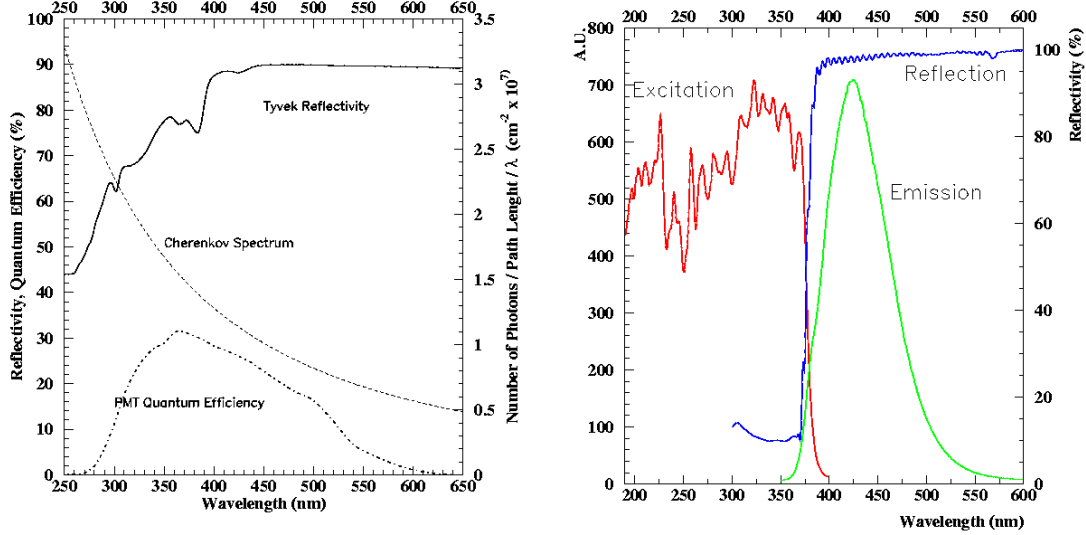
Figure 27: Left: The spectral reflectivity of a 0.2 mm Tyvek plastic sheet is displayed together with the ETL 9356 photocathode efficiency and the primary Cherenkov spectrum. Right: Optical properties of the 3M radiant mirror foil. The excitation spectrum is well matched to the primary Cherenkov spectrum and the fluorescence to the PMT spectral sensitivity.

photomultiplier cathode or after (several) reflections from the Tyvek film. The diffuse character of the reflection distributes the photons over a large surface area and hence increases the number of triggered PMTs.

The overall shielding material in between the PMTs and the germanium diodes must be sufficient to reduce gamma emission by the radioactive impurities of the PMTs. Table 10 summarizes measurements of the radioactive impurity levels of the low-background glass used for PMT construction provided by Electron Tubes Limited (ETL). Comparison with earlier measurements [Arp 02] indicate variations of the impurity levels within a factor of two for ^{226}Ra and ^{228}Th, and a factor eight for potassium. The radioactivity of the glass dominates over the contribution from the other parts of the PMTs including their encapsulation [Arp 02]. Two different PMT arrangements are foreseen depending on the design of the cryogenic vessel.

For a super insulated copper cryostat the PMTs will be located on the wall of the water vessel to provide sufficient shielding as displayed in Figure 28. The ^{228}Th activity of the PMTs per unit area is $40 \cdot 10^{-3}$ Bq/m^2 compared to $< 6 \cdot 10^{-3}$ Bq/m^2 for copper. One meter of water buffer reduces the 2.6 MeV gamma flux to $1.4 \cdot 10^{-2}$ of the initial value, thus

Table 10: Radioactive impurities of low radiation glass supplied by ETL, of PMTs using this glass, and of the 3M radiant mirror foil VM2000 (86 g/m^2). 'Glass^a' refers to earlier measurements [Arp 02] and 'Glass^b' to a recent sample from the same supplier measured in August 2004. The total mass of glass per PMT is about 400 g. A PMT area density of one PMT per 2.8 m^2 is assumed.

		^{226}Ra	^{228}Th	^{40}K
Glass^a	[Bq/kg]	0.82	0.13	0.50
Glass^b	[Bq/kg]	1.80	0.30	3.80
Total^b / PMT	[Bq]	0.72	0.12	1.52
Activity/ area	[mBq/m^2]	260	40	540
VM2000	[mBq/kg]	< 8	< 11	76 ± 34
Activity/area	[mBq/m^2]	< 0.7	< 1	6.5 ± 2.9

providing sufficient shielding against the PMTs. About 170 PMTs are needed to cover the surface of 471 m^2 with a density of one PMT per 2.8 m^2.

In case of a steel/lead cryogenic vessel, the relevant area activity is that of steel of 1.8 Bq/m^2 which is large compared to that of the PMTs. Thus the contribution of the PMTs is negligible. In this design option the PMTs can mounted on the outer surface of the cryogenic vessel. For the same area density only 36 PMTs would be needed (Figure 28b). However, given the large difference between the radii of the vessels, a larger PMT area density is required to achieve the same pe yield. Monte Carlo studies will determine the exact PMT area density.

Given the absence of additional shielding in case of the copper cryostat, the water specific purity needs to be superior with respect to the steel/lead design. The impurity levels in water should not exceed those of copper. Assuming secular equilibrium the values translated in g/g are $< 1.6 \cdot 10^{-12}$ gU/g and $< 5.7 \cdot 10^{-12}$ gTh/g.

Water being purified by the BOREXINO Counting Test Facility (CTF) water plant can achieve values as low as $(3.0 \pm 0.4) \cdot 10^{-3}$ Bq/m^3 for ^{222}Rn [Sim 03], and $< 2 \cdot 10^{-3}$ Bq/m^3 for ^{226}Ra [MPI 03]. This is well below our requirements. Direct measurements of uranium and thorium were limited by the sensitivity of the measurements at 10^{-12}g/g.

Measurements inside the CTF tank showed typical ^{222}Rn concentrations in water at about 20 mBq/m^3, thus at the level of the copper impurity, and much higher than in the feeding water. The main source was the epoxy layer coating the carbon steel tank. In our design, the outer tank is build out of stainless steel, thus no protecting layer is required. Nevertheless care needs to be taken about the materials and their radon emanation used inside the water Cherenkov detector.

It should be emphasized that the dimensioning of the copper vessel is based on the ^{208}Tl (^{228}Th) contaminations. Given the different branching ratios of the ^{214}Bi line at 2.204 MeV with an emission probability of 4.86% and that of the ^{208}Tl 2.615 MeV with 35.6% with respect to ^{228}Th, the tolerable specific ^{226}Ra (^{238}U) activity is larger by a factor
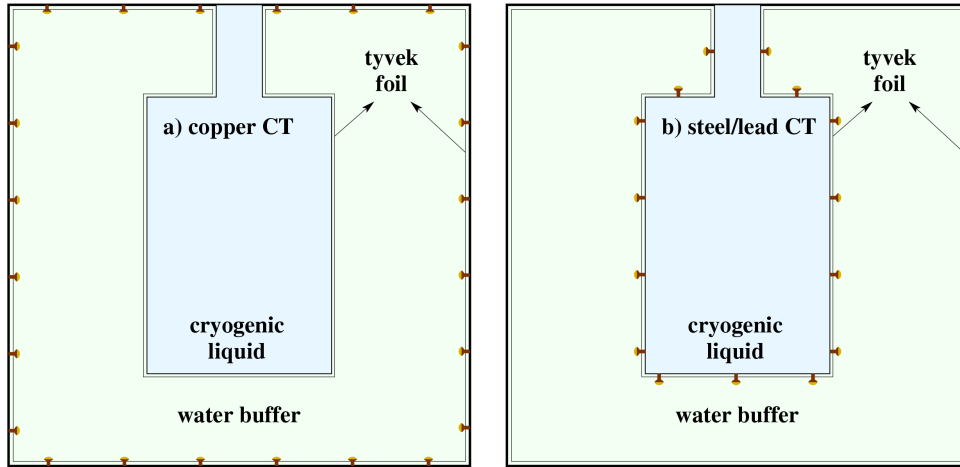
Figure 28: Reference design using Tyvek foil as a diffuse reflector. Location of PMTs in case of a copper (a) and a steel/lead (b) cryogenic vessel.

of seven. Moreover, the fact that the 2.204 MeV photon is attenuated stronger than the 2.615 MeV adds a further safety margin. In liquid argon, for example, the respective values for attenuation to 1/e of the initial flux are 16.9 cm and 18.6 cm.

Based on this estimate, we conclude that the design goal for the water purity in case of a copper cryostat is that the concentration should not exceed approximately 20 mBq/m^3 of ^{222}Rn or ^{226}Ra in the water. Somewhat more stringent values are required for ^{228}Th.

The encapsulation and water sealing of the PMTs follows the design developed for the BOREXINO CTF-2 as displayed in Figure 29 [Res 01]. The PMT is connected through a connector by a single cable carrying high voltage and signal. An optical fiber will be connected to each PMT, or to subgroups of PMTs to illuminate them at the single photoelectron level to provide precise timing and pulse height calibration. A VME card has been developed for the BOREXINO detector [Pei 03] which could be used for this purpose. The can is made out of stainless steel and is sealed to the glass with a flexible polyurethane layer and a heat shrinking tube glued from the outside. It is filled with reforming silicon gel to protect and electrically isolate the voltage divider and connecting pins. The design will be modified such that the connector and cable enters under 90 degrees with respect to the can.

After five years of operation of this PMT design in the CTF, an overall failure of approximately 20% has occurred.

Performance of the water Cherenkov detector. Optimization and performance studies of the muon veto still need to be carried out. Given the similarity of this design with that of BOREXINO, we report results of the Monte Carlo studies of the Outer Detector performed for BOREXINO [Obe 98].They are intended to illustrate the expected performance of the muon veto.
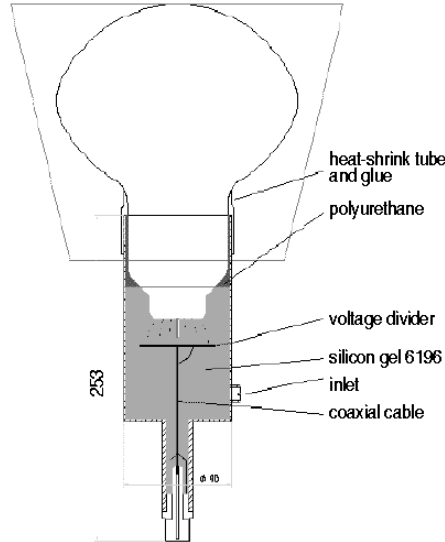
Figure 29: The BOREXINO CTF-2 waterproof PMT design [Res 01]

.

In BOREXINO, muons intersecting the nylon vessel have a path length of 4 m or more in the Outer Detector. These sample of muons generate about 260 photoelectrons (pe) distributed over 90 PMTs. The number of pe are not uniformly distributed on the triggered PMTs. 'Hot-spots' close to the intersection points of the muon track with the surface covered with PMTs are observed: up to hundred or more photoelectrons are collected by one or two PMTs while adjacent PMTs collect typically 10 pe's. PMTs at larger distances from the intersection point give signals at the single pe level. According to the MC simulation, muons passing through the non-scintillating buffer are tagged with an efficiency of 100% if requiring a coincidence of 10 PMTs. However, details of light obstructing objects or 'muon tunnels' in the detector, as cable bundles were not included in the simulation. The PMT area density has been chosen to allow a 20% failure rate within several years without deteriorating the efficiency of the veto system.

Alternative design. The Cherenkov light collection and conversion into photoelectrons can be increased using birefringent mirror foils. These foils are produced by 3M and distributed under the brand name radiant mirror foil, Vikuiti ESR, or earlier VM2000. To our knowledge, the foil has been first used in a prototype detector for a large cosmic ray calorimeter [Ste 02]. Later it has been employed in the LENS prototype detector as light guides [Mot 04] as well as in the design of the liquid argon scintillation read out as presented in this proposal.

The radiant mirror foil serves two functions in the design: 1) as a wavelength shifter and

66

b) as a high reflective mirror light guide. Cherenkov photons with wavelength below 380 nm are absorbed and re-emitted with a wavelength-dependent quantum efficiency between 30% and 50%. The fluorescence is emitted isotropically in 2π at wavelengths around 420 nm. This light is propagating in the water buffer and reflected off the walls which are covered by the mirror foil with a reflectivity of $(98.5 \pm 0.3)\%$ measured at 430 nm [Mot 04]. Provided that the attenuation of the water is of the order of several tens of meters, the shifted photons can be guided to the PMTs without undergoing substantial loss. Figure 27(right) shows the optical characteristics of the radiant mirror foil.

The intrinsic radioactivity of the mirror foil has been investigated with HP-Ge spectrometry at Lngs. With surface activities (Table 10) significantly lower than those of the copper cryostat, the mirror foil can be mounted at its outer surface without increasing the background index. Aging tests of the foil submersed in deionized water for one year, partially at elevated temperature (40 degrees Celsius), did not show any degradation of the optical properties.

With all surfaces covered with mirror foils, we can reduce the number of PMTs to approximately 1 every 8 m^2 compared to 1 every 2.8 m^2 in the Borexino layout. Monte Carlo studies need to be carried out to optimize the number of PMTs and their exact location.

6.6 Electronic readout

Figure 30 shows a schematic of the readout chain for one Ge diode. For optimum noise and speed the input FET of the charge integrating preamplifier is placed close to the detector within the cryofluid. The pre-amplified signal is sampled by a flash ADC (FADC); two such units of high and low gain may be needed if the dynamic range of one unit is not sufficient. Further signal processing including filtering will be done fully digital by digital signal processors (DSPs), field programmable gate arrays (FPGAs) or standard PCs. Algorithms for the real time digital synthesis of pulse shapes have been established [Jor 94, Jor 03] for deriving the optimum information on energy and time from a given signal.
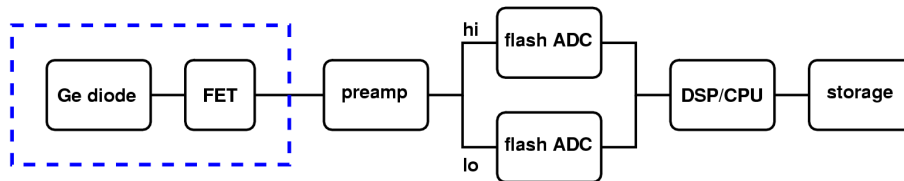
Figure 30: Schematics of the electronic readout chain.

The distance between Ge diode and preamplifier of more than 5 m is bridged by a cable that should be flexible, even at LN temperature, hold high voltages up to 4 or 5 kV, exhibit a low impedance for maintaining the pulse characteristics in the time domain, and be well shielded to minimize cross talk; in addition it should consist of radiopure materials only. Tests showed that Kapton cables with copper traces represent a promising candidate.

In cryostat-housed Ge detectors, the FET of the preamplifier stage is usually mounted close to the diode on the cool finger. A little piece of plastic between cool finger and FET serves as thermal impedance and makes the FET run at about 20°C above the LN temperature at optimum noise performance. This approach is presumably not possible in LN, and it has to be investigated if there are commercial FETs available which are suited to run at LN temperature, or a dedicated FET has to be designed which does not exhibit carrier freeze out. Since the cable between FET and preamplifier might be still several meters long, the most straightforward way to best performance will be to put not only the FET but the whole preamplifier close to the diode, which - on a few mm^2 large silicon die - can be realized by a fully integrated VLSI solution. The developments for γ ray tracking detectors like AGATA [AGA] have resulted in frontend electronics optimized for pulse shape analysis with segmented Ge detectors. Besides discrete hybrid solutions also fully integrated ASIC designs are pursued [Del 03]. Typical specifications include a noise level of 1 keV, a bandwidth of 20 to 30 MHz, a dynamic range of 1000, and a FET power of less than 25 mW which makes these frontends extremely interesting also for the present application. R&D on such a device can be done also at the Heidelberg ASIC laboratory where the MPI Kernphysik has developed VLSI readout ASICs for silicon strip detectors.

For the pulse shape sampling and digital signal processing units, several options are available. The commercial fully digital spectroscopy modules of XIA's DGF4C series [XIA] have been chosen as a reference by the MAJORANA collaboration [Maj 03]. The CAMAC based DGF-4C as well as the DGF Pixie-4 module in the CompactPCI/PXI standard provide digital spectrometry and waveform acquisition for four input signals per module with the possibility to combine several modules into a larger system. In the Pixie-4 the signals are digitized in a 14 bit FADC at 75 MHz. Triggering, filtering and time-stamping of the data stream is done in real time in a field programmable gate array (FPGA), and the resulting data can be read out by a computer at up to 109 MB/s. – An alternative more cost-effective solution is represented by the GRT4 VME pulse processing card which has been developed for the determination of position, energy and time of an γ event in a segmented Ge detector [Laz 03]. Each of its four channels has a 40 MHz low pass filter including an optional differentiation stage followed by a 14 bit 80 MHz FADC. The VHDL hardware language is used to implement the desired algorithms in the FPGA. An in-beam test with a 33% efficient Ge detector has shown that the energy resolution is the same as with conventional analog electronics. – A third even more cost-effective solution [Kih 03] uses the 8-channel SIS3300 VME FADC module with 100 MHz sampling rate at 12 bit precision. The module is self-triggering and has two memory banks which allow data transfers at 7 MB/s. A low noise amplifier in front of the FADC is used to adjust gain and dc offset. All digital signal processing including pulse shape analysis, integration and pole/zero cancellation was done by a VME CPU with an Intel p3/850 MHz processor running a Linux operating system. This system showed a similar energy resolution as an analog system at a maximum count rate of 4000 events/s and has been installed in the GENIUS test facility at LNGS [Kla 03a].

Alternatively, collaboration members are working with the pulse shape sampling system MD^{2}S (MARS Detector Digitizing System) that was developed for the segmented detector

MARS [Iso 02]. The compatibility between the preamplifier (PA) signals and the fast ADC (FADC) is ensured by a signal conditioning stage that can be easily changed to account for different input PA signals. It allows for gain and offset variation. Antialiasing of the signals is performed in order to remove high–frequency components above 30 MHz. The signals are then continuously digitized by a 12 bit 80/105 MHz FADC AD9432 (from Analog Devices) of following characteristics: range ± 1 V, integral linearity ± 0.5 LSB and differential linearity ± 0.25 LSB. The sampling frequency can be controlled by an external clock with frequencies up to 100 MHz. The sampled data are stored in a circular buffer from where they can be retrieved when a trigger arrives. The data readout is controlled by a FPGA. – The FADC and the signal conditioning card are mounted in a low noise environment (NIM) while the FPGA is mounted on a GIII PCI board developed at CERN. On the same board a 32 MB SDRAM memory bank is installed to store data and informations. The communication between the NIM modules and the PCI cards is done through a low–noise high–speed LVDS cable. Each NIM–PCI board system holds 4 channels. The PCI boards can be mounted in a PCI extender or directly in the PC on 32 bit PCI slots that allow a data throughput of up to 132 MB/s. – The system is controlled by a driver module inserted in the Linux kernel of a PC and works in interrupt–based data transfer. Data are stored on hard disk. Analysis of the data is done by a program package developed for the MARS detector running under Linux and Windows operating systems. Test measurements were performed with an 80% HPGe detector at a sampling rate of 60 Msps and 1 kHz of trigger rate using standard calibration sources and precision pulse generators. The measured electronic noise was about 1.1 keV and the quality of the spectra is the same as in the case of using standard analogue electronics.

In conclusion, various attractive readout systems are existing or are becoming available. The final choice will be in due time.

6.7 Data acquisition and Slow Control

The data acquisition system will gather the data of the Ge diodes and of the muon counters, and store them with a time stamp on tape. Neither channel count nor acquisition rate will represent a problem - even the muon count rate is only several 10^{-4} events per (m^{2}s). The major requirement will be rather the highest possible operational availability and stability.

The slow control system handles traditionally the non-time critical tasks. It transfers the whole detector system from the safe stand-by mode into the running state (or vice versa) by activating the low voltage power supplies and setting the high voltages for the photomultipliers and Ge-diodes. Concurrently it is reading at typically a few Hz the various system parameters, and stores any changes of their values with a time stamp in a data base for later retrieval. It also provides a graphical user interface for a breakdown of the status of the various subcomponents, as well as for loading experiment configuration files. Typical system parameters include

- from the vessel: pressure, temperature, gauge of cryogenic fluid and water,

- from the detectors: leakage currents and base currents of the photomultiplier tubes,

- from the electronics: power supply voltages and currents, status of crates, temperatures,

- from the cleanroom: air pressure, oxygen level, radon level, particle concentration,

- from the environment: barometric pressure, humidity, temperature, oxygen level, status of smoke detectors.

If safety relevant alarm conditions are detected, they are immediately communicated to the programmable logic controller (PLC) which forwards them to the LNGS general safety monitoring system. For most safety critical parameters, however, the detour via slow control is avoided and the monitoring hardware will send its alarm signals directly to the PLC.

The full computerization of the data acquisition and slow control system will allow the sharing of acquired data among all collaboration members practically in real-time, as well as the reliable remote monitoring and control of the whole experiment.

6.8 The LArGe Test Bench

The Liquid Argon Germanium Test Bench (LARGE-TB) is a shielded low-background cryogenic dewar system which will be operated underground at the LNGS using the former LENS Low-Background-Facility (LLBF) shielding system and cleanroom barrack. The LARGE-TB has several objectives:

1. to verify low background of HP Ge detectors prior to the operation of GERDA, establishing thus procedures of detector handling,

2. to investigate the performance of the background suppression by liquid argon scintillation light readout on a prototype scale, and

3. to provide a material's screening facility with so far unreached sensitivity.

One major milestone of the LArGe-TB project will be the operation of a segmented germanium detector with simultaneous liquid argon scintillation readout.

The LArGe-TB consists of a cylindrical dewar tank, equipped with photomultiplier tubes (PMTs), enclosed by a graded passive shielding system (Fig. 31). A double chamber
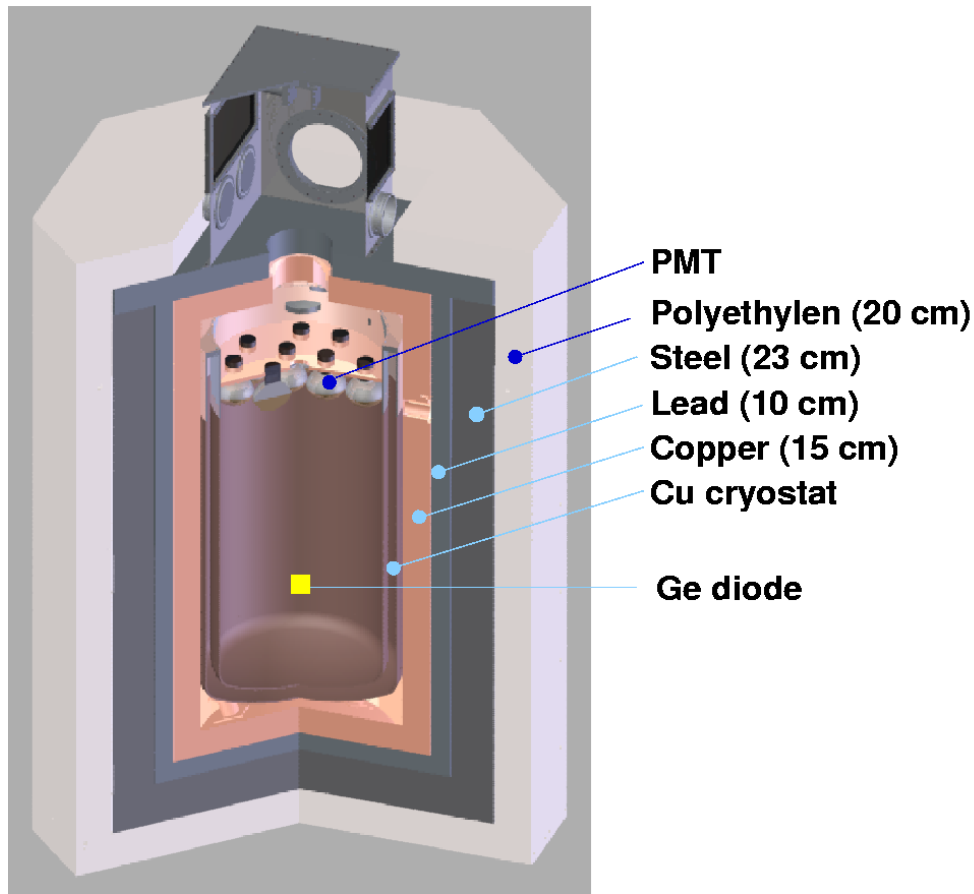
Figure 31: Artist's view of the LArGe-TB. The dewar has a diameter of 1 m and a height of 2.2 mm; the overall height of the shield is 3.6 m and its width is 2.5 m.

lock on top of the shield provides access for detector insertion. A handling and filling system for liquefied argon connects to the dewar.

A cylindrical super-insulated copper dewar with an inner diameter of 90 cm and a height of approximately 200 cm (volume 1.3 m^3) is located in the center of the LArGe-TB. Its inner walls are covered with wavelength shifting and reflecting foil (e.g. VM2000). Twelve 8" PMTs (ETL 9367 KFLB) mounted in the upper part view the LAr target. A graded

passive shielding system with increasing purity levels reduces the external background: 20 cm of polyethylene at the outside is followed by 23 cm of steel (7 mBq/kg ^{228}Th), 10 cm of lead ($< 22\mu$Bq/kg ^{228}Th) and 15 cm of copper ($< 23\mu$Bq/kg ^{228}Th). The final active shielding layer consists of 41 cm of liquid argon for a germanium diode with 4 cm radius suspended on the central axis of the dewar.

For normal incidence, the steel/lead/copper layer attenuates the 2.615 MeV gamma line from ^{208}Tl to $5 \cdot 10^{-8}$ of the initial flux. The graded shielding is designed such that the residual external gamma flux at the detector is dominated by the inner most copper layer. This is possible since the surface activity of the reflecting VM2000 foil (86 g/m^2) is small compared to that of the copper (see Table 7). Similarly, despite of the high specific activity of the ETL PMTs (see Table 10), their background contribution is below the copper limit due to their overall low mass and their minimum distance of 100 cm from the Ge diodes. Extensive MC studies have been carried out to simulate the external background coming from ^{208}Tl decays in the bulk of the shielding material. With passive shields of LN or LAr, the background index from ^{208}Tl at $Q_{\beta\beta}$=2039 keV is calculated to be 0.09 resp. 0.04 cts/(keV·kg·y). An active LAr shield yields an additional suppression by almost one order of magnitude.

It is planned to get the LArGe-TB operational already during 2005.

6.8.1 Instrumentation of liquid argon

The scintillation properties of liquid argon are well known [Kub 79, Dok 90, Hit 83, Cen 99]. About 40,000 photons per MeV are emitted at a wavelength of 128 nm. The decay times of the singlet state is $\tau_S = 6$ nsec and of the triplet $\tau_T = 1.6\,\mu$sec. Their intensity ratio I_T/I_T is 0.3 for electrons and 1.3 for alpha particles [Hit 83] thus providing the possibility for efficient pulse shape discrimination.

The potential to discriminate backgrounds by using the scintillation light depends critically on the efficient detection of 128 nm photons. The strategy which we pursue is to shift the XUV photons to wavelengths around 400 nm and guide them via reflecting foils to photomultipliers submerged in the liquid argon.

A further requirement is that materials for shifting and guiding the scintillation photons to the PMTs, as well as the PMTs themselves must not augment the background signal in the germanium detectors. Details on radio-purity measurements are given in section 6.8.

In laboratory experiments we investigated the feasibility of this novel background discrimination method [Sch 04]. The experimental set-up consists of a lead shielded, closed dewar system with approximately 30 cm diameter and 80 cm height in which a bare germanium crystal with a mass of 165 g is suspended in liquid argon. A wavelength shifting and light guiding foil (VM2000) in form of a cylinder with 20 cm diameter transports the scintillation light to an 8" PMT (ETL 9357 KFLB) which is covered by a wavelength shifting transparent window [Res 04].

Figure 32 (top) shows the spectrum of a ^{54}Mn gamma source (835 keV) with and without anti-coincidence of the scintillation light; the source was placed within the LAr about 4 cm away from the crystal. A Monte Carlo simulation reproduces the spectral shape
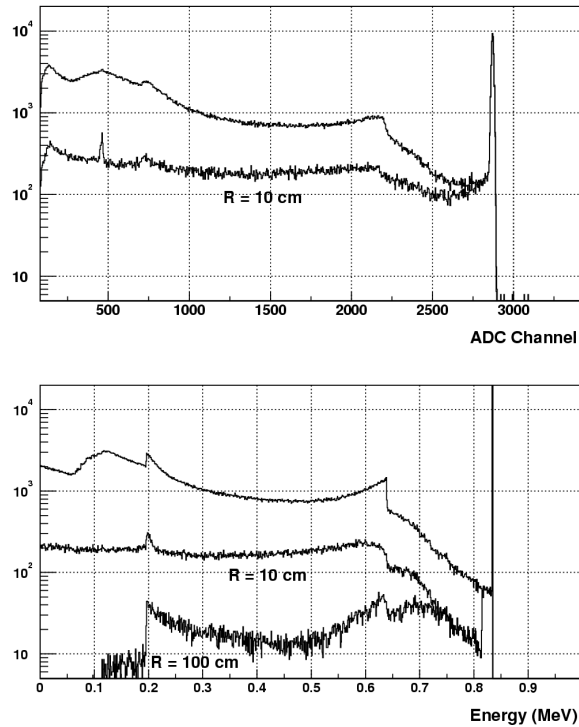
Figure 32: Operation of a HP-Ge detector in liquid argon with simultaneous scintillation light read out. Top: energy spectrum (experimental data) of ^{54}Mn gamma source with and without anti-coincidence scintillation signal. Bottom: Monte Carlo simulation of the experimental set-up. The radius of the cylindrical dewar is 10 cm. Infinite energy resolution is assumed in the simulation and an energy threshold of 20 keV with 100% efficiency. For comparison, the Monte Carlo result for a radius of 100 cm is shown.

and the reduction factor quite well. The discrimination power is limited in this set-up by the 20 cm diameter of the LAr active volume: a fraction of the gammas, which Compton scatter in the germanium crystal, escape the active argon volume without interaction, thus are invisible in the scintillation channel. To illustrate this effect we display the Monte Carlo results for a radius of 100 cm. Here, the suppression is limited by the lithium dead layer of the detector.

From comparison of data and Monte Carlo results, we derive a threshold of approximately 20 keV energy deposition in the liquid argon. A preliminary value for the photo electron yield is ≈150 pe/MeV.

Future laboratory R&D will focus on the following items:

- Optimization of the wavelength shifting and light guiding materials with the goal to further increase the number of detected photo electrons;

- Measurements of the attenuation and scattering lengths at 128 and 420 nm and their

dependence on impurities;

- improvements of the read-out electronics using flash ADCs to record the full pulse shape information;

- Monte Carlo studies on light shadowing for an array of germanium diodes dispersed in liquid argon.

6.9   Rn-reduced air

The ^{222}Rn concentration in the air of the Gran Sasso laboratory is about 50 Bq/m^3. For the handling of germanium crystals this concentration is prohibitively high because of radon progenies which will be deposited on the detector surfaces. Therefore we consider the possibility to supply radon-reduced air to the cleanroom on top of the vessel. Radon can be removed from air by adsorption on an activated carbon column. In our case we would like to have a continuous supply of radon-reduced air without regeneration of the column. Therefore the retention time t_{Ret} for radon in the column has to be long enough to let decay ^{222}Rn before it would leave the column (several ^{222}Rn halflifes). t_{Ret} is related to Henry's constant H which describes the adsorption equilibrium by $t_{Ret} = H \cdot R \cdot T \cdot m / \phi$. R is the gas constant, T is the temperature, m is the mass of the adsorber and ϕ is the air flow-rate. [Mau 00] has derived a semi-empirical formula for the adsorption of spherical gas particles on activated carbon. According to this model Henry's constant H is given by:

$$H\left[\frac{\text{mol}}{\text{kg} \cdot \text{Pa}}\right] = \exp\left\{ \left(-0.05 + \frac{81}{T[\text{K}]}\right) \cdot \frac{T_C[\text{K}]}{\sqrt{p_C[\text{bar}]}} - 17.5 \right\} \tag{12}$$

T_C and p_C are the critical temperature and pressure of the gas to be adsorbed. For radon $T_C/\sqrt{p_C}$ is 47.6 K/$\sqrt{\text{bar}}$.

A reasonable goal for the ^{222}Rn activity in the purified air would be 100 mBq/m^3 at a flow-rate of 15 m^3/h. This means a reduction of a factor 500 is required which corresponds to a retention time t_{Ret} of 35 days. In general there are two ways to achieve this: The carbon column can be operated at room temperature or it can be cooled. Applying the given formulas one finds that for the first case about 3.5 tons of activated carbon would be required. Because the density of activated carbon is usually about 0.5 g/cm^3, such a solution would require a column with a size of the order of 7 m^3. The limited space in Hall A could exclude this solution. If the activated carbon would be permanently cooled to −40 °C about 180 kg would be sufficient. In this case, however, it would be required to dry the air before it enters the column. In the Super Kamiokande experiment both solutions are combined [Tak 04]: 4 tons of activated carbon reduce the radon concentration by a factor of 5000. Another 50 kg are cooled at −40 °C and provide a further reduction by a factor 10. The expected reduction factors according to the model of [Mau 00] for these cases are 1000 and 2.5, respectively. Thus the results of Super Kamiokande show

that the model is conservative and slightly better results can be obtained in practice. It is also possible to operate the column at lower temperatures. At -60 °C only 40 kg of activated carbon are required and at -80 °C the required amount is 7 kg. However at low temperatures the amount of CO_2 which is adsorbed in the column is not negligible and it might have an impact on the capacity of the column for radon. Laboratory tests will clarify this question.

For the production of radon-reduced air it is not necessary to use the highly-pure activated carbon CarboAct which will be used for the purification of nitrogen or argon (see section 8.1.2). Standard purity products that are much cheaper than the CarboAct have a ^{222}Rn emanation rate of about 300 mBq/kg [Heu 00] which is low enough for this purpose. Thus the prize of the carbon will be small compared to the rest of the installation.

For small volumes in the cleanroom (flowbox, air lock) synthetic air with a very low radon concentration can be supplied. Nitrogen can be purified from radon to the sub-μBq-level [Heu 00]. It can be mixed with oxygen from standard gas bottles. The BOREXINO collaboration has shown that the ^{222}Rn concentration in synthetic air produced in this way is smaller than 100 μBq/m^3.

6.10   Water purification

The water shield will serve also as Cherenkov medium for the detection of incident muons. Purification of the water is necessary in order to keep the light transmissivity as high as possible. Origins of turbidity are dust and metal ions as well as biological activity from bacteria, for example. Contaminations from radioactive materials like Rn, Ra and Th should be a fraction of those of the vessel's construction materials (see section 6.2).

Water purification systems are essential for water Cherenkov detectors like Super-Kamiokande [SuK 03], [SNO 00], Auger [Aug 97] or the BOREXINO counting test facility (CTF) [Ali 98] where the design goal for the radiopurity of the water shield is 10^{-6} Bq/kg. The radon content of the LNGS water is 10 Bq/kg.

The purification systems consist in general of several components including μm absolute filters, ion exchangers for the removal of metal ions, ultra violet sterilizers to kill bacteria, and ultra filters to remove nanometer sized particles [Aug 97, Ali 98, SuK 03]. The purity of the water is monitored by measuring in particular its resistivity which reaches after the ultra filter the chemical limit of 18 MΩ·cm [SuK 03]. Radon may be removed either by a vacuum de-gasifier [SuK 03] or by a counter-flow of nitrogen like in the BOREXINO CTF [Ali 98].

The capacity of the BOREXINO CTF purification system is designed for 1000 tons of water. In order to save cost and space, we propose to use this system for producing the 400 to 700 tons of water needed for the planned experiment. In view of the sealed and rust-protected water container, a small and dedicated continuous re-circulation system with a sub-micron filter and an ultra violet sterilizer will be sufficient to maintain the water quality.

6.11   Liquid gas storage

Storage tanks are needed to provide timely the LN (or LAr) lost by evaporation. This loss will range - dependent on vessel volume and type of insulation - from 0.1 to 1 m^3 per day. Hermetic storage of freshly delivered liquid gas over a few weeks is also a cheap yet efficient method to reduce the content of radon by profiting from its half-life of less than 4 days.

Close to Hall A two storage tanks are located with a capacity of 5 m^3 each. So far, they have been used by the GNO experiment. These tanks might be suitable for the planned experiment and we propose to allocate them to it. However, their compatibility with the required low Ar, Kr and Rn concentrations has to be checked.

7 Fabrication of enriched detectors

7.1 Procurement of enriched ^{76}Ge

It is our intent to procure 30 kg of enriched ^{76}Ge to build a new batch of detectors for phase II of the experiment. These new detectors are expected to be segmented, and laid out in such a way as to maximize background rejection via pulse shape measurements. The process for acquiring the enriched ^{76}Ge has begun, and it is expected that we will receive the 30 kg by mid-2005.

We review the steps required towards the production of new, optimized detectors and the current status in the following sections.

7.2 Purification and production of metallic ^{76}Ge

The process of producing enriched ^{76}Ge begins with the acquisition of raw germanium. The naturally occurring abundance of different isotopes of germanium is:

$$
\begin{array}{ll}
^{70}\text{Ge} & 20.8\ \% \\
^{72}\text{Ge} & 27.6\ \% \\
^{73}\text{Ge} & 7.7\ \% \\
^{74}\text{Ge} & 36.3\ \% \\
^{76}\text{Ge} & 7.6\ \% \\
\end{array}
$$

Only the isotope ^{76}Ge undergoes double beta decay. There are three important reasons for enriching the sample in ^{76}Ge.

1. The cost of detector fabrication is substantial. For a given mass of ^{76}Ge, it is cost effective to first enrich and then build the detectors. An enrichment at the level of 50 % or more is needed to make the detector fabrication cost less than the enrichment cost.

2. Many backgrounds are expected to scale with the total mass of the detector, whereas the signal will only scale with the mass of ^{76}Ge.

3. The intrinsic background from cosmogenic production of ^{68}Ge depends strongly on the initial concentration of ^{70}Ge, cf. e.g. [Maj 03]. It is therefore important to reduce the fraction of ^{70}Ge in the detector. This consideration produces the strongest requirement on the enrichment. Requiring a mass fraction of ^{76}Ge greater than 86 % guarantees that the mass fraction of ^{70}Ge is less than 0.2 % of the enriched sample.

We therefore choose an enrichment level of ^{76}Ge of 86 %. Enrichment will be done at *PA Electrochemical Plant* (ECP) in Zelenogorsk, Russia. The enrichment is performed in the gas phase (GeF$_4$) in a cascaded centrifuge system. The centrifuges used for the enrichment of the germanium for phase II of the experiment will be new devices, a virgin fluorine

gas sample will be used, and the enrichment will take place in a controlled clean room environment. The purity of the extracted sample depends in part on the purity of the initial sample. It is expected that up to 0.2% of the enriched material will be made up by the following elements: (Cr, Cu, Fe, Ni, Si, Mg, Al, Co, Mn, Zn, Mb, Sr, Cd, Ca), provided zone refined germanium is used as input to the enrichment process. A further purification step after enrichment is therefore necessary before crystal growing can begin. Several firms have been contacted concerning the purification step, and we anticipate purifying the sample to electronic grade material (6N level, 99.9999% Ge) before starting the crystal growing. We have received quotes for the combined enrichment and purification steps which are in line with our cost expectations.

We foresee a three step procedure for procurement of the enriched material:

- We will first procure 15 kg of natural Ge purified to electronic grade, 6N purity, via the ECP plant in Krasnoyarsk. The material will be transported to our detector fabrication destination, and detectors will be constructed from this material. In this way, all steps of the detector production process apart from the costly enrichment step will be tested. The quality of the purified material will be checked with full scale detectors, and the time needed for the transport will also be determined.

- The enrichment will first be performed for a 2 kg test sample. All steps in the procurement and testing will be worked out with this sample, including quality control measurements, underground storage, etc. We expect this first sample to be delivered within 4 weeks of concluding the contract to purchase the purified, enriched germanium.

- The remaining 28 kg will be delivered over a period of 6-7 months. Given the long procurement times, it is foreseen to store the germanium underground (600 m w.e.) to prevent undue cosmogenic activation. This sample will be transported in one batch.

The transports will likely be land or sea based, and will be performed in the most expeditious manner possible, in order to minimize cosmogenic activation. Immediately upon receipt, the samples will be brought underground and stored either at the detector manufacturer or at the LNGS site until the optimization of the detector construction has been finalized.

7.3   Quality control of enriched ^{76}Ge

Impurity concentrations of the enriched samples will be measured at several stages of the enrichment process. The first measurements will be performed on a sample of natural germanium before the centrifugal enrichment step, the second sample will come after the enrichment, and the third after the purification.

The Russian groups participating in the experiment (Institute for Nuclear Research, Kurchatov Institute) will take the responsibility for these tests, and will acquire samples

from ECP. The final round of tests will be performed by these two institutes after the purification step in sensitive mass spectrometer systems (ICPMS) capable of detecting impurities at the level of 0.1 ppb. The impurity concentrations will be measured again by the Milano/LNGS groups once the enriched sample has reached the underground storage site.

The results of these tests will be used to track the quality of the germanium through the different steps in the process, and will yield valuable information in understanding detector performance. The data from these tests will also be invaluable in possible future enrichment plans. The tolerable limits for different impurities is currently being worked out. In some cases, the limits just reflect the measurement capabilities of existing instruments.

7.4   Crystal and detector fabrication

The crystal growing and fabrication of detectors with the enriched germanium for phase II of the experiment will take place once the optimal detector segmentation and geometry have been determined.

The steps involved in the crystal growing and detector fabrication:

1. *Zone refinement.* This serves to further reduce the remaining level of impurities. Impurity concentrations are 1 ppb after polyzone refining and 0.01 ppb after a successive mono zone refining step.

2. *Crystal pulling*, which leads to a further purification of the germanium by an order of magnitude ('detector grade material') [Umi 04].

3. *Quality control* of the produced crystals and *crystal dimensioning*. The produced crystals will be stored underground while awaiting transfer to the detector manufacturer.

Crystal growing is expected to require approx. 3 days from the start of crystal pulling, and detector fabrication will take another ≈ 4 days. In order to minimize the production of radioactive isotopes via cosmogenic activation, the enriched germanium will be stored underground at the crystal grower's and detector manufacturer's sites overnight and for the waiting time between the different processing steps. It has been verified in a benchmark test with non-enriched germanium that the entire procedure of crystal growing and detector fabrication can be performed such that the above mentioned figures for cosmic ray exposure of the material can be met (see next section).

The optimal size of the detectors still has do be worked out with the help of simulation studies. We anticipate, however, that typical sizes will be in the range of $1 - 2.5$ kg. In the reference layout with liquid nitrogen as a shielding and cooling medium, it is desirable to pack the detectors in the closest possible manner, in order to maximize background suppression capability by exploitation of anti-coincidences between adjacent detectors, cf. section 3.4.

Diode production implies drilling of the central bore and doing the implantation and electrodes for high voltage and readout. In order not to introduce radioactive impurities, it is important that the electrical contacts of the detectors have minimum mass.

^{nat}Ge-diode production bench mark test

The exposure of the germanium crystals to cosmic ray radiation needs to be minimized to achieve the required background index of 10^{-3} cts/(keV·kg·y). Ten days of exposure results in 0.17 μBq/kg ^{60}Co-activity, which gives a background index of $0.9 \cdot 10^{-3}$ cts/(keV·kg·y) if no further discrimination method is applied (cf. discussion and references in section 3.3.1). The goal is therefore to limit the time of detector handling above ground to approximately 10 days after the last purification step, i.e. crystal pulling, in which elements like cobalt are reduced by segregation. This includes the last steps of crystal production, the diode fabrication and transport.

To test whether a detector production is feasible within such a short time frame, we organized the logistics of the production of a non-enriched 2 kg p-type HP-Ge detector together with the company which is growing the crystal and the company which produces the diode, both located in Olen, Belgium. Underground storage was arranged nearby in the HADES underground facility at a depth of 500 m w.e.

Table 11 summarizes the operations and time periods related to the crystal growing and diode fabrication. The overall exposure to cosmic rays above ground - exclusive mono-zone refinement, inclusive crystal pulling - corresponds to 7.4 days. The transport to Gran Sasso by car will add about one more day. A further reduction of exposure could be achieved by storing the crystals over night in the HADES facility during detector manufacturing.

Table 11: Details of the production sequence of a 2 kg p-type HP-Ge diode minimizing cosmic ray exposure. The overall exposure for crystal production starting from the crystal pulling corresponds to 3.2 days and for the diode production 4.2 days.

Operation	Start	Stop
Mono-zone refinement	17/05/04	24/05/04
Crystal pulling	8 am, 25/05/04	26/05/04
Crystal meas. & selection	27/05/04	27/05/04
Crystal dimens.	28/05/04	28/05/04
Underground storage	1 pm, 28/05/04	
Retrieval from underground	21/06/04	
Diode production	8 am, 21/06/04	25/05/04
Underground storage	1 pm, 25/05/04	

The diode currently is in the HADES underground facility and will be brought underground to the LNGS after completion of the required infrastructure for detector handling and testing at LNGS. Based on this experience, an exposure time of less than ten days for crystal pulling and detector fabrication seems realistic.

7.5 Detector Optimization

Optimization studies will be performed concerning segmentation and pulse shape discrimination before new enriched ^{76}Ge detectors will be fabricated. The goal of these studies is to minimize the background as measured in the experiment. Single site energy deposits can in principle be distinguished from multi-site energy deposits via the time spectrum of the measured signal or by measuring the separated energy deposits in different detector segments. In the electric field regime which we anticipate using, the electrons and holes have saturated drift speeds of about 0.1 mm/ns. A 1 MeV electron has a range of about 1 mm in germanium. On the other hand, a 1 MeV γ has an absorption length of about 2 cm in germanium. The task is therefore to distinguish energy deposits localized on a mm scale from energy deposits distributed over ≥ 1 cm.

Detector Segmentation

Increased detector segmentation can facilitate the direct observation of separated energy deposits. However, the level of segmentation needs to be optimized since more segments implies more cabling and readout electronics, which will be sources of background. Even more relevant might be practical limitation in the detector fabrication. A dialogue will be opened with possible detector manufacturers to understand which detector geometries can be realized, and the geometry will be chosen which optimizes the multi-site energy deposit rejection. This optimization will be done in the context of a simulation of the full experiment, since considerations such as packing density of the detectors are closely coupled to the final background rejection.

In view of the large number of detectors needed for the full scale experiment, R&D with commercial suppliers of germanium diodes will also focus on the efficient manufacturing of axially segmented p-type detectors. These devices are easier to build than n-type diodes, and their robust outside dead-layer does both ease the handling and provide an integrated shield against α particles. The experimental program will be accompanied by Monte Carlo simulations (see chapter 5).

Pulse Shape Discrimination

In addition to directly measuring the geographical separation of energy deposits, it is also possible to recognize multi-site energy depositions via distortions in the expected time evolution of the signal.

The Majorana Collaboration [Maj 03] has estimated that pulse shape discrimination can yield a factor four in background rejection at an 80 % efficiency for keeping single-site energy deposits. We intend to pursue our own detailed studies of rejection via pulse shape discrimination. Besides the methods used in the Heidelberg-Moscow experiment [Pet 93, Kla 04] or proposed for Majorana, there is the possibility of adopting the methods developed for PSA in proportional counters for the GALLEX and GNO solar neutrino experiments [Alt 96, Pan 04].

In this context, 3-D simulations will be performed on different detector geometries to understand the electric field distribution in the segmented detectors. The calculated electric

field distributions will be used to understand the time development of pulses as measured at the anode and cathode. The results will lead to an optimized detector geometry which will take into account also the simulation results for the full experiment.

Reference and 'zero effect' detectors

To unambiguously establish the signal of neutrinoless double beta decay, it will be most revealing to have in the same setup Ge diodes which are expected to exhibit this signal with strongly reduced intensity. Such Ge diodes can be produced from natural germanium for example. It would be even more convincing if the material for these detectors had very much the same history as the enriched ^{76}Ge material. This is the case if the ^{76}Ge depleted 'waste' material were used which is produced during the enrichment process. Such material would still have an appreciable amount of ^{76}Ge and ^{70}Ge, the latter exhibiting by far the largest cross section for ^{68}Ge production. Using the stripped GeF_4 waste material, an additional centrifuge step would yield highly enriched ^{72,73,74}Ge material (97.5%) the rest being ^{70}Ge and ^{76}Ge with less than 2% and 0.5%, respectively. Such a separation step could be done rather economically at the RRC Kurchatov at Moscow. 'Zero effect' detectors made from such material will exhibit no signals from double beta decay, and are thus not only a reference for background events but also good detectors for other interesting physics like dark matter search. Disposing of the Ge diodes of different isotopic composition and known history, it would be also possible to arrive at a better quantitative understanding of cosmogenic ^{68}Ge production.

Within an array of Ge detectors, any reference detector will of course serve also as an active shield against external background as well as a veto device that is able to record signals from intrinsic background processes in neighboured diodes.

7.6   Long term R&D for Phase III

New techniques for germanium enrichment

The current standard technology for isotope enrichment utilizes centrifuges with GeF_4 as operating gas. Researchers at the Institute of Molecular Physics of the Kurchatov Institute have developed a new Ge isotope selection technique based on $GeCl_4$. This method is potentially advantageous concerning purity of the enriched material and waste recycling. The new technique has been proven to work by producing a few grams of ^{76}Ge.

$GeCl_4$ is a commercially available compound with high chemical purity, and the disadvantages of GeF_4 – high cost, danger of contamination from eventual previous utilization in uranium enrichment – are avoided. The main limitation of this approach stems from the fact that chlorine has two stable isotopes (^{35}Cl and ^{37}Cl) and the heavier one has only an abundance of 24%. The maximum possible enrichment fraction amounts to about 40%, i.e. for higher enrichments the GeF_4 technology has to be used.

The extension of the $GeCl_4$ technology to produce the necessary amount of enriched material for an estimate of its economical efficiency is one of the foreseen R&D topics. Its isotope selection and all other technological processes connected with $GeCl_4$ will be

studied in detail. In addition it is planned to develop measurement techniques to identify the U/Th contamination in the raw and enriched germanium material. Once established they will be applied for monitoring the separation process.

Underground detector fabrication

In order to minimize cosmogenic activation, the fabrication of new enriched germanium diodes should be done preferentially underground. Establishing our own underground production would not only offer the additional benefit that control of the cleanliness of the entire production cycle becomes possible, but might, as is known from estimates of the AGATA collaboration, even be more cost-effective than ordering from a commercial supplier. Obviously, realizing this strategy would imply a long term engagement. It is interesting to note, however, that similar considerations exist within the AGATA collaboration. A merge of the interested parties might turn out to be beneficial for both sides with respect to sharing of resources, know-how transfer and training for the fabrication of germanium diodes.

8 Radiopurity assessment

A major background reduction requires that ultrapure materials are used for the construction and operation of the detector. We have developed different techniques to measure very low levels of radioactivity and to purify gases and liquids. The potential of these techniques will be summarized in this section.

8.1 Gas purification

8.1.1 Purity requirements

The liquid gases (nitrogen or argon) used in the experiment are produced by air separation. Therefore these gases can still contain traces of atmospheric noble gases. The most abundant radioactive noble gas nuclides in the atmosphere are ^{39}Ar, ^{85}Kr and ^{222}Rn (see Table 12). ^{39}Ar and ^{85}Kr have Q-values below 700 keV and will not contribute to the background in the $0\nu\beta\beta$-region. However, the ^{222}Rn-decay chain is more complex, since γ-rays of more than 2 MeV energy are emitted in the decays of ^{214}Bi and ^{210}Tl. Monte-Carlo-simulations have shown (see section 3.3.2) that a ^{222}Rn activity of 0.3 μBq/m^3 of nitrogen (STP) leads to a count rate of less than 10^{-4} events/(kg·y·keV) in the energy window between 2 MeV and 2.08 MeV. Consequently nitrogen of this ^{222}Rn-purity is sufficient for the experiment.

Table 12: The most abundant radioactive noble gas nuclides in the atmosphere (all gas volumes are given at STP).

	^{39}Ar	^{85}Kr	^{222}Rn
Activity concentration	1.8 Bq/m^3 argon 13 mBq/m^3 air	1.2 MBq/m^3 krypton 1.4 Bq/m^3 air	10 to >100 Bq/m^3 air
Reference	[Loo 83]	[Bfs 01]	

Similar purity levels are required for liquid argon. Moreover when the scintillation of argon is utilized it might become necessary to remove ^{85}Kr from the argon in order to reduce the overall count rate. ^{39}Ar obviously cannot be removed from the argon. Its volumetric activity of 1.8 Bq/m^3 (STP) translates to a count rate of $5 \cdot 10^4$ Hz in an active volume of 30 m^3 liquid argon. The ^{85}Kr activity should not exceed this number. Therefore the volumetric krypton concentration in the argon has to be 1 ppm or lower. The purity requirements will be more stringent for the dark matter search at low energies.

8.1.2 Adsorption technique

Ultrapure gases are produced by adsorption of the impurities on dedicated adsorbers. Since activated carbon usually has a wide pore size distribution, it is suited to trap different kind of impurities independent of their molecular size. A simple model for the adsorption of spherical gas particles on activated carbon was already presented in section 6.9. Henry's constants for the gases of interest can be calculated according to equation (12). They are summarized in Table 13.

Table 13: The critical pressures and temperatures for different gases and the calculated Henry coefficients for the adsorption on activated carbon.

Gas	T_C [K]	P_C [bar]	$T_C/\sqrt{P_C}$ $\left[\text{K}/\sqrt{\text{bar}}\right]$	H [mol/(kg·Pa)] 15 °C	-100 °C	-196 °C	Ref.
Ar	150.7	48.6	21.6	$4 \cdot 10^{-6}$	$2 \cdot 10^{-4}$	63	[Atk 96]
N_2	126.3	34.0	21.6	$4 \cdot 10^{-6}$	$2 \cdot 10^{-4}$	63	[Atk 96]
Kr	209.4	55.0	28.2	$2 \cdot 10^{-5}$	$3 \cdot 10^{-3}$	$5 \cdot 10^{4}$	[Atk 96]
Rn	377.0	62.8	47.6	$2 \cdot 10^{-3}$	10	$1 \cdot 10^{13}$	[Fle 03]

At room temperature none of the gases are significantly adsorbed. From all the gases radon is by far the heaviest and has the highest polarizability. Consequently, it can already be adsorbed efficiently at rather high temperatures (-100 °C). At liquid nitrogen temperature Henry's constant for radon becomes huge, so the radon is completely transferred from the gas phase to the adsorbed phase. Therefore, no radon should remain in liquid nitrogen after running over an activated carbon column at -196 °C. In practice re-contamination due to [222]Rn emanation of the activated carbon limits the obtainable purity. We found a synthetic activated carbon (CarboAct) on the market whose [222]Rn emanation is (0.3 ± 0.1) mBq/kg [Heu 00] measured by the technique described in section 8.3.1. This is more than two orders of magnitude less than the emanation rate of other commercially available products. The BOREXINO collaboration has demonstrated that a [222]Rn concentration in nitrogen of less than 0.3 μBq/m³ (STP) can be reached if CarboAct is used as the adsorber [MPI 03].

Nitrogen and argon are very similar with respect to their adsorption behaviour. This can be seen by comparing their Henry's constants given by equation (12). Table 13 shows that $T_C/\sqrt{p_C}$ is 21.6 K/$\sqrt{\text{bar}}$ for argon as well as for nitrogen. Therefore the purification of argon from radon can be performed in the same way as the nitrogen purification. The only difference is that liquid argon has a 10 °C higher critical temperature than liquid nitrogen. Although Henry's constant is somewhat smaller at -186 °C it is by far large enough to completely trap radon on the adsorber. Consequently by applying liquid phase adsorption on [226]Ra-free activated carbon, argon can be purified from radon to the same

purity as nitrogen.

The situation for krypton is less favorable. Due to the similar adsorption properties of krypton and nitrogen/argon (see Table 13) a single component adsorption model fails to predict the equilibrium. Multi-component adsorption equilibria are difficult to predict quantitatively when the components of the gas mixture have similar adsorption properties. In that case there is a strong interference between the different components resulting in a much weaker adsorption of the trace impurity. However, the situation can be improved substantially if the adsorption happens in the gas phase at temperatures slightly above the boiling point of the gas to be purified. A further improvement has been demonstrated, if carbon adsorbers with optimized pore size distributions are used. Using this technique we have demonstrated that we will be able to purify more than 500 m^3 of nitrogen (STP) from krypton with only 1 kg of adsorber. Due to the similarity of nitrogen and argon the purification of argon from krypton can be performed in the same way.

Because their adsorption properties are identical, the purification of nitrogen from argon is impossible by adsorption. A separation can only be achieved by rectification as it is done during the production of nitrogen in air separation plants. The BOREXINO collaboration has investigated high purity nitrogen from different suppliers [Zuz 04]. The best quality that could be found (from the German company WESTFALEN AG) has a volumetric argon concentration of 0.5 ppb and is therefore pure enough for the experiment. Furthermore, the volumetric krypton concentration was 0.06 ppt. Such low values show that air separation plants are able to remove gaseous trace impurities. Therefore, it might not be necessary to build purification plants for krypton and argon for the proposed experiment. However, radon re-contamination may occur before the detector is filled due emanation from surfaces.

If the scintillation of argon is utilized also residual oxygen has to be removed. The ICARUS collaboration has successfully operated a commercially available oxygen purification unit with liquid argon [Cen 93]. The achieved oxygen purity is also sufficient for our experiment. By purifying liquid argon with a high throughput time and costs can be saved, because evaporation and re-condensation can be avoided.

8.2 Germanium spectroscopy

A standard technique for material screening is low level germanium spectroscopy. We have access to several germanium spectrometers at the MPIK/Heidelberg, at the Baksan laboratory and at the Gran Sasso laboratory.

In the underground facilities of the Baksan Neutrino Observatory (BNO) there are several spectrometers located. For a first analysis the low background gamma-spectrometer on the base of well-type NaI scintillator can be used. In this way a material selection at the level of sensitivity of about 10^{-9} g Th,U,K/g (for 1 kg sample measured for 1 week) can be obtained. For higher sensitivity measurements, two HPGe spectrometers are available.

For materials which are available in large mass (up to 20 kg) the best way is to use the IGEX/Baksan four HPGe setup. This spectrometer is an assembly of 4 ultra low background HPGe detectors of 1 kg each and operates now in the specially constructed low background facility at 660 m w.e. depth. A detailed description of the setup is given

in [Kli 98]. The IGEX/Baksan four HPGe setup operates at the background level of the IGEX ^{76}Ge double beta decay experiment, that means the background count rate is about 0.15 cts/(keV·kg·y) in the energy region near 2 MeV ($\approx$25 cts/(keV·kg·y) below 500 keV). Such ultra low background gives us the possibility to measure Th and U contaminations in screening materials with sensitivity up to 10^{-13} g/g. Additional advantages of this spectrometer is the large sample volume (30 x 30 x 30 cm) and the possibility to detect cascade gamma rays by several detectors in coincidence.

For materials which are available only in small masses (up to 1 kg) the more suitable way is to use a setup with one HPGe diode which is practically finished now. The effective detector mass is about 1 kg (in the nearest future 2 kg) and it is placed in the new Deep Underground Low Background Laboratory (DULB) situated at a depth of 4900 m w.e. To increase the sensitivity both the NaI and the IGEX/Baksan four HPGe setup will be moved in the near future to this new laboratory.

In Heidelberg the spectrometers are located in an underground laboratory (15 m w.e.). The rather shallow depth is sufficient to reduce the primary hadronic component of the cosmic ray down to a level which is negligible compared to neutrons from fission and (α, n) reactions. Secondary hadrons produced by muon interactions present the dominant hadronic component in the laboratory. They can effectively be rejected by muon veto devices, gas counters or plastic scintillators, which are installed at all spectrometers. Typical sensitivities are in the range of a few to a few ten mBq/kg for the U/Th chain activities and for ^{40}K depending on the sample mass.

Several spectrometers are available in the germanium laboratory of the Gran Sasso underground laboratory. The cosmic ray muon flux is reduced to $\sim$1 m^{-2}h^{-1} - about six orders of magnitude less than at ground level. The most sensitive instrument among those detectors and one of the most sensitive spectrometers worldwide is the GeMPI detector [Ned 00]. The sample chamber can house large samples of up to 22.4 liters. The background rate in the strongest lines of the uranium and thorium chain as well as for the ^{60}Co and the ^{40}K lines is less than 1 event per day. The continuous background is about 10000 events/(kg·y) in the energy range from 100 keV to 2730 keV. The GeMPI operates at background levels of current ^{76}Ge double beta decay experiments. This very low background results in a low detection limit. However, the ultimate sensitivity of a few 10 μBq/kg for the U/Th chain activities and for ^{40}K can only be reached after measuring for about 3 months. This limits the number of samples that can be tested in a given time. The situation will be improved because two new detectors (GeMPI II and III) which are similar to GeMPI I will be installed at Gran Sasso soon. GeMPI II is built in the frame of the M-Cavern project [Har 03] while GeMPI III is a joint project of the MPIK and the INFN.

8.3   Radon monitoring

The radioactive noble gas radon represents a major source of background due to its mobility and because it is permanently produced by radium contamination in most materials. Consequently we developed methods to measure the ^{222}Rn concentration in liquids and

gases at very low levels. Furthermore, we are able to determine the ^{222}Rn emanation rate from solids at similar low levels. The highest sensitivity is reached if low background proportional counters are used to detect the decay of ^{222}Rn. If lower sensitivities are sufficient, a system based on the electrostatic collection of radon progenies on an α-counter can be used. It allows radon concentration in gases to be monitored online.

8.3.1 ^{222}Rn measurements with proportional counters

Low background proportional counters as used in the GALLEX/GNO solar neutrino experiments can be used for ^{222}Rn detection [Heu 00, Rau 00, Sim 03]. Background rates of less than one event per day can be achieved for an energy threshold of 50 keV. The achievable sensitivity depends on the number of ^{222}Rn atoms which can be transferred in the counters for a given sample. Therefore, the preparation of the sample is crucial.

^{222}Rn emanation measurements. For emanation measurements two electropolished stainless steel chambers are available, housing samples of 20 ℓ and 80 ℓ, respectively. After putting the sample inside the ambient air is removed and the chamber is filled with radon-free helium (or nitrogen). After several days the emanated radon is flushed out of the chambers and collected on a carbon trap at liquid nitrogen temperature. Next, the carbon trap is connected to a counter filling line, where the sample is purified and mixed with a standard counting gas, before it is transferred to the proportional counter. There are three α-decays in the ^{222}Rn-decay chain until the long-lived ^{210}Pb is reached and on average half of them are detected (50 keV threshold).

The detection limit of the described technique depends on the blank contribution of the chambers and is about 60 μBq for the small and about 150 μBq for the large chamber. Small samples with volumes below 1 ℓ can be put into glass vials that can be connected directly to the counter filling line. In this case the blank contribution is lower and a detection limit of 30 μBq is achieved.

^{222}Rn and ^{226}Ra measurements in liquids. If the radon concentration in liquid samples has to be measured the dissolved radon has to be extracted from the liquid phase. This can be done by sparging with helium or nitrogen, and the chambers described previously can be used for that purpose. We have also developed a system which is used for the radon assay of water [Sim 03]). It is composed of a 480 ℓ water tank equipped with a gas distribution line for the sparging. The extracted radon is collected on a carbon trap. The saturation blank activity of the tank is 1 mBq, but since an extraction can be done in about 2 hours, a detection limit for ^{222}Rn of 0.1 mBq/m^3 of water can be achieved.

The technique can be extended to measure ^{226}Ra. After removing the primary radon component new ^{222}Rn will emerge only from the decay of ^{226}Ra dissolved in the water. Thus, a second extraction after several days determines the ^{226}Ra concentration. The detection limit is worse for ^{226}Ra, about 1 mBq/m^3, because a measurement takes several days, resulting in a higher blank contribution due to the ^{222}Rn emanation from the tank.

Radon measurements in gases. Proportional counters can also be used to determine the amount of radon in nitrogen and argon. In the BOREXINO experiment it has been demonstrated that ^{222}Rn in nitrogen can be measured at the sub-μBq-level [Heu 00]. The technique consists of leading several 100 m^3 of nitrogen over a $\sim$150 g activated carbon column which is immersed in liquid nitrogen. After removing the nitrogen by pumping on the column at -100 °C the sample is transferred to the proportional counter. As already discussed in section 8.1.2 the synthetic activated carbon CarboAct has a very low ^{222}Rn emanation rate and hardly contributes to the background. The achievable detection limit is about 50 μBq allowing the sub-μBq-level to be reached with nitrogen samples of about 100 m^3.

The detection of ^{222}Rn in argon can be performed in the same way as in nitrogen. The activated carbon column has to be cooled at liquid argon temperature. It has been mentioned in section 8.1.2 that argon and nitrogen have very similar adsorption properties. Therefore the nitrogen/radon-system and the argon/nitrogen-system behave similarly and the same ^{222}Rn detection limits as obtained for nitrogen can be achieved for argon.

Proportional counting can also be applied to detect other radioactive noble gas nuclides like ^{39}Ar and ^{85}Kr. Theses procedures are summarized in [Sim 04]. The absolute sensitivities are comparable with the sensitivities for ^{222}Rn, however it is more difficult to collect theses gases efficiently on adsorber columns. Thus, the relative sensitivities will probably be lower.

8.3.2 Online radon monitoring in gases

If lower sensitivities are sufficient, the ^{222}Rn concentration in air or other gases can be measured online with an electrostatic chamber. Since the ^{222}Rn progenies ^{218}Po and ^{214}Po are positively charged in most cases, they can be collected by an electric field [Tak 99]. Such a system was developed for the BOREXINO experiment and is described in details in [Kik 01]. A silicon PIN diode is used as a detector and a high voltage of 30 kV is applied between a vessel of 418 ℓ volume and the detector. Laboratory studies show that collection efficiencies of 80 % are possible. ^{222}Rn concentration measurements with a detection limit down to $\sim$100 μBq can be performed.

To achieve lower detection limits the next generation of these detectors will use an active volume of about 800 ℓ, an improved geometry and voltages up to 50 kV to collect the ions. The detector can be used to measure the radon concentration either in ambient air or in a closed cycle inside a volume of interest.

8.4 Noble gas mass spectrometry

There are very limited possibilities of measuring radioactive noble gas nuclides at very low concentrations. The first one (already mentioned in section 8.3.1) is direct counting using low-level proportional counters. It requires pre-concentration of ^{39}Ar and ^{85}Kr from big volumes and later purification of the samples. A more indirect but easier way is to investigate natural argon and krypton using special tuned rare gas mass spectrometry.

^{39}Ar and ^{85}Kr activities can be next calculated taking into account the fairly known specific concentrations of both isotopes in the atmosphere. For such measurements we use a VG3600 mass spectrometer (MS) devoted to investigate rare gases at low concentrations in terrestrial and extraterrestrial samples [MPI 92].

8.4.1   Argon and krypton in nitrogen gas

In case of nitrogen, argon and krypton concentration can be measured in a rather simple way. A gaseous sample is introduced directly into the preparation section of the MS, where the volume of the aliquot is set and measured (usually about 1 cm^3) and next, in the purification sector the nitrogen is absorbed by a getter pump. In the following step the remaining rare gases are transferred into the MS and analyzed.

Taking into account the intrinsic background of the entire system and measuring 1 cm^3 of nitrogen we can achieve the following detection limits: $1 \cdot 10^{-9}$ m^3/m^3 (1 ppb) for Ar in N$_2$ ($\sim$1.4 nBq/m^3 for ^{39}Ar in N$_2$) and $1 \cdot 10^{-13}$ m^3/m^3 (0.1 ppt) for Kr in N$_2$ ($\sim$0.1 μBq/m^3 for ^{85}Kr in N$_2$). For an even lower limit, the volume of the sample can be enlarged up to several cm^3 [Zuz 04].

8.4.2   Krypton in argon gas

To determine the krypton concentration in argon gas an extension of the technique applied for the determination of argon/krypton in nitrogen is required. The reason is that the mass spectrometer cannot handle macroscopic amounts of noble gases (argon in our case) and the reduction of the sample volume is limited by the sensitivity of the device for krypton detection. There are two possible ways to solve the problem: Reduction of the argon volume in the sample (with no losses of krypton), or increasing the krypton content by concentration from a large argon sample.

In the first case, the reduction of the argon volume can be done before the sample is introduced into the sample preparation section of the MS using a special gas chromatography unit, already built and tested at MPIK [Sim 04]. Another way is to separate argon and krypton in the purification sector of the MS. For this purpose a special cryostat can be used. After freezing the whole sample on its carbon trap, different gases can be released sequentially by increasing the temperature. This method is extensively used to separate e.g. helium from argon, krypton or neon. However, due to their similar adsorption properties the separation of argon and krypton needs more detailed investigations.

To increase the krypton content in the sample (the second possibility) it is necessary to collect it from a suitable volume of argon (gas phase is preferred) on the trap filled with an appropriate adsorber kept at low enough temperature. In the next step the gases are released into the preparation section of the spectrometer, where the volume can be precisely determined and reduced, if necessary.

8.5 ICPMS and neutron activation analysis

The collaboration has access to two additional powerful tools to determine trace contaminations of materials: these are ICPMS (Induced Coupled Plasma Mass Spectrometry) and Instrumental Neutron Activation Analysis (INAA). The ICPMS instrument available at LNGS is an Agilent Technologies ChemStation series 7500. It is installed at the outside lab inside a clean room of class 1000, equipped with ultrapure water. It can measure trace elements as low as one part per trillion (ppt) or quickly scan more then 70 elements to determine the composition of an unknown sample. Moreover it allows isotopic analysis with an accuracy of better than 1%. The Agilent 7500 ChemStation software automates the analysis and accurately interprets the resulting data. The LNGS ICPMS has been already used by several collaborations to determine trace elements in water, and U and Th contaminations in Cu, Pb, $CdWO_4$ crystals. Recently an interesting research of Ir, Pt, and rare earths elements at the level of ppt has been performed to analyze rocks from the geological boundary between the Creteceous and the Terziary age. The goal is to determine the extraterrestrial origin of a field of craters recently discovered in the Abruzzo mountains.

INAA is another powerful elemental determination technique that depending on the matrix and element under investigation could be either associated or complementary to ICPMS. In Pavia (Italy) there is a 250 kW power TRIGA MARK II research reactor with a thermal neutron flux of $4 \cdot 10^{12}$ n/(cm²s). Several irradiation channels are available for research and industrial applications. The reactor is managed by CNR and the University of Pavia. It has been used by INFN researchers to determine K,U,Th concentrations in materials like plastics or for elemental characterization of samples of archeological interest. The associated gamma ray spectrometry can be performed both directly at the reactor site for short life isotopes and at LNGS for long lived isotopes in low background spectrometers to improve the sensitivity. The typical sensitivity of this technique is ppt or better.

9 Safety and Environment

The discussion in this section is based on the baseline and alternative design described in section 6.2. Many details of the experiment are not yet finalized. Nevertheless, the major generic safety aspects and environmental impacts of the experiment are known, and this chapter serves to discuss them.

Tables 14 and 15 identify potential hazards which may be caused by the installation of the proposed experiment. The still incomplete tables follow the initial safety information

Table 14: Initial safety information for the proposed experiment, excluding the construction phase.

SPOKESPERSON:...... tbd RAE:....... tbd GLIMOS:...... tbd				
(1) GASES, LIQUIDS, CRYOFLUIDS (used in detectors or kept nearby)				
Device Type	Fluid	Volume	Abs. Press.	environm. impact
$*$ Exp. tank	LN2 or LAr	<60 m^3	1.2 atm	none
$*$ Exp. tank	water	<700 m^3	1.0 atm	none
(2) OTHER CHEMICALS				
(Toxic/Corrosive/Flammable solvents, additives etc):				
$*$ small amounts of acids for germanium detector fabrication				
$*$ small amounts of cleaning fluids like alcohol				
(3) ELECTRICITY				
MAGNETS: > NONE				
High Voltage (>1 kV)				
Detector Type	Voltage	Current	Stored Energy	No of HV channels
$*$ PM	<3 kV	<3 mA		$\mathcal{O}(100)$
$*$ Ge diode	<5 kV	<1 nA		<50
$*$ Rn monitor	50 kV	<1 nA		1–2
SHORT-CIRCUIT current >5 mA for >50V possible anywhere? $*$ (NO)				
POWER dissipated by all electronics				
a) on detectors: $*$ negligible b) off detectors: $*$ 55 kW (table 23)				
SPECIAL GROUNDING REQUIREMENTS? $*$ NONE				

requested for experiments at CERN [Ced 72]. Table 14 shows that an impact on the environment by toxic or corrosive materials is excluded. No flammable gases and liquids are used. The radioactive sources needed for the energy calibration of the Ge detectors will be all encapsulated, and their activity will be low enough so that no regulations beyond the standard radiation protection rules are needed.

The major potential hazard is due to the cryostat of the experiment which will contain a maximum of 60 m^3 of liquid nitrogen (LN) or liquid argon (LAr). Table 16 gives a

Table 15: Initial safety information for the proposed experiment, excluding the construction phase (continued).

(4) LIFTING AND HANDLING			
Weight of heaviest single piece to install?	∗ to be specified		
Specially designed handling equipment?	For which max. weight?		

(5) VACUUM TANK, PRESSURE TANK, CRYO-TANK			
Tank	Abs. pressure	Volume	Weakest part of wall
∗ Cryo-tank (exp.)	1.2 atm.	<60 m^3	
∗ Cryo-tank1 (storage)	to be specified		
∗ Cryo-tank2 (storage)	to be specified		

(6) IONIZING RADIATION (radioact. sources, depleted uranium, etc.)	
Radioactive source	∗ for calibration, to be specified

(7) NON-IONIZING RADIATION (Laser, UV light, microwaves, rf)
∗ UV laser for PMT calibration
∗ possibly UV light for sterilizing water

(8) OTHER HAZARDS
∗ suffocation
∗ electric shorts induced by water leak

(9) RISK ANALYSIS (including environmental issues)
∗ to be done for LN/LAr/water vessel

compilation of the physical properties of these cryogenic liquids [TIS 98].

The amount of stored LN or LAr corresponds to a gaseous volume of about 46000m^3; this is about 2 times the volume of Hall A. The specified daily evaporation is less than 0.5% of the liquid, or less than 1% of the volume of Hall A. At standard operation, the present ventilation system guarantees that 40% of the air is exchanged per hour in each of the three halls, or an 'air-washing' of the total volume of each hall within 2.5 hours.

Argon and nitrogen are inert, non-toxic and non-flammable gases. Environmentally, they are not dangerous. However, if they replace part of the oxygen in the atmosphere, severe damage to human beings can occur. This hazard is increased in a confined space like an underground hall with limited ventilation. Thus, as a result of leakage, the hazards will be essentially that of asphyxiation and injuries due to the low temperature - frostbites, cryo-burns, hypothermia and others. Similarly, due to low temperature further damage could result to structures and equipment impinged on by the cryofluid. A risk analysis has to show which measures are needed to prevent a major accident, and to minimize the risks and effects of a major accident.

The large amount of water, ≈700 m^3, stored in the water vessel represents a hazard in case that a major leakage would develop suddenly. A risk analysis will show how the

Table 16: Physical properties of liquid nitrogen and argon

Characteristics	Argon	Nitrogen	Unit
Boiling point at 1 bar	-185.5	-195.8	°C
	87.3	77.3	K
Density of liquid at boiling point	1400	810	kg/m^3
Liters of gas at 20°C produced by 1 liter of liquid, 1 bar	841	693	liters
Density at 20°C compared to density of air	1.4	1.0	
Latent heat of evaporation for 1 liter of liquid	220	160	kJ
Ratio of enthalpy of vapor at 20°C and latent heat of evaporation	0.7	1.14	

impact of such a potential event can be minimized; this study will profit from the works being presently done by the Commissary at LNGS.

All other potential hazards are not aggravated due to the fact that the experiment will be operated underground. It is intended to plan and to build the experiment and its infrastructure following the 'Safety Guide of the LNGS'and the rules defined in the 'Environmental Management Manual'. In particular, it is intended to provide in due time documentation of the relevant components.
This documentation will include
- cryogenic tank cooling down and filling procedure,
- cryogenic tank emptying procedure,
- description/location of relieve and safety valves,
- description/location of temperature and pressure sensors,
- description/location of gas collector diffusers,
- description/location of oxygen monitors,
- description of gas control system and its operation,
- inventory of installed electrical cables,
- description of fire extinguishing system,
- risk analysis/matrix with respect to LN/LAr/water leakage,
- risk analysis/matrix considering earthquake, statics calculations
- risk analysis/matrix considering power black-out,
- risk analysis for the environmental hazards of the experiment.

The overall safety of the experiment will profit from a fully computerized control and monitoring system with remote access that will record all safety relevant parameters. The critical parts of this highly reliable and redundant detector safety system will be based on

an autonomously running programmable logic controller (PLC) front-end. In case of any alarm condition, the data will be communicated to the Lngs general safety monitoring system which will trigger the necessary action and contact the experiment's on-call duty. In case of electrical power outage, a UPS module makes it possible to continue data taking or to automatically bring all critical system components into a safe state.

To our knowledge none of the materials used in the experiment are classified as environmentally dangerous according to the classifications R52 or R53. The experiment will be built and operated in compliance with the UNI EN ISO 14001 Lngs protocol ('Environment Management Manual') and a risk analysis will determine possible environmental hazards. The requests for electrical power and cooling water are discussed in section 12.

10 Time schedule and milestones

The GERDA experiment is structured into two phases as shown in Table 17. A third phase is considered.

Phase I starts with the construction of the experimental facility in the summer of 2005, and measurements begin one year later using both natural Ge diodes as well as the existing $\approx$15 kg enriched ^{76}Ge diodes.

Phase II will have started already at the end of 2004 so that 30 kg of enriched material will be available by the end of 2005. One more year will be needed for the design, tests of prototypes and the optimization of segmented detectors so that measurements with enriched segmented ^{76}Ge diodes can commence early in 2007. With the new detectors the running will continue until $\approx$100 kg·years have been accumulated.

Table 17: Phases of the planned experiment

	2005	2006	2007	2008	2009	2010
Phase I						
Construction	▬					
Measurement with existing ^{76}Ge diodes		▬▬ ■	■ ■	■ ■	■ ■	
Phase II						
Procurement of enriched ^{76}Ge material	▬					
Design and tests of segmented Ge diodes	▬▬					
Production of new ^{76}Ge diodes		▬				
Measurement with all ^{76}Ge diodes			▬▬▬▬▬▬			

Table 18 shows in some detail milestones for the construction period in phase I. With the major part of funds being secured the installation of the vessel system can start as soon as Hall A is available for construction work. Time has been allocated for safety reviews and an european-wide call for tenders.

Table 19 shows milestones for phase II. Here the focus is on the development and fabrication of segmented ^{76}Ge diodes. The milestone for the order of enriched material has been already met by the end of September.

Table 18: Proposed milestones for Phase I of GERDA.
Months are quoted as numbers.

Year	'04		'05				'06			
Quarter	Q3	Q4	Q1	Q2	Q3	Q4	Q1	Q2	Q3	Q4
Proposal	9									
Begin of first run									7	
First bkg index result										10
Cryogenic & water vessel										
System design finalized			3							
System safety reviewed				5						
Materials screened				5						
Cryogenic vessel ordered				5						
Water vessel ordered					7					
Vessel system baseplate built					8					
Water vessel installed						12				
Cryogenic vessel installed							1			
Vessels filled								4		
System commissioned								5		
Cleanroom, lock										
Cleanroom design finalized			3							
Lock design finalized				6						
Lock prototype tested						10				
Platform frame installed						12				
Platform installed							2			
Cleanroom & Lock installed							3			
Muon veto system										
Design studies & MC done			1							
Components ordered			3							
Components assembled & tested					9					
Water Cherenkov installed							1			
Scintillator panels installed							2			
Infrastructure										
LArGe test bench installed					7					
Water pipe Borexino-GERDA built						11				
LN storage vessels installed						11				
Rn air filter installed							1			
Rn monitoring system installed							3			
Safety systems installed							2			

97

Table 18: Proposed milestones for Phase I of GERDA. Months are quoted as numbers.

Year	'04		'05				'06			
Quarter	Q3	Q4	Q1	Q2	Q3	Q4	Q1	Q2	Q3	Q4
Ge-76 diode refurbishment										
Underground lab room allocated	10									
Underground lab room installed		11								
All diodes at LNGS		11								
Performance in cryostats documented			2							
Contact materials screened			3							
Refurbishment designed & tested			3							
Refurbishment procedures documented				4						
Diodes dismantled from cryostats				4						
Diodes refurbished & tested				6						
Contacts redone - if needed					9					
Refurbishment finished						11				
Prototype diode string/array tested			3							
Materials for string/array screened					8					
Diode strings/arrays assembled						12				
Electronics										
Diode readout chain design finalized				5						
Readout chain for diodes available						11				
HV supply for Ge diodes delivered				4						
DAQ/database designed				4						
DAQ/database tested						10				
DAQ/database installed								4		
Slow control design finalized				4						
Slow control prototype tested						10				
Slow control system installed								4		

Table 19: Proposed milestones for Phase II of GERDA. Months are quoted as numbers.

Year	‘04		‘05				‘06			
Quarter	Q3	Q4	Q1	Q2	Q3	Q4	Q1	Q2	Q3	Q4
R&D for new segmented Ge-76 diodes										
Segmented prototype p-type detector ordered		12								
Segmented prototype detector tested				4						
Ge-nat ref. material from plant received		11								
Ge-nat ref. material processed thru all steps				4						
Ge-nat ref. detector built				6						
Ge-nat ref. detector tested					8					
Design for new segmented diodes finalized								6		
ASIC readout design available					7					
ASIC readout prototype produced & tested								4		
Fabrication of new Ge-76 diodes										
Enriched material ordered	9									
Test batch analyzed			1							
Transport procedures tested		11								
Full batch produced					7					
Full batch purified to 6N					9					
Full purified batch delivered						10				
Crystal pulling done									9	
Prototype enriched detector delivered										11

11 Institutional responsibilities

Table 20 lists the current distribution of tasks among the institutions of the collaboration. It reflects the interests and experiences of the collaborating groups as well as the financial support. Several topics like "readout electronics chain" and "modification of the existing detectors" are covered by a large number of institutions. For these a more detailed coordination is needed.

The naming abbreviation of the institutes are:

INR Institute for Nuclear Research of the Russian Academy of Sciences, Moscow,

ITEP Institute for Theoretical and Experimental Physics, Moscow,

JINR Joint Institute for Nuclear Research, Dubna,

KI Russian Research Center Kurchatov Institute, Moscow,

LNGS INFN Laboratori Nationali del Gran Sasso, Assergi,

MI Università di Milano Bicocca e INFN Milano,

MPIK Max-Planck-Institut für Kernphysik, Heidelberg,

MPIP Max-Planck-Institut für Physik, Munich,

PD Università and INFN Padova,

UK Jagiellonian University, Krakow,

EKUT Physikalisches Institut Universität Tübingen,

Also, some financial support is not guaranteed at the moment and consequently the task list may modify accordingly.

The table shows that there is enough expertise and resources within the collaboration to cover all tasks.

Table 20: Project coverage by institutions. If more than one institution is listed the first one is considered to be responsible. This list is not yet finalized.

item	institution
Cryogenic Vessel	
cryogenic vessel (design, material validation, production control)	MPIK, INR/ITEP
risk analysis	LNGS, PD
infrastructure for cryogenic liquid (storage tank, ventilation, pipes, ...)	LNGS
safety control	LNGS
liquid gas purification and monitoring	MPIK
Water Vessel	
water vessel (design, production)	LNGS, PD
baseplate for vessel system	LNGS, PD
water purification	LNGS
risk analysis	LNGS, PD

Table 20: Project coverage by institutions. If more than one institution is listed the first one is considered to be responsible. This list is not yet finalized.

Infrastructure on top of vessel	
clean room and interlock (design, fabrication, installation)	MPIP
detector suspension (design, simulation, fabrication)	MPIP, MPIK
calibration methods for Ge diodes	MI, PD, MPIP
radon reduced air	MPIK, MPIP, JINR
Modification of existing ^{76}Ge diodes	
supply of existing diodes	KI, INR/ITEP
new detector contacts and support (design, fabrication, material validation)	MPIK, KI, INR/ITEP, JINR, EKUT
new implantation for p-contact if needed	MPIK, JINR
infrastructure for modification (lab, glove box, ...)	LNGS, MI, EKUT
test and characterization	LNGS, MI, KI, INR/ITEP, PD, JINR
Germanium detector readout	
cold electronics, front-end, cables	MI, MPIK
digitization	PD, MPIK, MPIP
pulse shape analysis	LNGS, MI, PD, KI, MPIP
electronics calibration (pulser)	MPIK
high voltage	MPIK
data acquisition and slow control	MPIK, PD
Muon Veto (water Cherenkov)	
PMTs (design, fabrication)	LNGS, MI, INR
support structure for PMTs	EKUT
reflector foil	EKUT
high voltage	EKUT
analog electronics	LNGS, MI, INR
digital electronics and DAQ	EKUT
calibration	LNGS, MI, INR
Muon Veto (scintillator)	
scintillator panels (construction)	JINR, EKUT
PMTs, bases, HV	EKUT, JINR
readout	MI+EKUT

Table 20: Project coverage by institutions. If more than one institution is listed the first one is considered to be responsible. This list is not yet finalized.

Fabrication of new detectors	
procurement of enriched material	MPIP, INR/ITEP, KI
chemistry for separated material	MPIP, INR/ITEP, KI
enriched material control (impurity, enrichment fraction)	MPIP, INR/ITEP, KI, LNGS
design of segmentation and contact	MPIP, PD, JINR
fabrication and test of detectors	MPIP, EKUT, MPIK, LNGS, PD, MI
Material validation and monitoring	
gas purity of LN/LAr	MPIK
radon emanation and monitoring	MPIK, UK, JINR
material screening (ICPMS, Ge & α spectroscopy)	LNGS,MPIK,JINR,INR/ITEP,UK
LArGe construction	
modification of LLBF	MPIK, LNGS, JINR, EKUT
Simulation + analysis	
DAQ software and data distribution	MPIK, MPIP
offline analysis and simulation framework	MPIP, EKUT
monitoring software	MPIK, MPIP, EKUT
Additional R& D	
new germanium isotope separation methods	KI
LAr scintillation	MPIK, JINR, INR/ITEP
analog electronics	MI, MPIK
digital electronics	MPIP

12 Requests to LNGS

This section discusses the support needed from the LNGS for the construction and operation of the experiment. At present this list is preliminary and may change once the final design of the experiment is available.

Table 21 lists the **requested space** in the LNGS underground laboratory. The tank

Table 21: Space requested underground

item	size in m^2	purpose
LN/LAr/water tank	13x14	vessel for detectors, insulation and shielding
infrastructure at the tank		
cleanroom		on top of the tank for the installation of the detectors
electronics room		next to the cleanroom for the readout electronics (3 racks) and slow control
control room #1		next to the cleanroom for DAQ
stair case		for access to the top of the tank
elevator		for lifting of equipment to the top of the tank
additional infrastructure		
storage tanks	3×6	for storage of 20 m^3 of cryogenic fluid
germanium lab	20	for fabrication/repair of diodes
gas lab	20	analysis of contamination of LN/LAr
gas/water purification	25	^{222}Rn extraction, see sec. 6.10
Stirling engine	6	refrigeration of boiled-off fluid (optional)
LArGe-TB (former LENS)	12×4	detector and material screening, LAr instrumentation tests

with its immediate infrastructure (first part of Table 21) should fit in Hall A in front of LVD. For the storage tank(s) the current location of GNO storage tanks may be usable and the germanium lab could be part of the low background facility proposed for LNGS.

In addition some space is needed outside the tunnel. This is listed in Table 22.

Table 22: Space requested above ground

item	purpose
control room #2	monitoring/control of the experiment
office space	4 offices
construction area	~ 200 m^2 temporary space for vessel assembly

Table 23 lists the maximum **electrical power** for the underground equipment. For the

Table 23: Electrical power needed underground

item	power in kW
readout	4 (250 channels of $\sim$16 W each)
slow control	1
DAQ	2 (2 PCs with RAID arrays)
air conditioning for electronics	4
gas purification	9
evaporator for cryogenic liquid	5
Stirling engine (optional)	10
elevator	10
germanium lab	5
gas lab	5
total	55

part of the system that is needed to operate the experiment like electronic readout, slow control and DAQ, an un-interruptible power supply (UPS) is foreseen. This power adds up to 7 kW and should be provided and maintained by Lngs.

During the construction of the tank and for the operation of the experiment **additional support and infrastructure** is needed.

- **Technician/engineer:** During the construction time of the experiment, good coordination between the laboratory and different companies is mandatory. This is best accomplished by Lngs staff. Our current estimate is that support by two technicians/engineers during one year would be sufficient.

- **Workshops:** Support by the mechanical workshop for repairs of smaller items is needed. This will again apply mainly during the construction period.

- **Alarm supervision:** During the operation of the experiment a permanent monitoring of alarms has to be ensured. This should be provided by the Lngs central safety monitoring system.

- **Gas system:** It is desirable that the operation of the cryogenic fluid containers is provided by the LNGS. This applies also for the oxygen concentration monitoring.

- **Water purification:** We propose that the initial water purification is done with the Borexino plant.

- **Cooling water:** The Stirling engine needs cooling water and it would be desirable to cool the electronics the same way. In this case the air conditioning might be spared. In total about 2 m^3/h are needed.

- **Ventilation:** In the current design about 0.5% of the cryogenic fluid evaporates per day. This is less than 0.5 m^3 of liquid which expands to $\approx$400 m^3 of gas. The required ventilation is therefore at least 20 m^3/h. During the filling of the tank this value will be higher.

- **Screening measurements:** Sensitive screening of materials to a level less than 100 μBq/kg has to be performed for several materials, especially the ones used close to the detectors. Measurements at LNGS can reach this sensitivity and support from the laboratory for the task is extremely valuable.

In section 10 a preliminary version of the time table is given. From it one can conclude that for Phase I and II a **six year occupation of the resources** is planned at the moment.

13 Structure of the collaboration

The organization of the collaboration towards the construction of the new facility is defined in a Memorandum of Understanding (MoU) between the collaboration partners and follows the organizational concepts proven by past experiments in particle physics. The MoU also defines the sharing of construction tasks and the other contributions to the project. By particle physics standards, GERDA is a small collaboration and we therefore aim to keep the number of management levels modest.

A Collaboration Board defines the managerial and physics guidelines, makes key decisions concerning the experiment and the priorities, elects or approves collaboration officials etc.. A Spokesperson – elected by the Collaboration Board – and a Deputy Spokesperson represent the collaboration and guide the detailed design, construction, installation and operation of the instrument. A Technical Coordinator takes a crucial role in coordinating the construction and installation of the detector, and to define and monitor interfaces between components as well installation and commissioning procedures. The collaboration will furthermore appoint a Group Leader in Matters of Safety (GLIMOS) and an Environmental Experiment Responsible (RAE) to ensure that all relevant safety regulations and environmental regulations are followed. A LNGS contact person will be nominated, and be available on site.

The work of designing, constructing and commissioning the detector is divided in to reasonably self-contained tasks, to be handled by Task Groups chaired by Task Coordinators. Task Coordinators are proposed by the members of a Task Group and approved by the Collaboration Board. Currently, the following Task Groups are foreseen:

- Task 1: Modification and test of the existing Ge diodes

- Task 2: Design and production of new Ge diodes

- Task 3: Diode readout and signal processing

- Task 4: Cryogenic vessel

- Task 5: Infrastructure on top of vessel

- Task 6: Water vessel and muon veto water Cherenkov system

- Task 7: Scintillator muon veto on top of vessel

- Task 8: Infrastructure for GERDA

- Task 9: Software (online/offline/database/code management)

- Task 10: Simulation and background studies

Additional tasks concern future-oriented R&D, such as liquid-argon scintillation.

A project management group which includes the Task Coordinators, Spokespersons, Technical Coordinator and optionally other collaboration members serves to provide a forum for coordination between the Task Groups.

The Editorial Board regulates all publications generated by the GERDA collaboration which are based either on results of the experiment or which extensively use GERDA hardware or software. The members of the Editorial Board are proposed by the chairman of the Collaboration Board and approved by the Collaboration Board; ex officio members are the spokesperson and his/her deputy.

The structure of the GERDA collaboration is illustrated in Fig. 33.
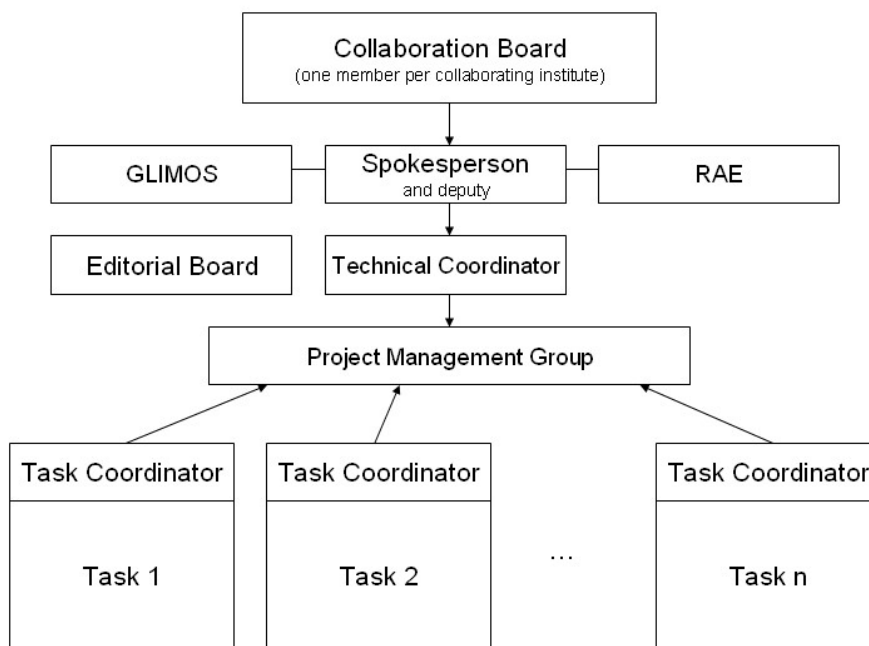
Figure 33: Schematic of the collaboration structure.

References

[Aal 99]   C.E. Aalseth et al., Phys. Rev. C59 (1999) 2108.

[AGA]   "Advanced GAmma Tracking Array" (AGATA) project,
           http://agata.pd.infn.it/index.html, and npg.dl.ac.uk/AGATA/

[Ake 04]   D.S. Akerib et al., (CDMS Collaboration), astro-ph/040533.

[Ali 98]   G. Alimonti et al., Nucl. Instr. Meth. A406 (1998) 411-426.

[Ali 98b] G. Alimonti et al., Astr. Part. Phys. 8 (1998) 141.

[All 03]   S.W. Allen, R.W. Schmidt and S.L. Bridle, Mon. Not. Roy. Astron. Soc. 346
           (2003) 593, and astro-ph/0306386.

[Alt 96]   M. Altmann et al., Nucl. Instr. Meth. A381 (1996) 398.

[Ang 04]   G. Angloher et al., (CRESST Collaboration), astro-ph/0408006.

[Arn 03]   C. Arnaboldi et al., (CUORE collaboration), Astropart. Phys. 20 (2003) 91.

[Arn 04]   C. Arnaboldi et al., Phys. Lett. B584 (2004) 260-268.

[Arno04]   R. Arnold et al., preprint submitted to Nucl. Instr. Meth. A, physics/0402115.

[Arp 92]   C. Arpesella, Nucl. Phys. B (Proc. Suppl.) 28A (1992) 420.

[Arp 02]   C. Arpesella et. al. (BOREXINO Collaboration), Astropart. Physics 18 (2002)
           1-25.

[Art 04]   A. Artikov et. al., arXiv: physics/0403079

[Ash 03]   V.D. Ashitkov et al., nucl-ex/0309001.

[Atk 96]   P.W. Atkins, Physikalische Chemie (1996) VCH Verlagsgesellschaft mbH,
           Weinheim.

[Aug 97]   Pierre Auger Project Design Report (1997)
           http://www.auger.org/admin/DesignReport

[Aug 03]   C. Augier, International Workshop on Weak Interactions in Nuclei and Astro-
           physics: Standard Model and Beyond ECT, Trento, 16 - 21 June (2003)

[Avi 92]   F.T. Avignone et al., Nucl. Phys. B (Proc. Suppl.) 28A, (1992) 280.

[Bak 03]   A.M. Bakalyarov et al., hep-ex/0309016.

[Bar 02]   A.S. Barabash, Proc. Int. Workshop on technique and application of xenon detectors, Edts. Y. Suzuki, M. Nakahata, Y. Koshio and S. Moriyama, Univ. of Tokyo, Japan Dec. 2001, World Scientific, (2002) p. 101-114.

[Bau 99a]   L. Baudis, Dissertation (1999), Universität Heidelberg.

[Bau 99b]   L. Baudis *et al.*, Phys. Rev. D59 (1999) 022001.

[Bel 01]   G. Bellini *et al.*, Eur. Phys. J. C19 (2001) 43.

[Ben 02]   A. Benoit *et al.*, (EDELWEISS Collaboration), Phys. Lett. B545 (2002) 43 and astro-ph/0206271.

[Ber 03]   R. Bernabei *et al.*, (DAMA Collaboration), Riv. N. Cim. 26 n.1. (2003) 1, and astro-ph/0307403.

[Bfs 01]   Bundesamt für Strahlenschutz (BfS), *'Künstliche Umweltradioaktivität'* Jahresbericht (2001) 63.

[Ced 72]   CERN EDMS # 383772

[Cen 93]   P. Cennini *et al.*, Nucl. Instr. Meth. A333 (1993) 567-570.

[Cen 99]   P. Cennini *et al.*, Nucl. Instr. Meth. A432 (1999) 240-248.

[Chk 04]   O. Chkvorets, internal report (2004).

[CRM 04]   Cryogenmash, Moscow, http://www.cryogenmash.ru/index_eng.htm

[Cmp 04]   CMP Arles, dept. cryogénie Soisson, 02201 Soisson, France.

[Dan 00]   F.A. Danevich *et al.*, Phys. Rev. C62 (2000) 044501.

[Del 03]   http://www-dapnia.cea.fr/Sphn/Deformes/Agata/preamps/index.shtml

[Dem 97]   A. Dementyev, V. Gurentsov, O. Ryazhskaya and N. Sobolevsky, INFN/AE-97/50 (1997)

[Die 99]   A. Dietz, Diplomarbeit (1999), Universität Heidelberg.

[Dör 03]   Ch. Dörr, H.V. Klapdor-Kleingrothaus, Nucl. Instr. Meth. A 513 (2003) 596-621, and Ch. Dörr, Diplomarbeit (2002), Universität Heidelberg.

[Dok 90]   T. Doke *et al.*, Nucl. Instr. Meth. A291 (1990) 617.

[Eji 00]   H. Eijiri *et al.*, Phys. Rev. Lett. 85 (2000) 2917.

[Elg 03]   Ø. Elgarøy, O. Lahav, JCAP 0304 (2003) 004.

[Ell 02]   S.R. Elliott and P. Vogel, Ann. Rev. Nucl. Part. Sci. 52 (2002) 115-151.

[Fer 03]   F. Feruglio *et al.*, Nucl. Phys. B659 (2003) 359-362.

[Fle 03]   Flexware Inc., http://www.flexwareinc.com/gasprop.htm .

[Ful 88]   N.J. Fulford and M.D. Slatter, Cryogenics 28 (1988) 810-817.

[GEA 03]   S. Agostinelli *et al.*, Nucl. Instr. Meth. A506 (2003) 250-303.

[Giu 03]   A. Giuliani, TAUP 2003 conf. proceedings., Nucl. Phys. B (Proc. Suppl.), in press.

[Hag 03]   T. Hagner *et al.*, Astropart. Phys. 14(1) (2000) 33-47

[Har 03]   F.X. Hartmann *et al.*, LNGS-LOI 31/2003.

[Heu 95]   G. Heusser, Ann. Rev. Nucl. Part. Sci. 45 (1995) 543.

[Heu 00]   G. Heusser *et al.*, Appl. Rad. and Isot. 52 (2000) 691-695.

[Hit 83]   A. Hitachi *et al.*, Phys. Rev. B 27 (1983) 5279.

[Ira 02]   I.G. Irastorza *et al.*, astro-ph/0211535.

[Iso 02]   R. Isocrate, "MD²S MARS Detector Digitising System", Contribution to the "AGATA LLP Meeting", November 2002, Munich.

[JLG 04]   JL Goslar GmbH, *'Untersuchung über den Bau eines Bleiabschirmtanks'* (2004).

[Jor 94]   V.T. Jordanov and G.F. Knoll, Nucl. Instr. Meth. A345 (1994) 337-345.

[Jor 03]   V.T. Jordanov, Nucl. Instr. Meth. A505 (2003) 347-351.

[Kih 03]   T. Kihm, V.F. Bobrakov, H.V. Klapdor-Kleingrothaus, Nucl. Instr. Meth. A498 (2003) 334-339.

[Kik 01]   J. Kiko, Nucl. Instr. Meth. A460 (2001) 272-277.

[Kla 99]   H.V. Klapdor-Kleingrothaus *et al.*, MPI-Report MPI-H-V26-1999, and hep-ph/9910205, and L. Baudis *et al.*, Nucl. Instr. Meth. A426 (1999) 425-435.

[Kla 01]   H.V. Klapdor-Kleingrothaus et al., Eur. Phys. J. A12 (2001) 147.

[Kla 03]   H.V. Klapdor-Kleingrothaus *et al.*, Nucl. Instr. Meth. A510 (2003) 281-289.

[Kla 03a]   H.V. Klapdor-Kleingrothaus *et al.*, Nucl. Instr. Meth. A511 (2003) 341-346.

[Kla 04]   H.V. Klapdor-Kleingrothaus *et al.*, *'Data acquisition and analysis of the ^{76}Ge double beta experiment in Gran Sasso 1990-2003'*, Nucl. Instr. Meth. A522 (2004) 371.

[Kli 98]   A.A. Klimenko *et al.*, JETP Lett. 67 (1998) 875-880.

[Krö 01]   Th. Kröll, D.Bazzacco, Nucl. Instr. Meth. A463 (2001) 227-249.

[Kub 79]   S. Kubota *et al.*, Phys. Rev. B20 (1979) 3486.

[Laz 03]   L.H. Lazarus, preprint 2003, http://nnsa.dl.ac.uk/GRT/

[LoI 04]   I. Abt *et al.*, Letter of Intent: 'A New 76Ge Double Beta Decay Experiment at LNGS, hep-ex/0404039.

[Loo 83]   H.H. Loosli, Earth and Planetary Sci. Lett. 63 (1983) 51-62.

[Mai 96]   B. Maier, Dissertation (1996), Universität Heidelberg; and J. Bockholt, Dissertation (1994), Universität Heidelberg.

[Maj 03]   White Paper on the Majorana Zero-Neutrino Double-Beta Decay Experiment, MAJORANA collaboration (2003), nucl-ex/0311013.

[Mau 00]   S. Maurer: *'Prediction of Single-Component Adsorption Equilibria'*, Dissertation, Technische University München, Herbert Utz Verlag – Wissenschaft (2000).

[Med 04]   P. Medina, C. Santos, D. Villaumé, Proceedings of the 21st IEEE Instrumentation and Technology Conference, Volume 3, Como, Italy, May 18-20 2004.

[Mot 04]   D. Motta, Dissertation (2004), Universität Heidelberg.

[MPI 92]   Max-Planck-Institut für Kernphysik, *Progress Report* (1992), Heidelberg.

[MPI 03]   Max-Planck-Institut für Kernphysik, *Progress Report* (2003), Heidelberg.

[Ned 00]   H. Neder, G. Heusser and M. Laubenstein, Appl. Rad. Isot. 53 (2000) 191-195.

[Obe 98]   L. Oberauer and S. Schönert, The Borexino muon identification system, Borexino internal report, 98-02-01 (1998)

[Osi 01]   A. Osipowicz *et al.* (KATRIN collaboration), hep-ex/0109033.

[Pan 04]   L. Pandola *et al.*, Nucl. Instr. Meth. A522 (2004) 521.

[Pei 03]   P. Peiffer, Diploma thesis (2003), Univ. Heidelberg.

[Pet 93]   F. Petry *et al.*, Nucl. Instr. Meth. A332 (1993) 107.

[pro 04]   pro-beam AG, München/Burg, http://www.pro-beam.de

[Rau 00]   W. Rau and G. Heusser, Appl. Rad. Isot. 53 (2000) 371-375.

[Res 01]   E. Resconi, Dissertation Univ. Genova, Italy (2001)

[Res 04]   E. Resconi and S. Schönert, to be submitted to Nucl. Instr. Meth. .

[Ric 96]   R.H. Richter et al., Nucl. Instr. Meth. A377 (1996) 412-421.

[Sch 04]   S. Schönert, D. Motta, P. Peiffer and H. Simgen, XXIst Int. Conf. on Neutrino Physics and Astrophysics, Paris, June 2004, Nucl. Phys. B (Proc. Supl.) in print.

[Sho 99]   A.L. Shoup (Milagro collaboration), astro-ph/9907214.

[Sim 03]   H. Simgen et al., Nucl. Instr. Meth. A497 (2003) 407-413.

[Sim 04]   H. Simgen, et al., Appl. Rad. Isot. 61 (2004) 213-217.

[SNO 00]   The SNO Collaboration, Nucl. Instr. Meth. A449 (2000) 172-207.

[Spe 03]   D.N. Spergel et al., ApJ Suppl. 148 (2003) 175.

[Ste 02]   F. Steinbuegel et. al., 7th Int. Conf. on advanced technology and particle physics 2001, Villa Olmo, Como, World Scientific, Singapore (2003)

[SuK 03]   The Super-Kamiokande Collaboration, Nucl. Instr. Meth. A501 (2003) 418-462.

[Tak 99]   Y. Takeuchi et al., Nucl. Instr. Meth. A421 (1999) 334.

[Tak 04]   Y. Takeuchi, personal communication (2004).

[TIS 98]   'The use of cryogenic fluids', (1998) CERN TIS IS 47.

[Umi 04]   Umicore Electro-Optic Materials, personal communication.

[Wul 03]   H.R.T. Wulandari, 'Study on Neutron-Induced Background in the Dark Matter Experiment CRESST', Dissertation (2003), Technische Universität München, and H.R.T. Wulandari et al., hep-ex/0401032.

[XIA]   X-Ray Instrumentation Associates (XIA), http://www.xia.com .

[Zde 01]   Yu.G. Zdesenko, O.A. Ponkratenko, V.I. Tretyak, J. Phys. G27 (2001) 2129.

[Zub 01]   K. Zuber, Phys. Lett. B 519 (2001) 1-7.

[Zuz 04]   G. Zuzel et al., Appl. Rad. Isot. 61 (2004) 197-201.